PhD degree in Systems Medicine (curriculum: Molecular Oncology)

European School of Molecular Medicine (SEMM)

University of Milan and University of Naples "Federico II"

Molecular Oncology

Prune-1 drives the recruitment and the polarization of Tumour-Associated Macrophages (TAMs) preparing the soil for lung metastases in Triple Negative Breast Cancer

Veronica Ferrucci

CEINGE, Biotecnologie Avanzate, Naples

Matricola n. R10737

Supervisor: Prof. Massimo Zollo

CEINGE, Biotecnologie Avanzate, Naples, Italy

Internal Advisor: Prof. Piero Pucci

CEINGE, Biotecnologie Avanzate, Naples, Italy

External Advisor: Prof. Kris Gevaert

VIB Medical Biotechnology Center, Gent, Belgium

Anno accademico 2016-2017

INDEX OF CONTENTS

ABSTRACT

Tumour microenvironment is a complex network of cells, including immune cells, with a role in tumorigenesis and metastatic spread. Among the immune cells, M2-polarized Tumour-Associated-Macrophages (M2-TAMs) show immunosuppressive activities by expressing inflammatory molecules, thus promoting tumorigenesis. Triple-Negative Breast Cancer (TNBC), lacking both hormone receptors (*i.e.* Progesterone Receptor [PgR] and Estrogen Receptor [ER]) and Human Epidermal growth factor Receptor 2 (HER2), is associated with poor prognosis and high probability of distant metastases. In TNBC, a large number of infiltrating M2-TAMs is positively correlated to higher risk of metastases and lower rates of Disease-Free Survival" (EFS) and Overall Survival (OS).

Prune-1 belongs to DHH (Asp-His-His) phosphoesterase superfamily with an exopolyphosphatase activity. The overexpression of Prune-1 is correlated with metastases and poor prognosis in several tumours including Breast Cancer (BC). Prune-1 was also found to induce Epithelial-Mesenchimal-Transition (EMT) and metastatic dissemination throught the enhancement of canonical TGF-β signaling by counterbalancing its inhibition operated by NDPK-A. Further evidences suggested that lung cancer progression is driven by Prune-1 through the canonical WNT signaling pathway in both autocrine and paracrine manner via Wnt3a cytokine secretion, thus suggesting a potential role for Prune-1 also in extracellular environment.

Here, we identified Prune-1 protein as overexpressed in TNBC patients and positively correlated to lynphnode metastases, inflammatory pathways and infiltrating M2-TAMs ($CD68^+/CD163^+$).

Furthermore, we developed a Genetically Engineered Mouse Model (GEMM) of metastatic TNBC over-expressing both Prune-1 and Wnt-1 in mammary glands (MMTV-Prune1/Wnt1). We found Prune-1 to recruit TAMs and to enhance their polarization toward a pro-tumorigenic M2-phenotype in the tumour microenvironment, thus promoting lung metastases in this GEMM. We also show that Prune-1 takes part to the communication between TNBC cells and TAMs through intracellular pathways activation (*i.e.,* TGF-β and NF-kB), but also in a paracrine manner by inducing the secretion of inflammatory cytokines (*e.g.,* IL-17F and IL-28) and modulating the exosome protein contents.

Finally, we found an anti-Prune-1 drug (AA7.1) with the ability to reduce the primary tumour growth by reducing the percentage of M2-TAMs in orthotopic xenograft immunocompetent models of TNBC.

In conclusion, our GEMM of metastatic TNBC driven by Prune-1 will be a useful source for future immunotherapy pre-clinical trials targeting M2-polarized TAMs within the tumour microenvironment to inhibit distant metastases in TNBC with poor prognosis.

1. INTRODUCTION

1.1 Triple Negative Breast Cancer (TNBC)

Breast Cancer (BC) is one of the most common cancers with estimated 252,710 new cases of diagnosed BC and 40,610 death among women in 2017 [1]. Clinically, this heterogeneous disease is categorized into three basic therapeutic groups. The Estrogen Receptor (ER) positive group is the most numerous and diverse, with several genomic tests to assist in predicting outcomes for ER patients receiving endocrine therapy. The Human Epidermal growth factor Receptor 2 (HER2) amplified group is a great clinical success because of effective therapeutic targeting of HER2, which has led to intense efforts to characterize other DNA copy number aberrations. Triple-Negative Breast Cancers (TNBCs, lacking expression of ER, Progesteron Receptor [PgR] and HER2) are a group with only chemotherapy options [2].

However, integrated molecular analyses reported that BC encompass several distinct molecular disease entities. In fact, supervised clustering of mRNA expression, genomic DNA mutations, DNA methylation, microRNA (miRNA) and protein expression data (using six different technology platforms) demonstrated the existance of different BC subtypes: Luminal/ER^+ (Luminal A and Luminal B subtypes), HER2-based (HER2E-mRNA/$HER2^+$ and luminal-mRNA-$HER2^+$ subtypes) and Basal-like [2].

Luminal/ER^+ BC are the most heterogeneous in term of gene expression, mutation spectrum, copy number changes and patient outcomes. The most dominant features are high mRNA and protein expression of GATA3, FOXOA1, ESR1, XBP1 and MYB. Most notably, GATA3 and FOXOA1 are mutated in a mutually exclusive fashion. Mutations in RUNX1, CBFB, PIK3CA, MAP3K1 and MAPK4 also occurred in this BC subgroup. Higher frequency of TP53 mutation, ATM loss, MDM2 and Cyclin D1 amplification are found in Luminal B (29%) compared to Luminal A (12%) subtype. In contrast, RB1 levels are higher in Luminal A tumours together with low levels of CDKN2C. These findings suggest Luminal A subtype, which has the best prognosis, is most likely to retain activity of tumour suppressors RB1 and TP53 [2].

This integrated molecular classification identified two subtypes within the HER2-based BC: the HER2E-mRNA/$HER2^+$ and luminal-mRNA/$HER2^+$ subtype. The first typically show high aneuploidy, the highest somatic mutation and DNA amplification rate, with higher expression of Receptor Tyrosine Kinase (RTK) including FGFR4, EGFR, HER2 itself, high levels of pSRC and pS6 and TP53 mutations. In contrast, luminal-mRNA/HER2+ subtype show higher expression of genes belonging to the “luminal cluster”, including GATA3, BCL2 and ESR1 [2].

The Basal-like BCs are often referred to as TNBCs because most Basal-like tumours are typically negative for ER, PgR and HER2. 'Basal-like' was the term chosen to define this subgroup because tumour cells express genes characteristic of normal basal/myoepithelial cells, such as KRT5, KRT14 and KRT17 (Cytokeratins -5, -14 and -17, respectively), and EGFR [3]. Basal-like tumours showed a high frequency of TP53 and PIK3CA mutations, RB1, BRCA1, PTEN and INPP4B loss and PIK3CA amplification. Interestingly, expression features of Basal-like tumours include a characteristic signature containing Keratins -5, -6 and -17 and high expression of genes associated with cell proliferation. Within this BC subgroup, hyperactivated FOXM1, MYC and HIF1α, ATM mutations, BRCA1 and BRCA2 inactivation (20% germline and/or somatic mutations), RB1 loss and cyclin E1 amplification are commonly found. A comprensive catalogue of likely genomic drivers in BC subtypes obtained from this recent integrated molecular features are listed in the Table 1 [2].

Table 1: Highlights of genomic, clinical and proteomic features of BC subtypes

Subtype	Luminal A	Luminal B	Basal-like	HER2E
(%) ER+/HER2−	87%	82%	10%	20%
(%) HER2+	7%	15%	2%	68%
(%) TNBCs	2%	1%	80%	9%
TP53 Pathway	TP53 mut (12%) Gain of MDM2 (14%)	TP53 mut (32%) Gain of MDM2 (31%)	TP53 mut (84%) Gain of MDM2 (14%)	TP53 mut (75%) Gain of MDM2 (30%)
PIK3CA/PTEN Pathway	PIK3CA mut (49%) PTEN mut/loss (13%) INPP4B loss (9%)	PIK3CA mut (32%) PTEN mut/loss (24%) INPP4B loss (16%)	PIK3CA mut (7%) PTEN mut/loss (35%) INPP4B loss (30%)	PIK3CA mut (42%) PTEN mut/loss (19%) INPP4B loss (30%)
RB1 Pathway	Cyclin D1 amp (29%) CDK4 gain (14%) Low expression of CDKN2C High expression of RB1	Cyclin D1 amp (58%) CDK4 gain (25%)	RB1 mut/loss (20%) Cyclin E1 amp (9%) High expression of CDKN2A Low expression of RB1	Cyclin D1 amp (38%) CDK4 gain (24%)
mRNA Expression	High ER cluster Low proliferation	Lower ER cluster High proliferation	Basal signature High proliferation	HER2 amplicon signature High proliferation
Copy Number	Most diploid Many with quiet genomes 1q, 8q, 8p11 gain 8p, 16q loss 11q13.3 amp (24%)	Most aneuploid Many with focal amps 1q, 8q, 8p11 gain 8p, 16q loss 11q13.3 amp (51%) 8p11.23 amp (28%)	Most aneuploid High genomic instability 1q, 10p gain 8p, 5q loss MYC focal gain (40%)	Most aneuploid High genomic instability 1q, 8q gain 8p loss 17q12 focal ERRB2 amp (71%)
DNA Mutations	PIK3CA (49%) TP53 (12%) GATA3 (14%) MAP3K1 (14%)	TP53 (32%) PIK3CA (32%) MAP3K1 (5%)	TP53 (84%) PIK3CA (7%)	TP53 (75%) PIK3CA (42%) PIK3R1 (8%)
DNA Methylation	-	Hyper-methylated phenotype for subset	Hypo-methylated	-
Protein Expression	High Estrogen-signaling High cMYB RPPA reactive subtypes	Less Estrogen-signaling High FOXM1 and cMYC RPPA reactive subtypes	High expression of DNA repair proteins, PTEN and INPP4B loss signature (p-AKT)	High protein and phos-protein expression of HER1 and HER2

Percentages are based on 466 tumours. Amp, amplification; Mut, mutation
from Koboldt *et al*., Nature (2012), 4; 490(7418): 61–70.

The definition of TNBC applies to all tumours that lack the expression of ER, PgR and HER2 (*i.e.,* ER^-, PgR^- and $HER2^-$), all of which are molecular targets of therapeutic agents. Nevertheless, chemotherapy is still the primary established treatment option for patients with both early-stage and those with advanced-stage (or metastatic) TNBC. Patients with TNBC typically have a relatively poorer outcome compared with those with other breast cancer subtypes owing to an inherently aggressive clinical behaviour and a lack of recognized molecular targets for therapy.

TNBC has several aggressive clinicopathological features, including young age at onset (<50 years) and large tumour size. Its histological hallmarks include high grade, proliferative activity, focal areas of necrosis, absence of infiltrative margin, absence of gland formation, presence of central scar/fibrotic foci and prominent lymphoplasmacytic inflammatory infiltrate [4].

The diagnosis of TNBC depends on the accurate assessment of ER and PgR protein expression levels by Immunohistochemistry (IHC), and of HER2 by IHC and/or Fluorescence In Situ Hybridization (FISH) by adopting a conservative cut-off point of <1% of ER/PgR-positive tumour cells [3].

The majority of TNBCs (95%) are histologically classified as invasive ductal carcinomas, but other different rare subtypes have been also described: invasive lobular (1-2%), metaplastic with squamous differentiation (<1%), spindle-cell metaplastic (<1%), adenoid cystic (<1%), secretory (<1%), medullary (<1%) and apocrine carcinoma (<1%) (Figure 1).

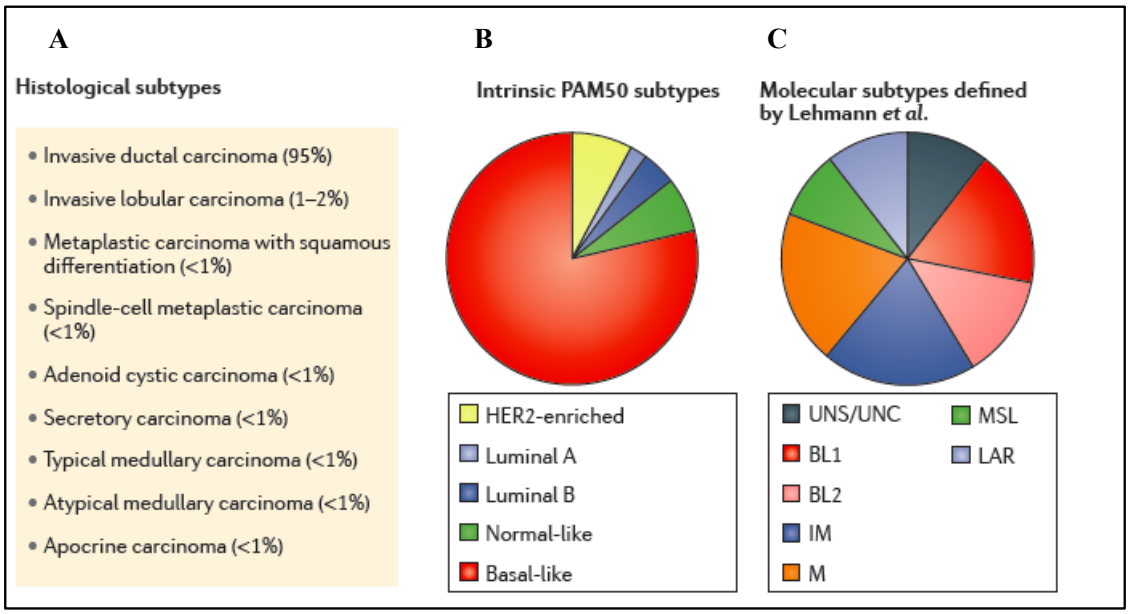

Figure 1: The heterogenous landscape of triple-negative breast cancer. Different approaches to dissect the complex molecular landscape of TNBCs are presented. **(A)** Histological subtypes. Some rare but relevant subtypes are shown for illustrative purposes. **(B)** Gene-expression-based subtypes of triple-negative breast cancer (TNBC) according to PAM50 (Prat *et al*., Oncology 2013; 18: 123-133). **(C)** Gene-expression-based subtypes defined by Lehmann et al., (J. Clin. Invest. 2011; 121: 2750-2767). BL1, basal-like 1; BL2, basal-like 2; M, mesenchymal; MSL, mesenchymal stem-like; IM, immunomodulatory subgroup; LAR, luminal androgen receptor group. From Bianchini *et al*., Nat Rev Clin Oncol, 2016, 13(11): 674-690.

TNBC patients have heterogeneous clinical behaviour and frequently have a poor prognosis. Interestingly, at the time of diagnosis TNBC exhibit a wide and continuous spectrum of genomic evolution, with some having only a handful of coding somatic aberrations in few pathways, whereas others contain hundreds of coding somatic mutations. TP53, PIK3CA and PTEN somatic mutations seem to be clonally dominant compared to other genes, while mutations in cytoskeletal, cell shape and motility proteins occurred at lower clonal frequencies, suggesting that they occurred later during tumour progression. Nervertheless, in some tumours the clonal frequencies of these "drivers" are incompatible with founder status, raising a question about what drives clonal expansion in these TNBC [5]. Thus, a concerted effort has been undertaken to understand the molecular basis of this heterogeneity and to discover actionable molecular targets for TNBC. Many of these efforts have focused on assigning TNBC molecular characteristics into subgroups [3]. More than 90% of Basal-like BCs are TNBCs. Conversely, Basal-like BC represents the most frequent subtype of TNBC (55–81%) (Figure 1B).

To better dissect TNBC-specific tumour heterogeneity, Lehmann and colleagues [6] defined six new TNBC subtypes on the basis of gene-expression profiles: two basal-like-related subgroups (basal-like 1 [BL1] and 2 [BL2]), two mesenchymal-related subgroups (mesenchymal [M] and mesenchymal stem-like [MSL]), one immunomodulatory subgroup (IM) and one luminal androgen receptor group (LAR) (Figure 1C). Interestingly, some of the TNBC subtypes are closely linked to histological types: IM tumours overlap with medullary breast cancer, M and MSL tumours with metaplastic breast cancer, and LAR tumours with apocrine tumours [6].

Among the most frequent mutations in TNBC, only TP53 mutations are found at a high frequency (60–70% of mutations), and are more common in TNBC-basal-like (62– 80%) than in TNBC-non-basal-like (43%). PIK3CA is the next most commonly mutated gene in TNBC (~10% globally), although mutations in this gene are significantly more frequent in TNBC-LAR (46.2%) than in the other subtypes (average 4.5%). Potentially actionable deletions (*e.g.,* PTEN or INPP4B) and amplifications (*e.g.,* PIK3CA, KRAS, BRAF, EGFR, FGFR1, FGFR2, IGFR1, KIT or MET) have been reported in TNBCs at variable frequencies (1–40%). Moreover, a frequent Phosphoinositide 3-Kinase PI3K/AKT pathway activation is also observed in TNBC. The presence of germline mutations in BRCA1/2 increases the lifetime risk of BC to 60–70% and occurs in ~10% of patients with TNBC [3].

The association between TNBC subtypes and response to neoadjuvant chemotherapy was evaluated in a retrospective analysis of 130 patients with TNBC treated with neoadjuvant Taxane and anthracycline-based regimens. This study reported patients with TNBC-BL1 subtype achieving the highest Pathological Complete Response (pCR) rate (52%) and patients with tumours classified as

TNBC-BL2, TNBC-LAR and TNBC-MSL having the lowest response rates (0%, 10% and 23%, respectively) [7].

Therapies for TNBC

Chemotherapy

Cytotoxic chemotherapy remains the mainstay of treatment for TNBC and approximately 30–40% of patients with early-stage TNBC treated with standard neoadjuvant anthracycline and taxane-based chemotherapy regimens achieve a pCR after treatment [8].

The intrinsic genomic instability of a subset of TNBCs with defects in DNA repair has generated a growing body of preclinical and clinical data examining the role of Platinum-based chemotherapy for TNBC. Platinum salts, including Carboplatin and Cisplatin, lead to DNA crosslink strand breaks that result in apoptosis specifically in cells unable to efficiently repair these lesions.

Several clinical studies have examined the role of platinum-based agents in the neoadjuvant treatment of patients with TNBC. Approximately 30% of women with TNBC treated with anthracycline and taxane-based neoadjuvant chemotherapy will achieve a pCR after treatment with an improved disease-free survival rates ($p<0.001$) [8], [9]. By contrast, a separate study reported that 50 out of 82 (61%) patients with stage I–III TNBC harbouring BRCA1 mutations achieved a pCR after neoadjuvant therapy with cisplatin [10].

In another small single-arm study in 28 women with stage II or III TNBC treated with four cycles of neoadjuvant single-agent Cisplatin, the pCR rate was 22% (including the only two patients with BRCA1 germline mutations), with four (14.2%) complete responses and 14 (50%) partial responses (overall clinical response rate 64%) [11].

These results suggest that platinum-based agents are effective as single-agent regimens (and/or bevacizumab) in patients with early-stage TNBC, and support the evaluation of addition of Platinum-based agents to standard Taxane– Anthracycline-based neoadjuvant regimens.

Two large randomized trials further explored the effect of platinum-based agents on TNBC in the neo-adjuvant setting. The CALGB40603 trial [12] evaluated the effect of adding Carboplatin and/or Bevacizumab to Paclitaxel followed by dose-dense Doxorubicin and Cyclophosphamide in 443 patients with stage II or III non-inflammatory TNBC. The addition of carboplatin increased the pCR rate in the breast from 46% to 60% ($p=0.0018$), and in breast/axilla from 41% to 54% ($p=0.0029$). The GeparSixto trial [8] included 315 patients with stage II or III that were randomly assigned to receive a regimen containing Anthracycline, Taxane and Bevacizumab, with or without Carboplatin. The pCR rate in breast/axilla increased from 36.9% to 53.2% ($p=0.005$) for those patients who received Carboplatin. In both trials, however, a substantially increased toxicity was observed, and many patients

(48% and 20%) were unable to complete therapy as planned. The addition of Cisplatin or Carboplatin to neoadjuvant treatment of TNBC is clearly associated with significantly higher rates of pCR, which suggests that the absence of ER/PgR/HER2 could be a potential therapeutic target for these drugs in patients with early-stage disease.

In the PrECOG 0105 single-arm neoadjuvant trial [13], 80 patients with TNBC were treated with Gemcitabine, Carboplatin and the Poly(ADP-Ribose) Polymerase (PARP) inhibitor Iniparib. Patients with mutations in BRCA1/2 had the highest response rate (75%). The patients with BRCA1/2 mutation achieved a remarkable response rate (59%); By contrast, in the group of patients without mutations in BRCA1/2, the favourable responses were only 8%.

The clinical utility of the addition of Platinum-based agents to standard neoadjuvant and adjuvant chemotherapy regimens, however, remains controversial mainly because of the added toxicities.

A multicentre phase II study evaluating Platinum monotherapy in 86 patients with metastatic TNBC Overall Response Rates (ORR) of 32% and 19% for Cisplatin and Carboplatin, were reported, respectively. Interestingly, patients who carried mutations in BRCA1/2 (n = 11) had a higher ORR (54.5%) than those with wild type BRCA1/2 (n = 66; ORR: 19.7%) [14]. In summary, the overall clinical efficacy of Platinum-based agents in patients with metastatic TNBC has been modest.

Targeted therapies

Given the heterogeneity of TNBC, personalized treatment strategies targeting molecular tumour-specific alterations would be the most appropriate to effectively treat the 60–70% of patients with TNBC who do not fully respond to chemotherapy. As many as 90% of TNBCs that persist after chemotherapy contain alterations in pathways that can be targeted with agents currently under clinical investigation, such as PARP inhibitors, PI3K inhibitors and MEK inhibitors.

PARP is a nuclear enzyme that catalyses the transfer of ADP-ribose from NAD+ to target proteins and facilitates DNA repair through poly(ADP)-ribosylation of several nuclear proteins involved in chromatin architecture and DNA metabolism. Immediate catalytic activation of PARP in response to DNA single-strand and double-strand breaks has been reported at levels up to 500-fold of basal levels [15]. Significant single-agent activity was reported with the PARP inhibitor Olaparib in patients with BRCA-deficient metastatic BC. Overall responses ranged from 22% to 41% with minimal toxicity [16].

Several phase III trials investigating the use of Olaparib in the metastatic (NCT02000622) and neoadjuvant (NCT02032823) setting, for patients with mutations in BRCA, are ongoing. Importantly, there are several additional PARP inhibitors currently being tested in clinical trials, such as Veliparib (phase III; NCT02163694), Talazoparib (phase III; NCT01945775), Niraparib (phase III; NCT01905592) and Rucaparib (phase I/II; NCT01074970).

Nevertheless, although PARP inhibitors clearly demonstrate benefit when administered as single agents, their benefit when used in addition to platinum agents is unclear in TNBC.

Mutations affecting 'hotspot' regions of the PIK3CA gene, which encodes the PI3K catalytic subunit-α, are the most frequent activating mutations in this gene in TNBC (10.2%). Additionally, loss of PTEN, a negative regulator of the PI3K pathway, occurs in 9.6% of TNBC and, in general, is mutually exclusive with PIK3CA hotspot mutations. A phase I study of the pan-PI3K inhibitor Buparlisib (BKM120, Novartis, Switzerland) in combination with Olaparib for patients with solid tumours that include metastatic TNBC is under way (NCT01623349).

Aberrant activation of the Ras/MAPK pathway can be attributed to activation or overexpression of growth factor receptors (such as EGFR, IGF1R, FGFR1 or VEGFR, among others), or to gene copy-number alterations (gains and amplifications) in key Ras/MAPK constituents such as BRAF and KRAS, which have been observed at moderate frequencies in Basal-like BC (30 and 33%, respectively), and result in increased gene expression. The use of MEK inhibitors in combination with chemotherapy or other targeted agents to treat TNBC is currently under clinical investigation. Further, in a phase I trial in patients with solid tumours (n.31) treated with Gemcitabine and Trametinib (an orally available potent inhibitor of MEK1/2), the only complete response to therapy occurred in a patient with metastatic TNBC [17].

Metastatic TNBC

Despite optimal systemic chemotherapy, fewer than 30% of women with metastatic BC survive 5 years after diagnosis, and virtually all women with metastatic TNBC will ultimately die of their disease.

The pattern of metastatic spread in TNBC patients was evaluated in a cohort of women with invasive BC (n.1608). Among those, 108 (11.2%) were TNBC. The mean time to distant recurrence in patients with TNBC was 2.6 years compared to 5.0 years for women with other cancer ($p<0.0001$). The excess risk of distant recurrence in TNBC versus other forms of cancer is attributable in large part to an excess of visceral metastases in the first 5 years following diagnosis ($p<0.0001$) [18]. TNBC has a propensity for visceral metastasis to brain and lung, rather than lynph nodes, bone or liver mostly due to the haematogenous than lynphatic spread [19]. This was confirmed in another study performed in a cohort of 205 TNBC patients, in which 193 patients (94.1%) had distant metastases. The most common site for the first metastasis to occur was the bone (22.9%), followed by lung (20%), liver (13.7%), pleura (8.8%) and brain (6.8%). Interestingly, TNBC patients with lung as the first metastatic site had the longest median post-metastatic overall survival (OS) of 16.6 months, followed by the bone (16.3 months), the liver (8.9 months), the pleura (7.5 months) and the brain (4.3 months) [20]. A more

comprehensive portrait of the features and clinical outcomes of patients with TNBC, relative to other BC subtypes, was provided in a study conducted on 15204 women presenting stage I-III BC. The women with TNBC in this cohort (n.2596, 17%) were more likely to experience a first recurrence in brain, lung, or loco-regional sites, and less likely to occur in bone. Further, TNBC subtype was associated with worse OS as compared to other BC subtypes ($p<0.0001$) [19].

Although there have been many new treatment options approved for metastatic BC, relatively few new agents have been approved for patients with metastatic TNBC. As a result, patients with metastatic TNBC continue to have a considerably worse OS when compared to their metastatic BC counterparts. In fact, the therapeutic approach for metastatic TNBC patients mimics that of other subsets of patients with metastatic BC based on single–agent chemotherapy (*e.g.,* Taxanes and Anthracyclines) or combination chemotherapy (Table 2).

Table 2: Commonly used systemic treatments in metastatic Triple Negative Breast Cancer

Drug	Dose	Frequency
Doxorubicin	60–75 mg/m^2	Day 1 of 21 day cycle
	20 mg/m^2	Weekly
Paclitaxel	175 mg/m^2	Day 1 of 21 day cycle
	80 mg/m^2	Weekly
Capecitabine*	1000–1250 mg/m^2	Twice a day, days 1–14 of a 21 day cycle
Gemcitabine	800–1200 mg/m^2	Days 1, 8, 15 of 28 day cycle
Vinorelbine	25 mg/m^2	Days 1, 8 of 21 day cycle
Eribulin	1.4 mg/m^2	Days 1, 8 of 21 day cycle
Cyclophosphamide*	50 mg	Days 1–21 of 28 day cycle
Carboplatin	AUC 6	Day 1 of 21–28 day cycle
	AUC 2	Days 1, 8 of 21 day cycle
Cisplatin	75 mg/m^2	Day 1 of 21 day cycle
Docetaxel	35–40 mg/m^2	Days 1, 8, 15 of 28 day cycle
	60–100 mg/m^2	Day 1 of 21 day cycle
Albumin-bound paclitaxel	100 mg/m^2	Days 1, 8, 15 of 21 day cycle
	260 mg/m^2	Day 1 of 21 day cycle
Epirubicin	60 mg/m^2	Days 1, 8 of 21 day cycle
	90 mg/m^2	Day 1 of 21 day cycle
Ixabepilone	40 mg/m^2	Day 1 of 21 day cycle
Doxorubicin	60 mg/m^2	Day 1 of 21 day cycle

Note: *Orally administered; AUC, area under the curve;
From Zeichner *et al.,* Breast Cancer: Basic and Clical Research. (2016):10 25-36.

Of importance, synergistic combinations produce a more significant response rates and survival outcomes in the setting of metastatic disease compared with monotherapy [21]. However, metastatic TNBC is not curable at this time and several preclinical/early phase studies have implicated other possible chemotherapeutic strategies and targettable pathways in metastatic TNBC, for which clinical trials are currently underway (Table 3) with the ultimate goal of improving the long-term ourcomes of this subset of patients [21].

Table 3: Clinical trials looking at targeted agents and chemotherapeutic, hormonal, immune strategies in metastatic Triple Negative Breast Cancer

Nct Number	Phase	Intervention	Target Of New Agent	(N)	Estimated Date Of Completion
NCT02120469	I	Eribulin mesylate and everolimus	MTOR	45	
NCT01939418	I/II	Gemcitabine, cisplatin and everolimus	MTOR	116	July 2017
NCT02506556	II	BYl719	PI3K	34	December 2018
NCT02485119	I	BAY94-9343	Mesothelin	15	November 2017
NCT01997333	II	Glembatumumab vedotin plus capecitabine	gpNMB	300	November 2018
NCT02370238	II	Paclitaxel in combination with reparixin	CXCR1/2	190	February 2018
NCT01837095	I	POL6326 in combination with eribulin	CXCR4	24	December 2016
NCT02227082	I	Olaparib and radiotherapy	PARP	36	August 2018
NCT02567396	I	Talazoparib	PARP	105	
NCT02158507	Pilot	Veliparib and lapatinib	PARP	25	June 2018
NCT01145430	I	Veliparib and pegylated liposomal doxorubicin	PARP	58	–
NCT02358200	I	BMN-673 with carboplatin and paclitaxel	PARP	20	May 2017
NCT02498613	II	Cediranib maleate and olaparib	VEGF and PARP	121	
NCT01631552	I/II	Sacituzumab govitecan	TROP-2	250	June 2016
NCT02574455	III	Sacituzumab govitecan with eribulin, capecitabine, or gemcitabine	anti-TROP-2-SN-38	328	June 2019
NCT02071862	I	CB-839	Glutaminase	165	March 2016
NCT02048059	II	ANG1005	Taxane	56	October 2016
NCT01910870	II	Cisplatin and metronomic cyclophosphamide	–	35	–
NCT02263495	II	Eribulin plus gemcitabine	–	112	December 2018
NCT02207335	III	Gemcitabine and capecitabine versus gemcitabine and carboplatin	–	120	December 2015
NCT01898117	II	Carboplatin-cyclophosphamide versus paclitaxel with or without bevacizumab	VEGFR	304	December 2029
NCT02202746	II	Lucitanib	VEGFR-FGFR	201	November 2016
NCT00733408	II	Nab-paclitaxel and bevacizumab followed by bevacizumab and erlotinib	VEGFR and EGFR	63	–
NCT02362230	II	Icotinib	EGFR	67	December 2017
NCT01939054	II	Nimotuzumab plus docetaxel and capecitabine versus docetaxel and capecitabine	EGFR	90	September 2016
NCT01990209	II	Orteronel	CYP17A1	86	June 2018

(Continued)

Table 3: (continued)

Nct Number	Phase	Intervention	Target Of New Agent	(N)	Estimated Date Of Completion
NCT02580448	I/II	VT-464	CYP17A1	81	December 2017
NCT02353988	II	Bicalutamide	AR	60	May 2017
NCT02348281	II	Bicalutamide	AR	44	June 2018
NCT02014337	I	Mifepristone and eribulin	Anti-progestogen and -glucocorticoid	40	February 2016
NCT02457910	I/II	Taselisib and enzalutamide	PIK3CA and AR	74	–
NCT02322814	II	Cobimetinib in combination with paclitaxel	MEK	112	April 2018
NCT01964924	II	Trametinib and Akt inhibitor GSK2141795	MEK and AKT	41	–
NCT02423603	II	AZD5363 in combination with paclitaxel	AKT	140	January 2017
NCT02162719	II	Ipatasertib in combination with paclitaxel	AKT	120	February 2017
NCT02476955	Ib	ARQ 092 in combination with carboplatin plus paclitaxel	AKT	49	June 2017
NCT02543645	I/II	Varlilumab and atezolizumab	Anti-CD27 and Anti-PDL1	55	June 2019
NCT02478099	II	MPDL3280A	Anti-PDL1	40	August 2017
NCT01928394	I	Nivolumab monotherapy or nivolumab combined with ipilimumab	Anti-PD1, Anti-CTLA4	1100	December 2017
NCT02309177	I	Nivolumab with nab-paclitaxel	Anti-PD1	138	July 2018
NCT02447003	II	Pembrolizumab	Anti-PD1	245	November 2019
NCT02513472	I/II	Eribulin mesylate plus pembrolizumab	Anti-PD1	95	January 2018
NCT02555657	III	Pembrolizumab vs. chemotherapy	Anti-PD1	600	September 2017
NCT02187991	II	Alisertib with paclitaxel	Aurora A kinase	252	September 2017
NCT01837602	I	cMet CAR RNA T cells		15	April 2017
NCT02402764	II	Selinexor	SINE XPO1	34	–
NCT02041429	I/II	Ruxolitinib lus chemo	JAK1/2	24	January 2021
NCT01596751	Ib/II	PLX 3397 and eribulin	colony-stimulating factor 1 receptor	80	December 2016
NCT02203513	II	LY2606368	Chk1/2	108	June 2019
NCT02474173	I	AT13387 and paclitaxel	HSP-90	24	–
NCT02393794	I/II	Romidepsin plus cisplatin	HDAC	54	December 2018
NCT02425891	III	Atezolizumab in combination with nab-paclitaxel	Anti-CD52	350	May 2019
NCT02027376	II	LDE225 in combination with docetaxel	Hedgehog	18	May 2017

Abbreviations: PI3K, phosphatidylinositol 3-kinase; MEK, mitogen-activated protein kinase kinase; Akt, v-Akt murine thymoma viral oncogene; mTOR, mammalian target of rapamycin; HSP-90, heat shock protein 90; CXCR, chemokine receptor; HDAC, histone deacetylase; PARP, poly adenosine diphosphate-ribose polymerase; Trop-2, tumor-associated calcium signal transducer 2; GPNMB, glycoprotein nonmetastatic b; EGFR, epidermal growth factor receptor; VEGFR, vascular endothelial growth; PD1, programmed death 1; PDL1, programmed death ligand 1; CTLA4, cytotoxic T-lymphocyte-associated protein 4; AR, androgen receptor; CYP17A1, cytochrome P450 17A1; CSF1R, colony-stimulating factor 1 receptor; JAK1/2, janus kinase 1 and 2; Sine XPO1, selective inhibitor of nuclear export exportin 1; CHK1/2, checkpoint kinase 1 and 2; CD27, cluster of differentiation 27; CD52, cluster of differentiation 52. From Zeichner *et al.,* Breast Cancer (2016),10. 25-36.

1.2 Prune-1, a metastasis promoter protein

Prune-1 is a phosphoesterase DHH (Asp-His-His) family appertaining protein, with an hitherto unrecognized cyclic nucleotide phosphodiesterase (PDE) activity, catalyzing the hydrolysis of 3′,5′-cyclic nucleotides with a preferential affinity for cAMP over cGMP as substrate (Km values of 0.9 ± 0.03 μM and 2.3 ± 0.11 μM, respectively). It also has an exopolyphosphatase activity that shows higher affinity for short-chain over long-chain inorganic polyphosphates (Poly-P) [22].

To date, numerous studies highlighting the association between a deregulated Prune-1 activity and tumour progression have been described in patients with metastatic BC [23], gastric and oesophageal cancer [24], Non Small Cell Lung Cancer (NSCLC) [25], metastatic colorectal cancer [26], Neuroblastoma [27] and highly metastatic Medulloblastoma Group 3 [28].

On the other hand, Prune-1 biallelic homozygous mutations were recently found in several individuals in extended families with tubulinopathies: Microcephaly (MIM#251200) and PEHO-syndrome (MIM#260565) [29], [30], [31], [32], [33]. The "gain of function" mutations identified in Prune-1 (*e.g.,* pD30N and pR297W) enhanced its enzymatic exopolyphosphatase (PPase/PPX) activity, through augmenting the catalytic ability of Prune-1 to hydrolyze tetrapolyphosphates (P4) in inorganic polyphosphates (*i.e.* PPi and Pi). Prune-1 protein was also found to colocalize with Microtubules (MT) to mitotic-spindle via binding to β-Tubulin. Our genotype/phenotype correlation studies demonstrate that Prune-1 mutants (*e.g.,* pD30N and pR297W) caused a delay in MT-polymerization *in-vitro*, mostly affecting the "nucleation" phase, thus resulting in impaired cell proliferation and migration processes in neuronal system [29].

Prune-1 is an unfolded multi-domain adaptor protein that can interact with several intracellular binding partners and modulate different signaling cascades, such as Wnt and TGF-β canonical pathways. This pathways activation is primarily due to the physical interactions of Prune-1 with Glycogen Synthase Kinase 3β (GSK-3β) and NDPK-A (also known as NM23-H1 or NME1) [25, 34, 35].

Regarding the interaction between Prune-1 and GSK-3β proteins [25], [36], the silencing of Prune-1 or inhibition of GSK-3β reduced cell motility in colorectal tumours by impairing the focal adhesions [36]. These data suggested that Prune-1 and GSK-β cooperatively act to regulate the disassembly of focal adhesions to promote cell migration in colorectal tumours.

Of importance, the ability of Prune-1 to induce activation of canonical Wnt/β-catenin signaling was also reported in NSCLC. Prune-1-driven Wnt signaling activation occurred by promoting sequestration of GSK-3β inside MVBs, which are essential components of the WNT signal-transduction pathway,. Interestingly, Prune-1 was shown to activate canonical Wnt signaling also in a paracrine manner, through Wnt3a increased secretion, thus suggesting a role for Prune-1 in intercellular communication in extracellular environment [25].

Recently, we identified a role for Prune-1 in metastatic behaviour of pediatric Medulloblastoma Group 3 [28]. In detail, we demonstrated both *in vitro* and *in vivo* that Prune-1 enhances the canonical TGF-β signaling pathway (mediated by SMAD2/3) through the binding to NDPK-A, that is already known to inhibit TGF-β activation cascade. Furthermore, we proposed a novel "metastatic axis" for Prune-1 through up-regulation of OTX2 and inhibition of tumour suppressor PTEN. In our model, Prune-1 (through its binding to NDPK-A) initiates a cascade of events that culminate in the promotion of EMT throught SNAIL-1 and N-Cadherin up-regulation and E-Cadherin down-regulation [28] (Figure 2). This data also confirm the Prune-1-induced EMT that had been previously found in liver metastases generated from colorectal tumours [26].

Altogether, these data highlight the pro-metastatic role of Prune-1 in several solid tumours, through the activation of different signaling cascade (*i.e.,* TGF-β, Wnt) and the induction of EMT process.

Prune-1/NDPK-A interaction has been found conserved in different species, with a potential role in the regulation of some important mechanisms during embryonic development. In fact, both proteins PRUNE-M1 and NM23-M1 (murine homologues of human Prune-1 and NDPK-A, respectively) showed the same spatio-temporal expression pattern in several areas of the developing nervous system (from E10.5 to adulthood), thus suggesting their fundamental function during cell proliferation, migration and differentiation processes during brain and cerebellum development [37]. Of note an additional role of the complex was observed in Müller gliogenesis during Xenopus retinal development [38], thus indicating an important role for Prune-1 and NDPK-A during the development of the retina and eye morphogenesis. Later, the ability of Prune-1 to bind NDPK-A was finally confirmed in human TNBC cells (*i.e.,* MDA-MB-435) via co-immunoprecipitation assays [39].

In mammalian cells, alterations of the equilibrium within Prune-1/NDPK-A interaction complex have been described to be responsible for the switch to pathological conditions (*i.e.,* cancer), by affecting specific related protein networks [40]. Furthermore, the role of the protein-protein interaction (PPI) between Prune-1 and NDPK-A in modulating cell motility, also in BC cellular models, was reported, thus showing this protein complex as a novel intracellular target for metastatic tumour treatment.

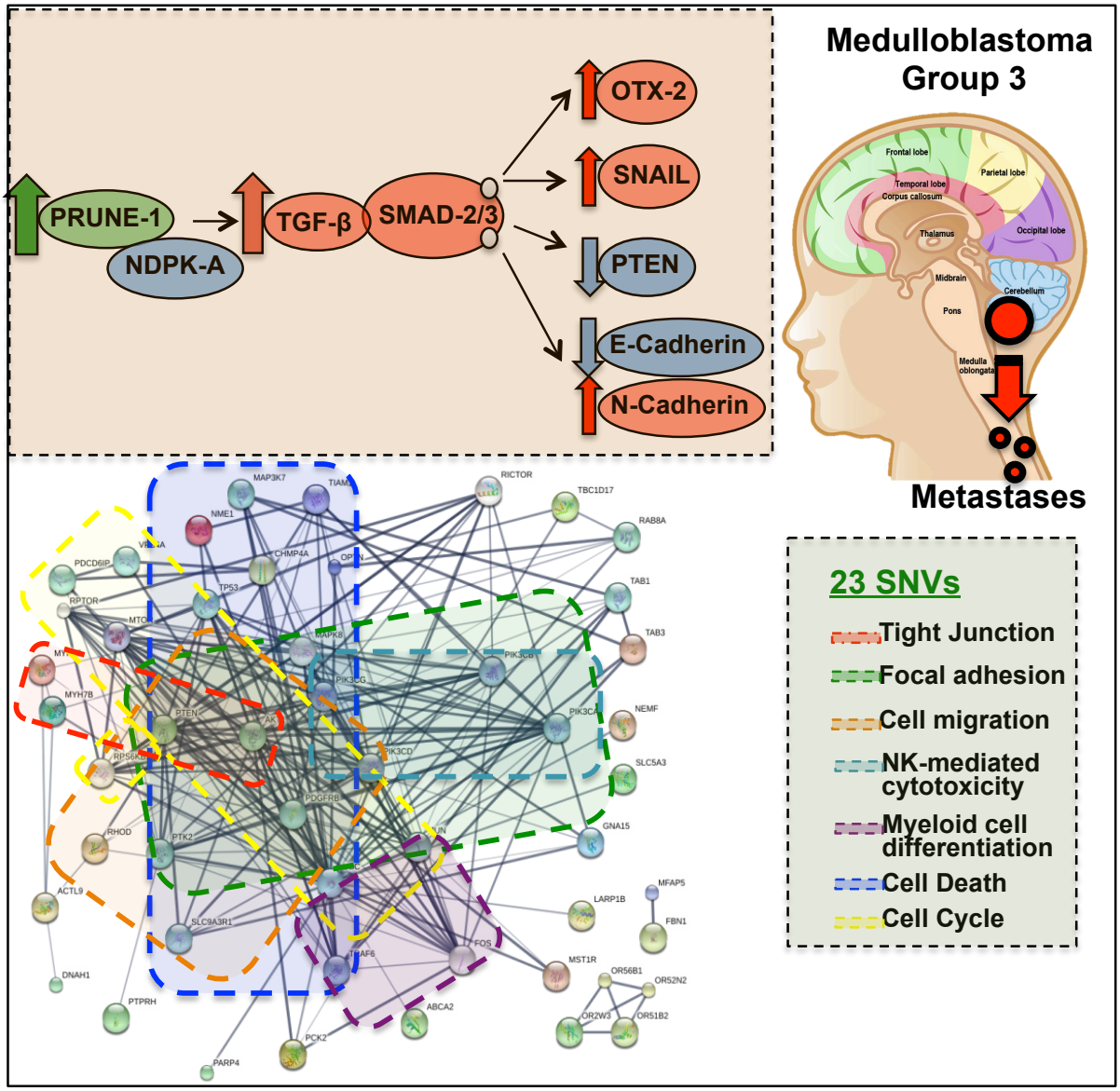

Figure 2: Prune-1 drives metastatic Medulloblastoma progression through a "metastatic axis". The organge box summarizes the proposed mechanism by which Prune-1 enhances canonical TGF-β signalling activation through binding to NDPK-A, which thus enhances OTX2 up-regulation and PTEN inhibition in metastatic Medulloblastoma Group 3, as dissected out *in vitro* from different cell models and *in vivo* using orthotopic xenograft of Medulloblastoma Group 3. The 'Pro-metastatic' protein network generated via Search Tool for Retrieval of Interacting Genes/Proteins (STRING) database using deleterious homozygous non-synonymous variants (NSVs) common to primary cells derived from metastatic Medulloblastoma Group3-4 patients is shown at the bottom of the panel. This network allowed us to select 23 potential deleterious mutations (as shown within the green box) that, together with the Prune-1-driven axis, take part in the networks characterised by proteins involved in tight junctions (red dashed box), focal adhesions (green dashed box), regulation of cell migration (orange dashed box), regulation of cell death (blue dashed box), regulation of cell cycle (yellow dashed box), natural-killer-cell-mediated cytotoxicity (light blue dashed box), and positive regulation of myeloid leukocyte differentiation (purple dashed box). Together with the newly identified Prune-1-driven axis, these variants take part in this pro-metastatic interactions network. From Ferrucci V *et al.*, Brain. 2018. *In press*

Metastatic Breast Cancer influenced by Prune-1

In metastatic BC, the amplification of 1q21-q22 chromosomal region occurred more frequently than in primary lesions and is associated with short OS and chemotherapy resistance [41]. Prune-1 gene is located on 1q21.3 amplified chromosomal region and its amplification has been analysed in advanced BCs. Interestingly, the primary cases of advanced BCs showing moderate amplification and high of Prune-1 expression levels, were classified as moderate or high-grade tumours. Of interest, the overexpression of Prune-1 was found in those tumours that were also characterized by higher NDPK-A expression levels. These results suggested that for some tumours showing high NDPK-A expression levels, the increase Prune-1 levels might interfere with the metastatis suppressor action of NDPK-A, thus promoting progression and metastatic dissemination [42].

Later, the distribution of Prune-1 was examinated in a larger and better-characterized tissue cohorts of invasive BCs. These analyses revealed that the over-expression of Prune-1, as observed in the majority (54%) of the BC tumours tested, was significantly correlated with the presence of advanced nodal status (N2–N3 cases; p=0.017) and distant metastases (p=0.029). These data strongly suggest the potential application of Prune-1 as a marker for the identification of subsets of aggressive metastatic BC patients [23].

Interestingly, high tissue levels of NDPK-A were shown in patients with BC and a significant positive association whit poor OS and EFS was also reported. Further, a positive correlation between extracellular NDPK-A secreted from TNBC cells (*i.e.* MDA-MB-231) and tumour size was found to be consistent with its potential role in metastatic progression of BC [43]. However, NDPK-A has also been reported to reduce cell motility when overexpressed in BC cells by influencing the cell anchorage-independent colonization [44]. Importantly, this “anti-motility” activitiy of NDPK-A was reverted Prune-1 in BC cells through its PDE activity [45], thus indicating a role of the protein complex in enhancing cell motility in BC.

The biochemical significance of NDPK-A/Prune-1 interaction complex in BC was further investigated. In fact, the PDE activity of Prune-1 (as measured by cAMP-PDE activity *in vitro*) was found enhanced (2-fold) after the interaction with NDPK-A. This direct correlation between the increased Prune-1 cAMP-PDE activity (due to the interaction with NDPK-A) and the induction of cell motility was also validated in BC cells *in vitro* [45].

All these studies suggest the Prune-1/NDPK-A protein complex with a role in promoting cell motility of BC cells. The formation of this complex has been hypothesized to impair the level of free NDPK-A functioning as an anti-metastatic protein.

The first attempt to reduce this complex formation in BC was made through the inhibition of NDPK-A phosphorilation mediated by Casein Kinase I (that is necessary in the binding to Prune-1) by using

IC261 molecule (an ATP-competitive inhibitor selective for CKIδ and CKIε) in BC cell lines. These results suggest that the IC261 (through impairment of NDPK-A phosphorilation) impaired the formation of the NDPK-A/Prune-1 complex, decreased the PDE Prune-1 enzymatic activity and reduced cell migration in BC cellular model [39]. These data further confirmed the involvement of Prune-1/NDPK-A protein complex in the migration properties of BC cells.

Later, the regions of interaction between Prune-1 and NDPK-A were also mapped in human BC cell lines and the amino acid residues on the surface regions of Prune-1 that are involved into the interaction with NDPK-A were identified [27], [46].

These findings allow a cell Competitive Permeable Peptide (CPP), mimiking the minimal region of interaction of NDPK-A (amino acids 115-128, including three Serine residues [120, 122 and 125] that are phosphorilated by Casein Kinase I) to be developed [27], [39], [47]. This mimetic peptide (CPP) represents a promising route to impair the NDPK-A/Prune-1 interaction complex with a pharmaceutical aim for cancer treatment especially for those tumours driven by alteration Prune-1/NDPK-A protein complex, including BC. In fact, this specific peptide (CPP) was found with the ability to reduce the cell motility in Prune-1-overexpressing BC cells in a dose-dependent manner by specifically impairing the phosphorylation of NDPK-A and consequently its interaction with Prune-1, so acting in a similar manner to IC261 inhibitor [39].

Then, the therapeutic properties of CPP were further addressed *in vitro* using several BC cell lines [48]. This study reported that CPP reduced the proliferation of BC cells, including TNBC cells (*i.e.* MCF7 and MDA-MB-231), through inhibition of Prune-1/NDPK-A complex [48].

These results show the potential therapeutic application of CPP in the treatment of metastatic TNBC. Future studies will be necessary to address its efficacy to inhibit metastatic dissemination also in vivo in those aggressive TNBC that are driven by amplification and/or over-expression of both Prune-1 and NDPK-A.

1.3 TGF-β signaling in TNBC

TGF-β pathway has been established as essential for cancer progression, because of its prominent role in the regulation of cell growth, differentiation and migration. TGF-β instigates cellular phenotypical changes that mediate its role as both a tumour suppressor and a tumour promoter. Indeed during the early stages of tumorigenesis, TGF-β functions as a tumour suppressor. However, as tumours progress, tumour cells may lose their growth-inhibitory response to TGF-β and may instead respond by initiating epithelial-to-mesenchymal transition and by increasing cell migration.

TGF-β signaling cascade

TGF-β1, TGF-β2 and TGF-β3 ligands function as the primary mediators of TGF-β signaling, and are secreted as inactive homodimeric polypeptides that can bind to latent TGF-β-binding proteins, which promote extra cellular sequestration. On activation, the ligands bind to the type 2 TGF-β receptor (TGFBR2), which causes recruitment and phosphorylation of TGFBR1 (also known as ALK5), resulting in downstream signaling activation. The final heterotetrameric form of the active receptors initiates downstream signaling through either SMAD-mediated canonical signaling or SMAD-independent non-canonical signaling. The canonical signaling pathway involves phosphorylation of the carboxy-terminal serine residue of the internal modulator SMAD proteins, SMAD2 or SMAD3, by the activated receptors. This phosphorylation induces oligomerization of SMAD2 or SMAD3 with SMAD4, which is necessary for nuclear translocation. Through interactions with a variety of transcription cofactors, the nuclear-localized SMAD complex initiates transcriptional activation or transcriptional repression of several genes. The non-canonical branch of the signaling pathway involves activation of the PI3K–AKT and Mitogen-Activated Protein Kinase (MAPK) pathways, among others, by the activated heterotetrameric receptors (Figure 3) [49].

A majority of the cytostatic response to TGF-β stimulation can be attributed to the activation of canonical SMAD activation that depends on the expression of other transcription factors and intracellular signaling proteins. An important determinant of SMAD2 and SMAD3 activation is the status of SMAD7 expression. SMAD7 is considered to be an inhibitory SMAD in the context of canonical TGF-β signaling. SMAD7 can block activation of SMAD2 and SMAD3 via competitive inhibition. SMAD7 also has the ability to promote de-phosphorylation of the activated receptor complex [50].

The outcome of these signaling pathways in epithelial cells is either suppression of cell proliferation or induction of cellular migration and invasion. Studies investigating the cytostatic phenotype induced by TGF-β have established numerous pathways through which this is achieved, including repression of MYC and cyclin-dependent kinase 4 (CDK4; [51]). Furthermore, the SMAD-dependent activation of the pro-apoptotic protein BCL-2-Interacting Mediator of Cell Death (BIM) triggers programmed cell death [52].

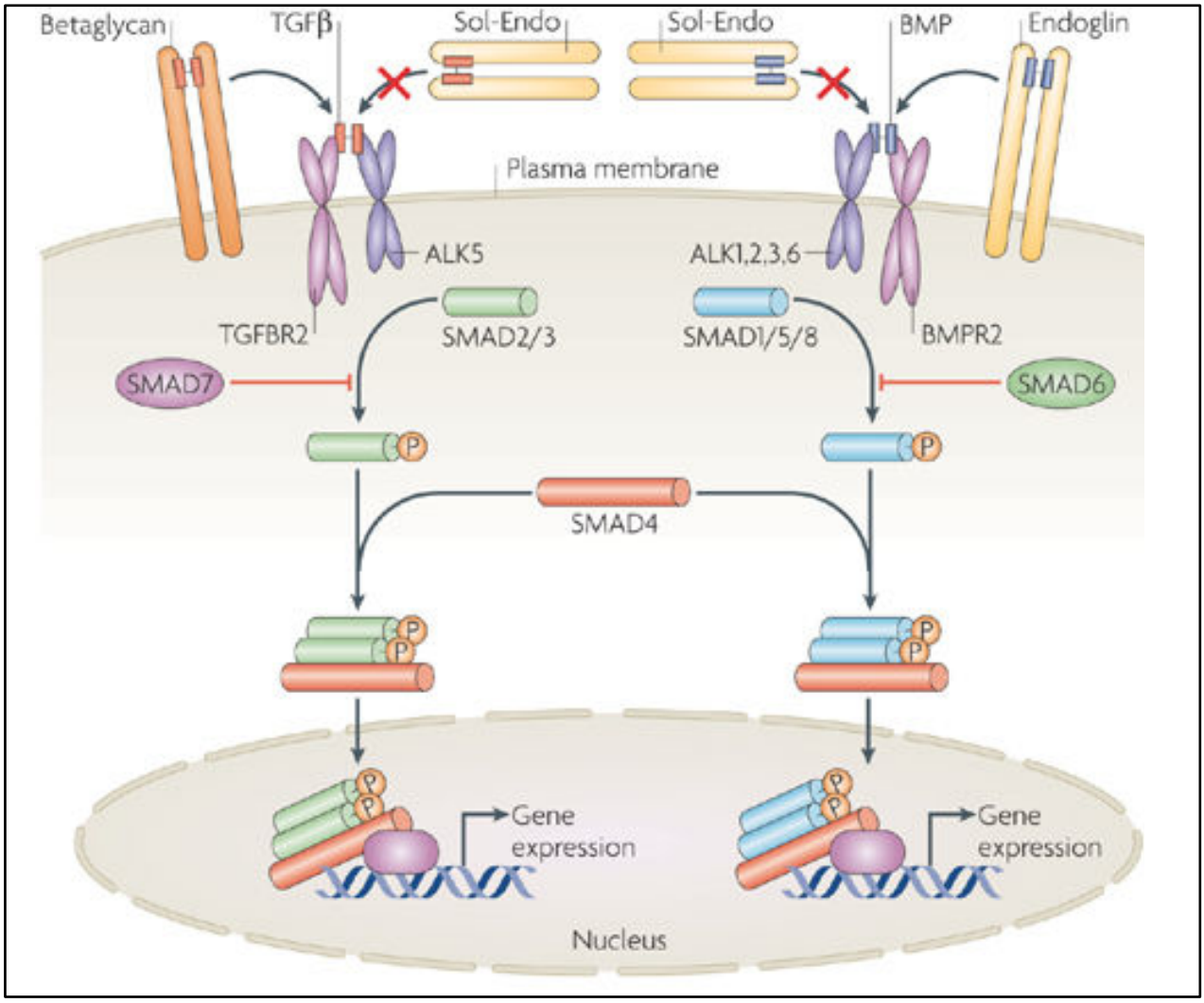

Figure 3: Signal transduction by TGF-β family members. Canonical signaling by TGF-β superfamily members can be divided into two main intracellular pathways according to the SMAD mediators: either SMAD2/3 or SMAD1/5/8. Members of the TGF-β family bind to specific Ser/ Thr kinase type II and type I receptors; in most cells, TGF-β signals via TGFBR2 and ALK5 (TGFBR1), and bone morphogenetic proteins (BMPs) signal via the BMP type II receptor (BMPR2) and ALK1, -2, -3 and -6. The accessory receptors betaglycan and endoglin can modulate signalling via the type II and type I receptors. Betaglycan enhances TGF-β2 binding to TGF-β receptors, whereas endoglin may perform a similar function for selected TGFβ family members and their receptors. Activated type I receptors induce the phosphorylation of specific receptor regulated (R-) SMADs, which are the intracellular effectors of TGFβ family members. In most cell types, TGF-β induces SMAD2/3 phosphorylation and BMPs induce SMAD1/5/8 phosphorylation. Activated R-SMADs form heteromeric complexes with SMAD4 that accumulate in the nucleus, where they regulate the expression of target genes in cooperation with transcription factors, co-activators and co-repressors. Inhibitory SMADs, such as SMAD6 and SMAD7, can antagonize TGF-β signalling by inhibiting the activation of R-SMADs.From ten Dijke *et al*., Nature Reviews Molecular Cell Biology. (2007).8, 857–869

Expression of constitutively active TGF-β1 by mammary epithelium resulted in a decreased incidence of tumorigenesis induced by infection with the Mouse Mammary Tumour Virus (MMTV) [53]. In contrast it was shown in several mouse models that specific expression of an activated TGF-β ligand or expression of a constitutively active TGFBRI in mammary epithelial cells could enhance breast cancer associated lung metastases *in vivo* [54]. Together, the results suggested that TGF-β could suppress primary tumour growth while promoting metastases (through EMT) of the responding carcinoma cells. Indeed a gene signature derived from BC cells that had been stimulated with TGF-β correlated with a poor prognosis in human (ER^-)-BC [55].

A central paradox of TGF-β is that it is a potent suppressor of proliferation in normal epithelial cells, notably breast, but it converts to a promoter during cancer development. Normal mammary epithelial cells are very sensitive to proliferative inhibition by TGF-β. Early stage breast tumours and transformed (non-tumorigenic) BC cell lines are also growth inhibited. With the acquisition of more advanced malignant characteristics, however, most BC cells show profound TGF-β resistance. In turn, the escape from TGF-β allows the tumours and stromal cells to produce more TGF-β to indirectly augment tumour growth by modulating angiogenesis, immune response and ECM production. Understanding TGF-β biology during this transition from normal to malignant in the breast is crucial to determining whether this period may offer a window for chemoprevention using TGF-β inhibitors in those high-risk patients who can benefit. Notably, treatment of mouse models of TNBC with TGF-β neutralizing antibodies or receptor kinase inhibitors strongly inhibits development of lung and bone metastases [56], [57].

Studies elucidating the tumour suppressor role of TGF-β corroborated evidence that the loss of TGF-β-signaling components was associated with carcinoma progression. The signaling pathway downstream of EMT induction by TGF-β has also been also mapped. In this regard, Inhibitor Of DNA Binding 1 (ID1; a transcriptional regulator) is inhibited by TGF-β. This results in decreased expression of E-Cadherin and Zona Occludens 1 (ZO1) which are two factors known to help maintain an epithelial phenotype. TGF-β signaling also induces the expression of EMT-associated transcription factors, such as Snail family zinc finger -1 and II (SNAI-1 and -2), Zinc Finger E-Box Binding Homeobox -1 and II (ZEB-1 and -2), and Lymphoid Enhancer-Binding Factor 1 (LEF1), which help to promote the loss of cellular adhesions and cytoskeletal rearrangement [58].

As tumours progress, the growth-inhibitory effects of TGF-β are overcome by the loss of TGF-β pathway elements or of downstream signaling targets. Loss of TGF-β responsiveness in tumour cells has substantial effects on tumour progression, not only through altered epithelial cell characteristics but also through gene expression changes that affect the tumour microenvironment. So TGF-β signaling as an important mediator not only of changes to the epithelial phenotype but also of changes

in the stromal environment that are essential for tumour progression. The functional role of TGF-β signaling in modulating the tumour microenvironment has also been addressed.

Targeting TGF-β in metastatic TNBC

The elevated TGF-β signature score in human BC cell lines with Basal-like gene expression compared to those with Luminal gene expression, is suggestive of an association with the Basal-like subtype of BC. Further, *in vitro* studies previously showed that TGF-β1 expression promoted the invasion and migration of MDA-MB-231 cells (as TNBC cellular model), via overexpression of SMAD2 protein, thus suggesting TGF-β canonical pathway with a crucial role in metastatic TNBC [59]. Importantly, high levels of TGF-β1 expression were significantly associated with tumour histological grade and lymph node metastases ($P<0.05$) in TNBC [59].

Recent data suggest that the TGF-β family of cytokines plays a role in BC stem cells (also known as Cancer Stem Cells [CSCs] or Tumour Initiating Cells) mainteinance that are known to be also responsible for the tumour recurrence after chemoterapy in metastatic TNBC patients. Importantly, chemotherapy-treated BC tissues were found with increased markers of TGF-β signaling by analyzing RNA from 17 matched breast tumour biopsies before and after neoadjuvant chemotherapy. Further, also CSCs-related genes (*i.e.,* CD44 and Aldehyde Dehydrogenase 1 Family Member A1 [ALDH1A1]) were found increased in samples after chemotherapy [60].

Studies *in vitro* showed that Paclitaxel, one of the most commonly used chemotherapies in patients with TNBC, enriched a CSCs population with increased TGF-β signaling in TNBC cell line (*i.e.,* MDA-MB-231) by inducing the expression of IL-8 in a SMAD4-dependent manner. Of importance, the pharmacological inhibition of TGF-β both *in vitro* and *in vivo* reduces those Paclitaxel-resistant CSCs, thus confirming the role of TGF-β in chemoresistant CSCs in TNBC [60].

Altogether, these data suggest the use of TGF-β inhibitors in combination with chemotherapy to target those drug-resistant CSCs in TNBC.

1.4 Tumour Microenvironment

A plethora of intrinsic and extrinsic factors, including communication between tumorigenic cells and infiltrating immune cells, fibroblasts, epithelial cells, vascular and lymphatic endothelial cells, cytokines and chemokines, constitute the tumour microenvironment. Although cancer cells can be immunogenic, tumour progression is associated with the evasion of immune surveillance, the promotion of tumour tolerance, and even the production of pro-tumorigenic factors by tumorinfiltrating immune cells [61].

The tumour microenvironment is a bidirectional, dynamic, and intricate network of interactions between the cells of the stromal tissue and the cancer cells. An important role in tumour development and malignant progression is played by the tumor-infiltrating immune inflammatory cells. Once recruited into the tumour microenvironment, these cells can contribute to the malignant progression of the cancer-cell phenotype. Moreover, they establish a complex network of interplay that contributes to the promotion and maintenance of an immunosuppressive microenvironment, which itself promotes immune escape, and as a consequence, enhances tumour progression [62].

There is a growing body of evidence that indicates that the immune system has both positive and negative effects on tumour development and progression. The immune system can identify cancerous cells on the basis of their expression of tumour-specific antigens or molecules induced by cellular stress, and eliminate them before they can cause harm. This latter process is referred to as tumour immune surveillance. Despite tumour immune surveillance, tumours do develop in the presence of a functioning immune system [62].

Therefore, a more complete explanation for the role of the immune system in tumour development has been formulated, thus leading to the concept of "cancer immunoediting." According to this theory, the immune system not only protects the host against tumour development but can also sculpt the immunogenic phenotype of a developing tumour, resulting in promoting or selecting tumour variants with reduced immunogenicity that are better suited to survive in an immunologically intact environment. Thereby, this process provides developing tumours with a mechanism to "escape" immunologic detection and elimination.

The tumour immunoediting is divided into three phases, called elimination, equilibrium, and escape. In the elimination phase of cancer immunoediting, corresponding to tumour immune surveillance, the immune system detects and eliminates tumour cells that have developed as a result of failed intrinsic tumour suppressor mechanisms [62]. The elimination phase can be complete, when all tumour cells are cleared, or incomplete, when only a portion of tumour cells are eliminated. In case of partial tumour elimination, the host immune system and any tumour cell variant that has survived the elimination process enter into a dynamic equilibrium. In the equilibrium phase, the immune system exerts a potent selection pressure on the tumour cells that is enough to contain, but not fully extinguish, a tumour containing many genetically unstable and rapidly mutating tumour cells. During this period of selection, many of the original escape variants of the tumour cell are destroyed, but new variants arise, carrying different mutations that provide them with increased resistance to immune attack [62].

In conclusion, the failure of immune system to completely eliminate the tumour results in the selection of tumour cell variants that are able to resist, avoid, or suppress the anti-tumour immune response, leading to the escape phase.

Another tumour immune escape mechanism arises from the ability of the progressing tumour to interfere with the host immune system. To this end, the tumour induces and/or recruits immunosuppressive cells which normally serve as safeguards against overwhelming inflammation or autoimmunity. By turning the host immune system against itself, tumours can gain an impressive arsenal of weapons to hamper the induction and progression of anti-tumour immune activity [62].

Within the tumour microenvironment, the tumour-promoting inflammatory cells include Tumour-Associated Macrophages (TAMs), neutrophils and lymphocytes. These cells can secrete several signaling molecules that serve as effectors of their tumour-promoting actions. These include Epidermal Growth Factor (EGF), the angiogenic growth factor Vascular Endothelial Growth Factor (VEGF), other proangiogenic factors, such as Fibroblast Growth Factor 2 (FGF2), and several chemokines and cytokines that amplify the inflammatory state.

In addition, these infiltrating immune cells can produce proangiogenic and/or proinvasive matrix degrading enzymes, including Matrix Metalloproteinase 9 (MMP-9). As a consequence, these cells induce and support tumour angiogenesis, facilitate tissue invasion, and sustain metastatic dissemination. Furthermore, within the tumour mass, a variety of partially differentiated myeloid progenitors have been identified. The myeloid-derived suppressor cells (MDSCs), are characterized by the expression of the macrophage marker CD11b and the neutrophil marker Gr1, and they show significant immunosuppressive activity [62]. The main cellular constituents of the tumour microenvironment are depicted in the Figure 4.

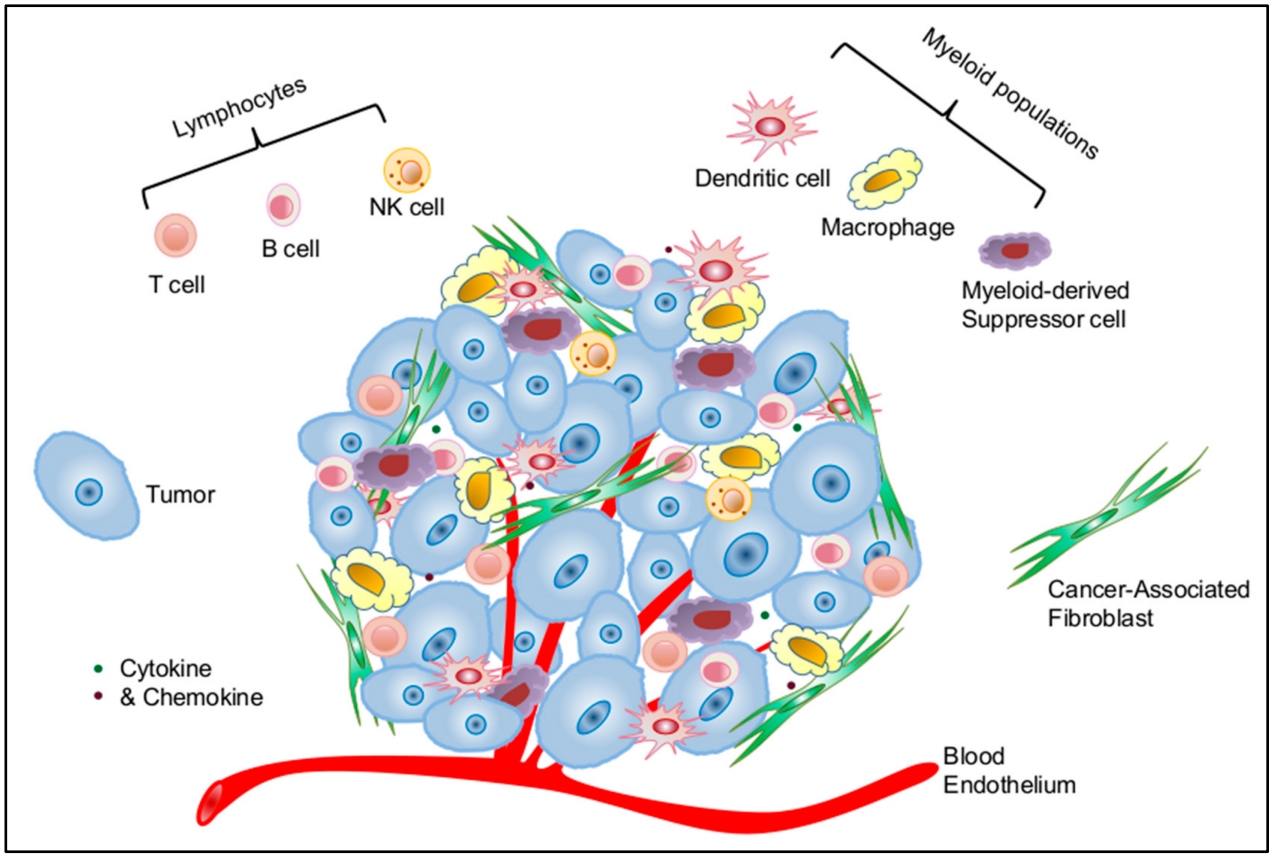

Figure 4: Cellular constituents of the tumor microenvironment that shape tumour immunological landscape. The tumour microenvironment consists of complex cellular and molecular and constituents. The cellular constituents consist of immune cells of hematopoietic origin and stromal cells of non-hematopoietic origin. The immune cell compartment comprises tumor-infiltrating lymphocytes (TILs) of T, B, and natural killer (NK) cells and tumour-associated myeloid populations of dendritic cells (DCs), macrophages (TAMs), and myeloid-derived suppressor cells (MDSCs). The stromal compartment consists of cancer-associated fibroblasts (CAFs) and endothelial cells of the lymphatic and blood vasculature. From Cui *et al*., Int. J. Mol. Sci. (2016),17(11):1942.

Tumour-Associated Macrophages

Macrophages originate from blood monocytes that can differentiate rapidly into distinct, mature macrophages, which have specific immunological functions. Tumour-Associated Macrophages (TAMs) are mature macrophages which originate from blood monocytes that are recruited at a tumour site by molecules that are produced by neoplastic and stromal cells. Within the tumour mass, the monocytes are surrounded by several signals that can induce their differentiation towards mature M2-polarized macrophages. The M2 polarization factors are IL-4, IL-6, IL-10, IL-13, M-CSF, glucocorticoids, TGF-β, and prostaglandin E2 (PGE2), and these can be produced within the tumour mass by neoplastic cells and fibroblasts (*e.g.,* IL-10, TGF-β), and by Th2 lymphocytes (*e.g.,* IL-4, IL-13) (Figure 5) [63].

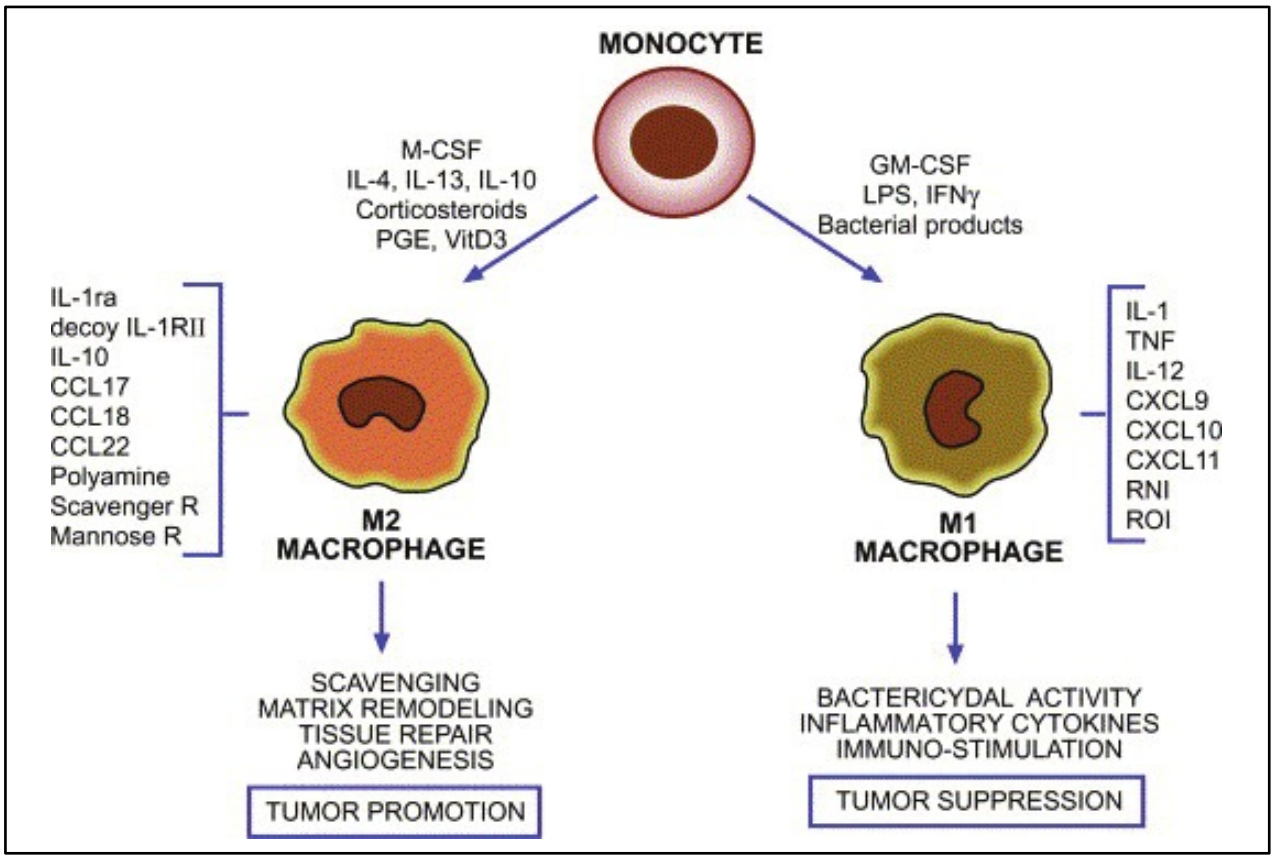

Figure 5: Macrophages polarization. The differentiation pathways of classically-activated M1 macrophages and alternatively-activated M2 macrophages are shown. From Quatromoni *et al*., Am J Transl Res. (2012); 4(4): 376–389.

M2 polarized TAMs stimulate the angiogenesis by secreting the growth factors VEGF, PDGF (Platelet-derived growth factor), TGF-β, and members of the FGF family, and angiogenesis-modulating enzymes (*e.g.,* MMP-2, MMP-7, MMP-9, MMP-12, and cyclooxygenase-2 [COX-2]), and several chemokines including CXCL12, CCL2, CXCL8, CXCL1, CXCL13, and CCL5 [61], [64].

Within the primary tumour microenvironment, at least two mechanisms have been proposed by which TAMs facilitate tumour metastasis. The first relates to the secretion of proteases within the tumour microenvironment, such as urokinase Plasminogen Activator (uPA), Cathepsins -B and -D, MMP-2, and MMP-9, which can digest the tumour basement membrane, thus facilitating tumor-cell escape. Finally, within the tumour microenvironment, TAMs have strong immunosuppressive activity, not only through their production of IL-10, but also by their secretion of chemokines (*e.g.,* CCL17 and CCL22), which preferentially attract regulatory T cells (Tregs) and Th2 lymphocytes (Figure 6) [64].

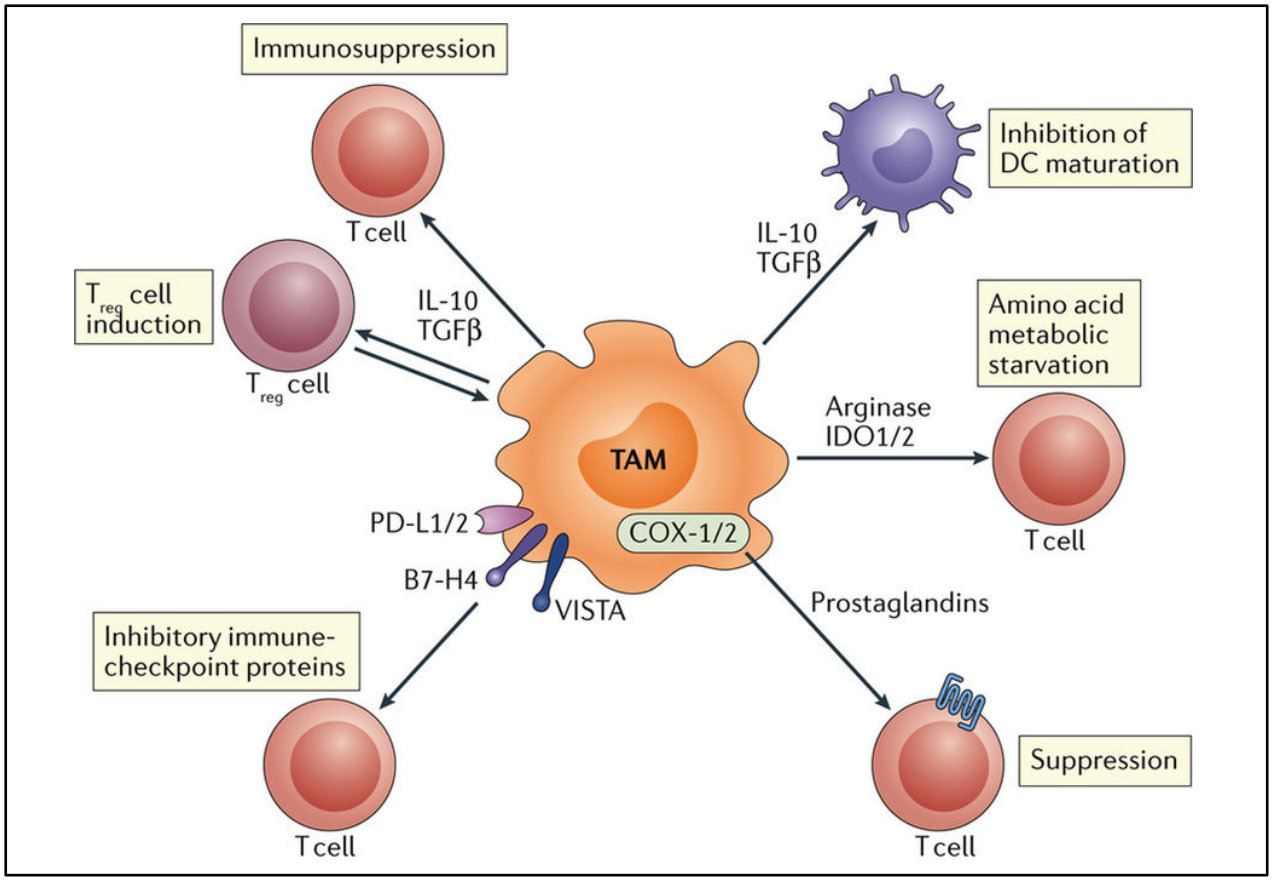

Figure 6: Mechanisms of tumour-associated macrophage (TAM)-mediated immune suppression. TAMs promote the immunosuppressive activity of regulatory T cells (Treg) via bidirectional interactions, which are mediated by immunosuppressive cytokines, including IL-10 and TGF-β. The same TAM-produced mediators inhibit Dendritic Cell (DC) maturation. The profile of amino acid metabolism in TAMs results in metabolic starvation of T cells via the activity of arginase and/or via production of immunosuppressive metabolites by the Indoleamine-Pyrrole 2,3-Dioxygenase 1/2 (IDO1/2) pathway. Prostaglandins produced by COX-1 and COX-2 expressed in TAMs have immunosuppressive effects, particularly on T cells. TAMs can also express Programmed death-ligand -1 and -2 (PD-L1 and PD-L2), which trigger the inhibitory PD1-mediated immune checkpoint in T cells, as well as B7 Family Member (H4B7-H4), and V-domain Ig Suppressor of T Cell Activation (VISTA), which might have similar functions. Together, these immunosuppressive activities of TAMs dampen adaptive antitumour immune responses. From Mantovani *et al*., Nature Reviews Clinical Oncology. (2017). 14, 399–416.

Myeloid-Derived Suppressor Cells

An additional class of immune cells within the tumour microenvironment is the Myeloid-Derived Suppressor Cells (MDSCs). These cells comprise a phenotypically heterogeneous population of immature myeloid cells at different stages of differentiation. They derive from bone marrow progenitors that have not completed their maturation into granulocytes, monocytes, or dendritic cells (DCs). In mice, these cells express the membrane Granulocyte-Differentiation Antigen-1 (Gr1) and Integrin Subunit Alpha M (or CD11b) [62].

Pro-inflammatory cytokines (*e.g.,* IL-1β, IL-6) and bioactive lipids (*e.g.,* PGE2) can induce MDSCs in primary tumour. The Calcium-Binding Protein S100A8 and S100A9 are pro-inflammatory proteins released by neutrophils highly expressed at tumour sites that also recruit and induce MDSCs. Furthermore, MDSCs produce and secrete these proteins, which can lead to an autocrine loop of engagement. Within the tumour microenvironment, the main factors responsible for expansion of MDSCs are VEGF and MMP-9, which play a role also in the maintenance of MDSCs. The recruitment of MDSCs to tumour sites is also driven by chemoattractant molecules, such as CCL2/CCR2, Stromal-Cell-Derived Factor 1 (SDF1)/CXCR4, CXCL5/CXCR2, and uPA [62], [65].

The major function of MDSCs is to promote an immunosuppressive and anti-inflammatory phenotype, which results in tumour immune escape. The suppressive function of MDSCs is turned on by several factors, including IL-4, IL-13, IFN-γ, IL-1β, and TGF-β. Activated MDSCs suppress the anti-tumour immune response in the tumour microenvironment directly through the expression of inducible Nitric Oxide Synthase (iNOS) and Arginase 1 (ARG1). MDSCs that express ARG1 deplete L-arginine from the microenvironment, and thus limit its availability to T cells. Consequently, T cells are deficient in the CD3ζ chain of the T-cell receptor (TCR), and they are arrested in the G0–G1 phase of the cell cycle. This results in inhibition of both their function and their proliferation. The high expression of iNOS in MDSCs increases the production of nitric oxide (NO) and reactive oxygen species (ROS). ROS inhibit MDSC maturation, induce DNA damage in immune cells in the tumour microenvironment, inhibit the differentiation of MDSCs into functional DCs, and recruit MDSCs to tumour sites. Moreover, extracellular ROS catalyze the nitration of TCR, which consequently inhibits the T cell-peptide-MHC interaction, which results in T-cell suppression. MDSCs also impair T-cell activation by abrogation of the expression of L-selectin on both CD4+ and CD8+ T cells, which thus suppresses the homing of these cells to tumour sites. Another mechanism by which MDSCs interfere with T-cell activation is their ability to expand the Tregs population that also inhibits the anti-tumour immune response in the tumour microenvironment (Figure 7) [65].

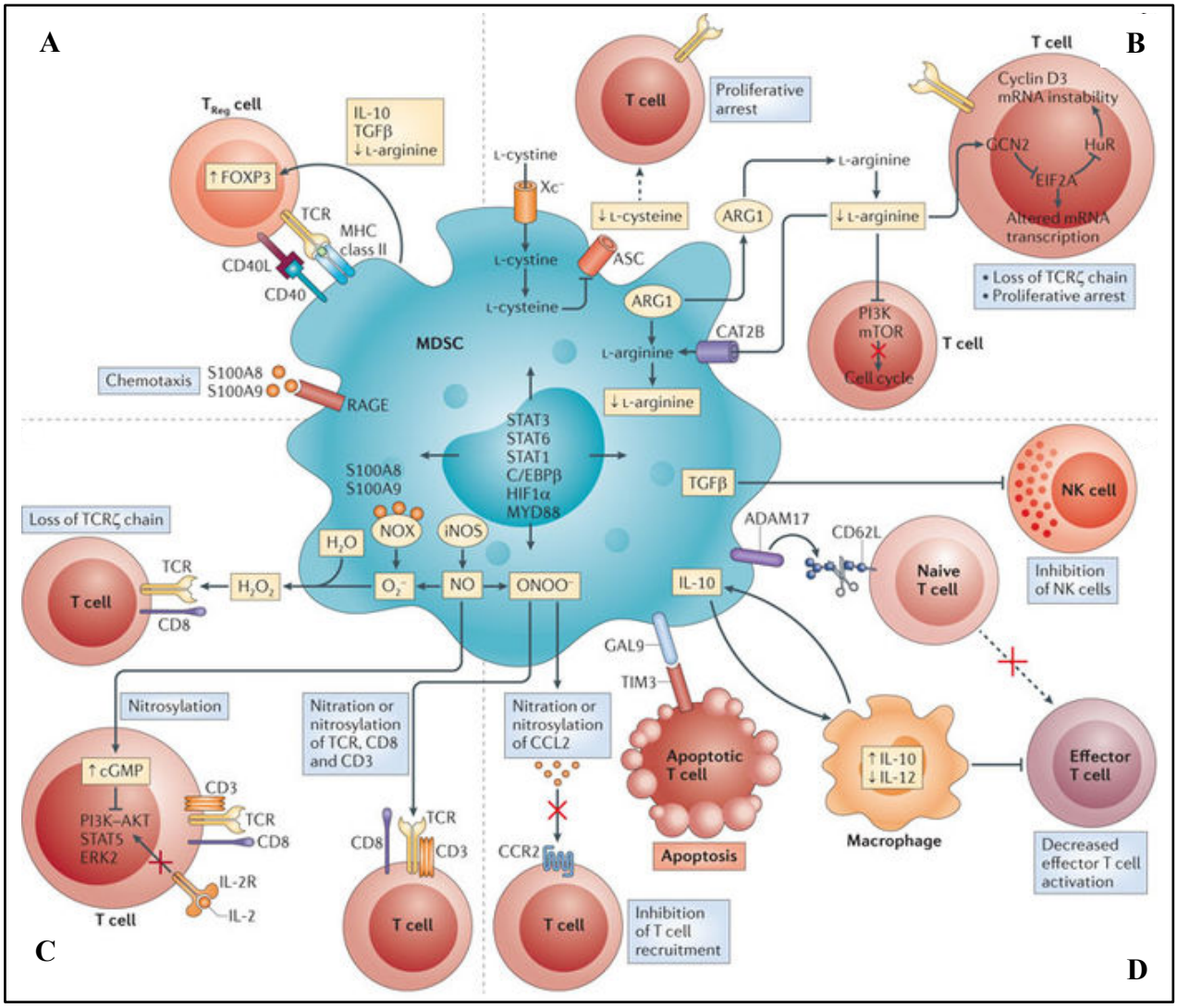

Figure 7: Coordinated regulation of myeloid cells by tumour cells. Myeloid-derived suppressor cells (MDSCs) can inhibit efficient antitumour T cell responses through a number of mechanisms. **(A)** MDSCs induce and expand regulatory T (T_{Reg}) cells. S100A8 and S100A9 are part of the NADPH oxidase (NOX) complex responsible for the increased production of reactive oxygen species (ROS) by MDSCs. **(B)** MDSCs deprive T cells of amino acids essential for their growth and differentiation. **(C)** MDSCs release oxidizing molecules, such as hydrogen peroxide (H_2O_2) and peroxynitrite ($ONOO^-$). Peroxynitrite causes nitration and nitrosylation of components of the T cell receptor (TCR) signalling complex, and H_2O_2 causes the loss of the TCR ζ-chain, thereby inhibiting T cell activation through the TCR. **(D)** MDSCs interfere with T cell migration and viability. The metalloproteinase ADAM17 (Disintegrin And Metalloproteinase Domain-containing Protein 17) cleaves CD62L, which is necessary for T cell migration to draining lymph nodes, and Galectin 9 (GAL9) can engage T Cell Immunoglobulin And Mucin Domain-containing Protein 3 (TIM3) on T cells to induce apoptosis. As the induction of the immunosuppressive pathways that are depicted in the figure is regulated by common transcription factors, these pathways can operate in more than one myeloid cell type. From Gabrilovich *et al.*, Nat Rev Immunol. (2012).22;12(4): 253-68.

Regulatory T Cells

Another mechanism by which tumours can evade immune response is the recruitment of Tregs into the tumour microenvironment. These cells actively suppress immune responses, thereby contributing to the maintenance of immunological self-tolerance.

Tregs represent a family of specialized T cells that are subdivided into two major groups: natural Tregs and induced or adaptive Tregs. Natural Tregs express CD4 and the IL-2 receptor α chain (CD25). These cells are physiologically produced by the normal thymus as a functionally mature and distinct population, and their development and function depend on the expression of the transcription factor forkhead box P3 (FOXP3). Adaptive Tregs are induced from *naive* T cells by specific modes of antigenic stimulation.

CD4+ CD25+ FOXP3+ natural Tregs suppress the activation and/or expansion of multiple types of immunocompetent cells [62]. In fact, they suppress the activation and/or proliferation and cytokine formation of CD4+ and CD8+ T cells, the B-cell proliferation and immunoglobulin production and class switch, the cytotoxic functions of NK. It has been postulated that cytotoxic T-lymphocyte associated protein 4 (CTLA-4) on Tregs might interact with the CD80 and CD86 molecules on antigen-presenting cells (APCs; *e.g.,* Dendritic cells, macrophages, and B cells) and transduce a co-stimulatory signal to Tregs, thus resulting in the activation of Tregs to exert suppression [66].

Alternatively, CTLA-4 on Tregs might ligate CD80 and CD86 and directly transduce a negative signal to the activated responder T cells. The secretion of immunosuppressive cytokines by Tregs represents another mechanism by which Tregs mediate suppression or condition a suppressive milieu. Tregs secrete IL-10 and TGF-β that is required for the maintenance of natural Tregs and for the induction of Tregs from *naive* T cells (Figure 8) [66].

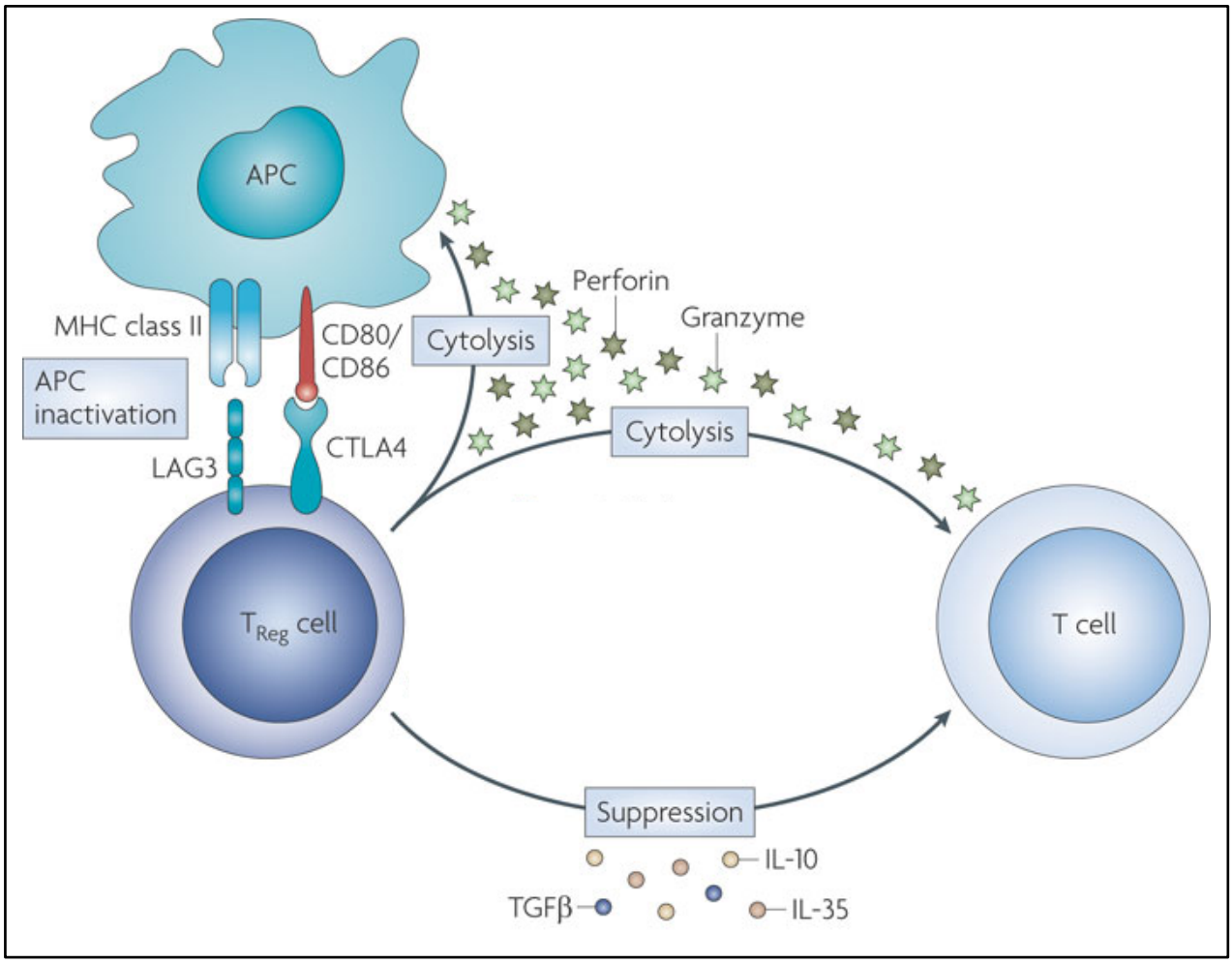

Figure 8: Mechanisms of T cell regulation by Regulatory T cells (Tregs) . Tregs use several mechanisms to inhibit the activation and proliferation of conventional T cells. Treg modulate the functions of antigen-presenting cells (APCs) by inhibiting their maturation and blocking the cell surface expression of MHC molecules and co-stimulatory molecules (CD80 and CD86), thereby attenuating interactions between APCs and T cells. Treg might have cytolytic effects on target T cells, as well as on APCs, through the secretion of granzymes and perforin. Treg suppress the activation and proliferation of T cells through the secretion of inhibitory cytokines, such as transforming growth factor-(TGF), interleukin-10 (IL-10) and IL-35. CTLA4, cytotoxic T lymphocyte antigen 4; LAG3, lymphocyte activation gene 3. From Rochman *et al*., Nat Rev Immunol. (2009). 9:480-490

TGF-β in the tumour microenvironment

Transforming growth factor-β (TGF-β) is an immunosuppressive cytokine produced by tumour cells and immune cells that can "polarize" many components of the immune system. Many studies indicate that TGF-β can promote cancer metastasis through effects on the tumour microenvironment by enhancing tumour cell invasion and modulating the function of immune cells. So, the overproduction of immunosuppressive cytokines, including TGF-β, by tumour cells and immune cells (*i.e.,* T-lynphocytes, APCs and MDSCs) contributes to an immunosuppressive microenvironment.

TGF-β has a crucial immunosuppressive role in both the innate and the adaptive arms of the immune response. In terms of the innate immune response, TGF-β inhibits IFNγ production by NK cells causing dampened $CD4^+$ Th1 cell responses. It downregulates expression of the activating receptor NKG2D on NK cells resulting in decreased cytolytic activity and overall poor antitumour responses. TGF-β also influences the presentation of tumour antigens to the adaptive immune system by decreasing DCs migration and promoting DC apoptosis in some tumour models. In general, TGF-β inhibits DCs maturation and cytokine production, thereby promoting a tolerogenic environment. In addition, TGF-β produced by tolerogenic DCs contributes to Treg cell differentiation. TGF-β favour the differentiation of M2 versus M1 macrophages by inhibiting NF-κB activation [83]. TGF-β also promotes the differentiation of N1 to N2 neutrophils, which, similar to M2 macrophages, are less cytotoxic.

Blocking TGF-β can induce an expression profile in the tumour microenvironment that promotes better antigen uptake and presentation, resulting in more robust priming and activation of the adaptive antitumour immune response. In terms of the adaptive immune response, TGF-β can also promote apoptosis of the short-lived effector $CD8^+$ T cells, directly dampen the function of both $CD8^+$ and $CD4^+$ T cells and induce the recruitment and differentiation of Tregs at the tumour bed.

In this regard, treatment of *naive* T cells with TGF-β induces the expression of FOXP3, which drives the phenotypical conversion of a *naive* T cell to a Treg cell [84]. Interestingly, Treg cell-induced suppression of the adaptive immune response is also mediated through the expression of TGF-β [85]. In contrast, the addition of IL-6 to TGF-β treatment of *naive* T cells induces a different phenotype with the suppression of FOXP3 and the activation of the transcription factor retinoic acid Receptor-Related Orphan Receptor γt (RORgt), thus inducing Th17 cell differentiation [86]. Various pro-tumorigenic and antitumorigenic functions of Th17 cells are primarily mediated through the expression of IL-17 in these cells. Interestingly, the function of IL-17 is also context dependent: IL-17 functions as a tumour promoter by inducing angiogenesis and tumour cell proliferation in immune-deficient hosts, but functions as a tumour suppressor in hosts with intact immune systems by enhancing anti- tumour immune functions [87].

In conclusion, the immunosuppressive effects of TGF-β on immune cell subsets leading to dampened antitumour immune responses as described above strongly support the development of TGF-β inhibitors to treat patients with cancer. Several inhibitors of TGF-β induced signaling within the tumour microenvironment are under development (Figure 9) [88], [89].

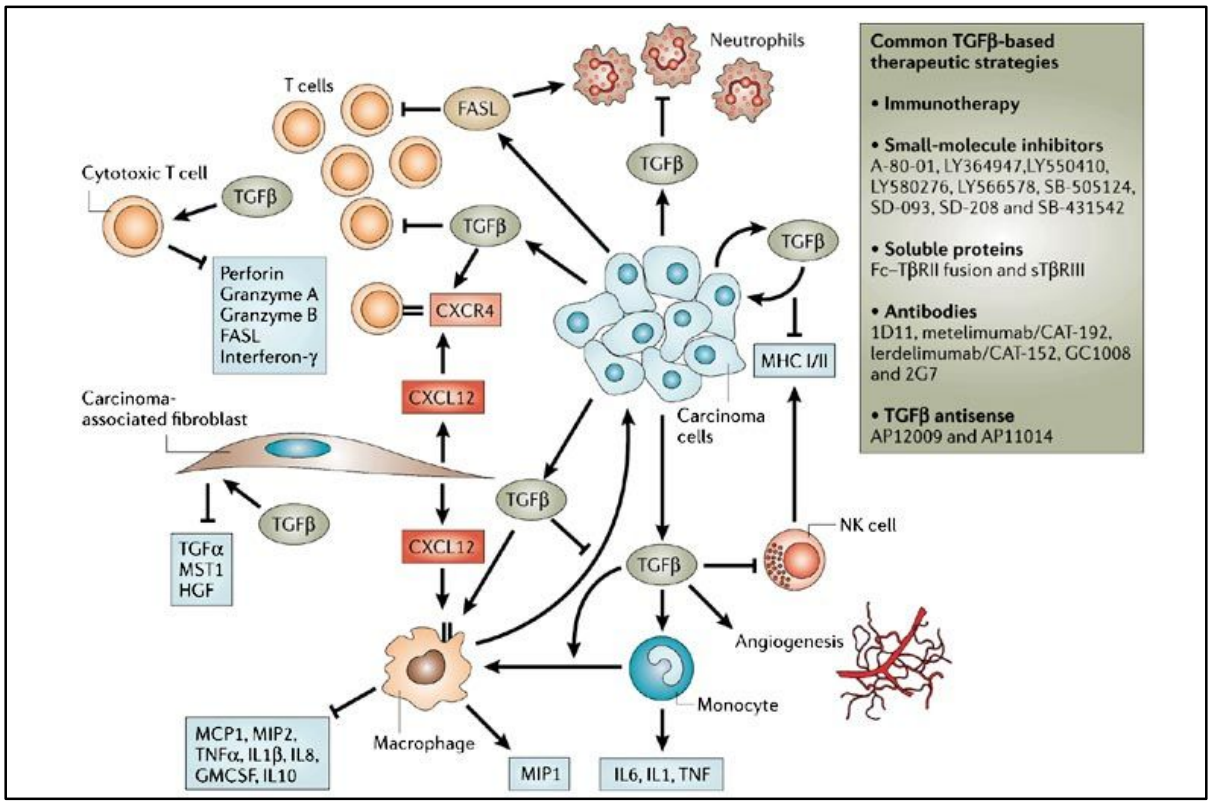

Figure 9: Targets for TGF-β-based therapeutic intervention in the tumour microenvironment. TGF-β is a potent regulator of T-cell, neutrophil, monocyte, macrophage, natural-killer (NK)-cell, carcinoma-associated fibroblast and carcinoma-cell-autonomous signaling in the tumour microenvironment. In addition, TGF-β contributes to the regulation of angiogenesis through direct and indirect mechanisms. TGF-β stimulates the migration of fibroblasts, T cells, neutrophils and monocytes, and influences their behaviour to suppress or promote tumour progression. TGF-β inhibits T-cell function, the secretion of cytolytic factors from cytotoxic T cells and stimulates monocytes to differentiate into macrophages, but inhibits the effector function of macrophages when present. TGF-β might stimulate tumour-homing T cells and macrophages through the upregulation of CXCR4 in response to CXCL12 secretion by carcinoma-associated fibroblasts. TGF-β enables the expression of FAS Ligand (FASL) by inhibiting the activation of neutrophils, cells that would normally kill FASL-expressing cells. This is an important role for TGFβ, as the expression of FASL promotes immune evasion by inducing cell death in FAS-expressing cells, including tumour-reactive T-cell populations. TGF-β signaling also results in a reduction of MHC class I and II gene expression that would normally induce NK-cell activation, but TGF-β has been shown to inhibit NK-cell activation, which further contributes to the promotion of tumour progression. Finally, TGF-β signalling influences tumour-cell-autonomous signaling that can suppress or promote progression and metastases depending on the context of stimulation. These interactions are often manipulated individually, through immunotherapy, or globally, through systemic inhibition strategies, in cancer research or clinical therapy. GMCSF, granulocyte-macrophage colony-stimulating factor; HGF, hepatocyte growth factor; IL, interleukin; MCP1, macrophage chemoattractant protein 1; MIP, macrophage inflammatory protein; MST1, macrophage stimulating 1; TNF, tumour-necrosis factor. From Bierie *et al.*, Nature Reviews Cancer. (2006). 6, 506–520.

The blockade of immune checkpoints in cancer immunotherapy

The growing body of evidence of the roles played by immune cells of tumour microenvironment in promoting tumour progression indicate that it is conceivable that these cells can serve as novel therapeutic targets in the treatment of cancers. Several immunotherapeutic approaches have been developed to target the immune cells that infiltrate the tumour, thus supporting the rationale for developing combinatorial strategies for targeting both tumour and immune cells. Some chemotherapies (*e.g.,* Dipyridamole [67] and Bindarit [68]) decrease the infiltration of TAMs and MDSCs in BC. These data raise the possibility that these treatment strategies might be effectively combined with immunotherapy to improve clinical outcomes.

The myriad of genetic and epigenetic alterations that are characteristic of all cancers provide a different set of antigens that the immune system can use to distinguish tumour cells from their normal counterparts. T cells, which is initiated through antigen recognition by TCR, is regulated by a balance between co-stimulatory and inhibitory signals. Immune checkpoints refer to a plethora of inhibitory pathways hardwired into the immune system that are crucial for maintaining self-tolerance and modulating the duration and amplitude of physiological immune responses in peripheral tissues in order to minimize collateral tissue damage [69].

However, the expression of immune-checkpoint proteins can be dysregulated by tumours as an important immune resistance mechanism particularly against T cells that are specific for tumour antigens. Because many of the immune checkpoints are initiated by ligand–receptor interactions, they can be readily blocked by antibodies or modulated by recombinant forms of ligands or receptors. Thus, agonists of co-stimulatory receptors or antagonists of inhibitory, both of which result in the amplification of antigen-specific T cell responses, are the primary agents in clinical testing (Table 4).

Antibodies against CTLA4 (which downmodulates the amplitude of T cell activation) were the first of this class of immunotherapeutics to achieve US Food and Drug Administration (FDA) approval. Preliminary clinical findings with blockers of additional immune-checkpoint proteins, such as Programmed Cell Death Protein 1 (PD1), indicate broad and diverse opportunities to enhance antitumour immunity with the potential to produce durable clinical responses [69].

The blockade of immune checkpoints is among the most promising approaches to activating therapeutic antitumour immunity.

Table 4: The clinical development of agents that target immune-checkpoint pathways

Target	Biological function	Antibody or Ig fusion protein
CTLA4	Inhibitory receptor	Ipilimumab
		Tremelimumab
PD1	Inhibitory receptor	MDX-1106 (also known as BMS-936558)
		MK3475
		CT-011‡
		AMP-224§
PDL1	Ligand for PD1	MDX-1105
		Multiple mAbs
LAG3	Inhibitory receptor	IMP321‖
		Multiple mAbs
B7-H3	Inhibitory ligand	MGA271
B7-H4	Inhibitory ligand	-
TIM3	Inhibitory receptor	-

CTLA4, cytotoxic T-lynphocytes-associated antigen 4: LAG3, lymphocyte activation gene 3; mAbs, monoclonal antibodies; PD1, programmed cell death protein 1; PDL, PD1 ligand; TIM3, T cell membrane protein 3. From Pardoll *et al.,* Nature Reviews Cancer. (2012). 12, 252–264.

1.5 The immune system in Triple Negative Breast Cancer microenvironment

Immune cells represent a major component of TNBC microenvironment [70]. The higher genomic instability and mutational burden of TNBC results in a higher propensity to generate neoantigens, which can be recognized as 'non-self' by the adaptive immune system [3]. Accordingly, TNBCs have a higher amount of tumour-infiltrating lymphocytes (TILs) and higher programmed cell death 1 ligand 1 (PD-L1) protein or mRNA expression compared with other BC subtypes.

High TILs infiltration has been associated with a lower risk of relapse in patients with BC. In this regard, after neoadjuvant chemotherapy in patients with TNBC with residual disease, the immune microenvironment can be turned from 'cold' (containing few TILs) to 'hot' (higher TILs presence) in some patients. Tumours that remain or become 'cold' after chemotherapy have a higher risk of relapse compared with tumours that remain or become 'hot' [71]. These data also support the concept of chemotherapeutic agents having immunomodulatory activity, and thus, acting as an immunological

adjuvant in the tumour microenvironment to stimulate antitumour immunity. Overall, a 'hot' immune microenvironment (*i.e.,* high levels of TILs) is associated with a better prognosis, a higher likelihood of benefit from chemotherapy, and a lower risk of relapse and/or death in patients with early-stage TNBC treated with systemic chemotherapy. These results also distinguish a subgroup of patients with TNBC characterized by a 'cold' immune microenvironment that has a high risk of relapse, despite treatment, and a low likelihood of benefit from cytotoxic chemotherapy. This subgroup is a high priority in the list of unmet needs in TNBCs.

The findings that a population of TNBC is immunogenic and actively engaged by the immune system provides a strong rationale for testing immunotherapies. In fact, different trials are ongoing to establish the role of immune-checkpoint inhibitors alone or in combination with other immunotherapies in TNBCs (Table 5).

Table 5: Clinical trials testing immunotherapies in patients with Triple Negative Breast Cancer

Disease setting	Phase	Clinical trial reference number	Breast cancer	Immunotherapies (alone or in combination)	Control arm treatment
Metastatic	I/II	NCT02513472	TNBC	Pembrolizumab*/eribulin mesylate	NA
	II	NCT02499367	TNBC	Nivolumab*/doxorubicin (low dose) or cyclophosphamide metronomic or radiation therapy or cisplatin	NA
		NCT02447003	TNBC	Pembrolizumab	NA
	III	NCT02555657	TNBC	Pembrolizumab	Single-agent CT (capecitabine, eribulin, gemcitabine or vinorelbine)
		NCT02425891	TNBC	Atezolizumab‡/nab-paclitaxel	Nab-paclitaxel
Adjuvant	II	NCT02539017	TNBC	Vaccine (DC-CIK)/EC followed by docetaxel	EC followed by docetaxel
Neoadjuvant	I/II	NCT02489448	TNBC	Durvalumab‡/nab-paclitaxel followed by ddAC	NA
	II	NCT02530489	TNBC	Atezolizumab/nab-paclitaxel	NA
	III	NCT02620280	TNBC (LABC only)	Atezolizumab/nab-paclitaxel/carboplatin	Nab-paclitaxel/ carboplatin

TNBC, triple-negative breast cancer; LABC, locally advanced breast cancer; DC-CIK, dendritic cells co-cultured with cytokine-induced killer cells; ddAC, dose-dense doxorubicin and cyclophosphamide; EC, epirubicin and cyclophosphamide; NA, not applicable; *Anti-programmed cell death protein 1 (PD-1) monoclonal antibodies (mAbs): nivolumab and pembrolizumab (anti-PD1). ‡Anti-programmed cell death 1 ligand 1 (PD-L1) mAbs: atezolizumab and durvalumab. From Bianchini *et al.,* Nat Rev Clin Oncol. (2016).13(11):674-690.

Three trials in patients with stage I–III TNBC are currently ongoing to evaluate the potential activity of immune checkpoint inhibitors in combination with chemotherapy in the neoadjuvant setting. In the phase III trial NeoTRIPaPDL1 (NCT02620280), patients with locally-advanced TNBC are randomly assigned to receive Nab-Paclitaxel and Carboplatin with or without a PD-L1-inhibitor (Atezolizumab). A phase II trial is evaluating Atezolizumab in combination with Nab-Paclitaxel (NCT02530489). A phase I/II trial is testing the safety and efficacy of Durvalumab, another anti-PD-L1 antibody, in combination with weekly Nab-Paclitaxel followed by dose-dense chemotherapy containing cyclophosphamide and doxorubicin (NCT02489448).

The importance of immune checkpoint inhibitors in metastatic TNBC, represent a very promising therapeutic option that is now ready for investigation in the setting of neoadjuvant and adjuvant therapy of early-stage TNBC [3].

The variegate nature of the immune microenvironment in TNBC considerably influences the risk of relapse and response to chemotherapy. In fact, recently new distinct TNBC subtypes were defined based on the immune and metabolic markers within the tumour microenvironment [72]. In details, the relashionship between TILs, immune response regulators (M2-polarized TAMs and Tregs) and glycolitic metabolism (*i.e.* Monocarboxylate transporter 4, MCT4) was evaluated in a cohort of 180 women affected by TNBC. This study confirms the already known positive correlation between high TILs in tumour microenvironment and improved OS in TNBC patients. Most importantly, it also shows for the first time that increased levels of PDL1, M2-Polarized TAMs ($CD163^+$), Tregs ($FOXP3^+$) and MCT4 (as glycolitic markers in the tumour stroma) are individually associated with signifincantly decreased OS in TNBC patients, thus differentiating the prognostic significance of TILs. This data highligth the existence of four new TNBC subtypes with a strong prognostic significance with the following features:

(i) low levels of immunosuppressive markers PD-L1 and FOXP3, high levels of stromal MCT4 and high levels of TILs;

(ii) low levels of immunosuppressive markers PD-L1 and FOXP3 (Tregs), low levels of stromal MCT4 and high levels of TILs;

(iii) high levels of immunosuppressive markers PD-L1, FOXP3 (Tregs), CD163 (M2-polarized TAMs), high levels of stromal MCT4 and low levels of TILs;

(iv) high levels of immunosuppressive markers PD-L1 and FOXP3 (Tregs), low levels of CD163 (M2-polarized TAMs), high levels of stromal MCT4 and low levels of TILs.

Importantly, survival correlation analyses show the first two groups ([i] and [ii]) had an overall good prognosis, while the latest groups ([iii] and [iv]) had poor survival. Altogheter, these data highligh the existance of a peculiar subgroup of patients (those belonging to the third group [iii]) with poor

prognosis characterized by high M2-Polarized TAMs ($CD163^+$) and Tregs ($FOXP3^+$) in a low TILs environment [72].

The role of Tumour-Associated Macrophages in Triple Negative Breast Cancer

Studies focusing on the mutual interaction between TAMs and TNBC cells reported that macrophages co-coltured with TNBC cells (*i.e.,* MDA-MB-231) revealed a more aggressive behaviour, with increased levels of macrophage M2 markers [73].

Several literature data highligh the role of TAMs in TNBC progression and clinical outcomes with prognostic significance. In this regard, data obtained from a tissue microarrays with tumours from 144 BC cases reported that infiltrating M2-TAMs ($CD163^+$) were positively correlate with ER negativity ($p<0.001$), PgR negativity ($p=0.001$), TNBC/Basal-like BC ($p<0.001$), higher grade ($P<.001$), larger size ($P<.001$) and higher proliferation index (as Ki67 positivity; $p=0.007$) [74]. In another study, the high numbers of M2-TAMs ($CD163^+$) were strongly associated with fast proliferation, poor differentiation, ER and HER2 negativity ($p<0.001$) in a cohort of 562 human primary BC [75]. Moreover, the increase of TAMs in TNBC patients after the surgery, were correlated to unfavorable prognosis [76].

The relationship of infiltrating TAMs with the clinicopathologic characteristics of TNBC was also evaluated [77] in a study performed on 287 TNBC patients. When patients were grouped according to the mean number of TAMs, the high-infiltration group was associated with lymph node involvement ($p=0.007$) and lymphovascular invasion ($p=0.032$). Further, the 8-years EFS and 5-years OS were shorter in "TAMs high infiltration" group compared to those of "TAMs low infiltration" group (EFS and OS: $p<0.0001$). Importantly, patients with “TAMs high-infiltration” had a significantly higher risk for developing distant metastasis (72.1% versus 86.8%; $p<0.001$). These data suggest that TAMs infiltration might serve as a prognostic indicator for poor outcomes among patients with TNBC [77]. More importantly, TAMs may serve as potential cellular targets for novel therapeutic interventions in TNBC due to their significantly correlation to poor prognosis and high risk of metastases.

TAMs exert their immunosuppressive functions by several mechanisms that include the secretion of inhibitory cytokines, the reduction of effector functions of TILs, the promotion of Tregs development and the production of reactive oxygen species (as previously shown in Figure 10). Importanly, TAMs reduce the effector activity of TILs by secreting several cytokines (including IFN-γ and TGF-β) which are involved in modulating the expression of PD-1/PD-L1 axis in TNBC. In particular, the “Janus kinase/signal transducers and activators of transcription 3” (JAK/STAT3) signaling is involved in IFN-γ-induced overexpression of PD-L1 [78].

Currently, a phase II study (NCT02876302) is investingating the anti-tumour activity of Ruxolitinib (as JAK1/2 inhibitor that reduces STAT3 phosphorylation**)**, in combination with chemotherapy for patients with TNBC (NCT02876302).

As mentioned above, TGF-β is implicated in M2 polarization and PD-L1 overexpression [79]. The evidence that TAMs result crucial in modulating the expression and activity of immunocheckpoints suggest that combined or sequential TAM-centered strategies should be developed, aimed to maximize the efficacy of anti-PD-1 and PD-L1 agents in this tumour. So targeting TAMs may represent a promising and effective approach to modulate the activity of anti-PD-1 and PD-L1 agents for TNBC cancer therapy. On this scenario, the role of TGF-β inhibitors in association with anti-PD-1/PD-L1 are under investigation. At this regard, a phase I study (NCT02947165) is ongoing to investigate anti-TGF-β monoclonal antibody (*i.e.,* NIS793) in combination with the anti-PD1 Spartalizumab (or PDR001) in patients with advanced malignancies including TNBC; and another phase I/II trial (NCT02423343) is evaluating the combination of Nivolumab and Galunisertib (small molecular PD-1 and TGF-β inhibitors, respectively) in patients with advanced malignancies including TNBC.

A better dissection of the exact molecular mechanisms of TAMs-dependent modulation of PD-1/PD-L1 axis may pave the way to innovative therapeutic strategies for TNBC patients [80].

Finally, the high density of TAMs in TNBC was also exploited to design a targeted therapy to more effectively control the tumour growth. By taking advantage of the slightly lower pH in solid tumour microenvironment and the fact that TAMs overexpress mannose receptors, TAMs were used as a target to deliver Doxorubicin (DOX), a chemotherapeutic agent, *in vivo* using nanoparticles surface-functionalized by acid-sensitive sheddable PEGylation and modified with mannose (*i.e.,* DOX-AS-M-PLGA-NPs). In details, the authors used M-Wnt cell line that are derived from mammary tumors spontaneously developed in MMTV-Wnt1, a Genetically Engineered Mouse Model [GEMM] of TNBC [81]. These primary TNBC cells were orthotopically injected into syngeneic mice and the resulting tumours (orthotopic M-Wnt1) were characterized by an higher density/population of TAMs [82]. In these orthotopic M-Wnt1, the modified-nanoparticles derivering DOX (*i.e.,* DOX-AS-M-PLGA-NPs) significantly inhibited M-Wnt tumour growth, compared to DOX alone, by reducing the density of macrophages in tumours. In summary, these data suggest that delivering DOX (which is commonly used in combination adjuvant chemotherapy of TNBC) using the TAM-targeting nanoparticles (*i.e.,* DOX-AS-M-PLGA-NPs) significantly increased the antitumour activity of DOX. It is expected that delivering other chemotherapeutic agents that are commonly used in TNBC chemotherapy, using the TAM-targeting nanoparticles, will also enhance their antitumour activity. So, these TAM-targeting nanoparticles may also be adopted to improve the chemotherapy of TNBC [82].

1.6 Extracellular vesicles

Intercellular communication plays an important role in cancer initiation and progression through secretory molecules, including growth factors and cytokines. Recent advances have revealed that small membrane vesicles, termed extracellular vesicles (EVs), served as regulatory agents in the intercellular communication of tumorigenic cells. In fact, EVs enable the transfer of functional molecules, including proteins, mRNA and microRNAs (miRNAs), into recipient cells. Cancer cells utilize EVs to dictate the unique phenotype of surrounding cells, thereby promoting cancer progression and metastatic spread [90].

EVs are an heterogenetic population categorized as exosomes, microvesicles (or ectosomes), and apoptotic bodies. These vesicles originate from different subcellular compartments. Microvesicles are 100–1000 nm in diameter and are produced directly from the plasma membrane via budding. The biogenesis of microvesicles is modulated by the interaction between phospholipid redistribution and the contraction of cytoskeletal structures [90].

Apoptotic bodies (500–4000 nm in diameter) are formed during the apoptotic process and contain organelles and nuclear fragments. Apoptotic bodies also contain DNA and RNA fragments and may participate in the intercellular communication of the cancer microenvironment [90].

Exosomes are small membrane vesicles, ranging from 50 to 150 nm in diameter with a lipid bilayer. They originate from the fusion (exocytosis) of the membrane of Multivesicular Bodies (MVBs) containing intraluminal vesicles with the plasma membrane. This releases their content of Intra-Lumenal Vesicles (ILVs) into the extracellular space as exosomes. Exosomes biogenesis and release are mainly modulated by Endosomal Sorting Complex Required For Transport (ESCRT) machinery and the ceramide-dependent pathway [91].

Interestingly the composition of exosomes appears to differ somewhat depending on their source tissue or cell type. For instance MHC class II is enriched in exosomes from B cells, DCs, mast cells, and intestinal epithelial cells while growth factors and their receptors are enriched in exosomes released from cancer cells [92].

Researchers in EV biology have identified several types of exosome markers, including Tetraspanins (CD9, CD63, CD81), Heat Shock Proteins (HSP-60, -70, and -90), membrane transporters and fusion proteins (Annexins and Flotillin), and MVB synthesis proteins (Alix and TSG101). Further**,** exosomes contain a variety of highly abundant cytosolic proteins including those involved in structure and motility (*e.g.,* Tubulin, Actin), energy metabolism (*e.g.,* Enolase), signal transduction (e.g., 14-3-3 proteins) and transcription and protein synthesis (*e.g.,* histones, ribosomal proteins). In addition to proteins, the lumen of exosomes also contain cytosolic RNA (*i.e.,* mRNAs and miRNAs), so called shuttle RNA that can be translated in the exosome's target cells [93].

Exosomes can move a distance by diffusion and can appear in biological fluids including blood, urine, amniotic fluid, saliva, lung surfactant, malignant effusions, breast milk and semen. The double-layer membrane, being characterized by a peculiar lipid composition along with protective proteins against complement, makes exosomes more stable than soluble proteins in the extracellular environment [91].

The role of EVs in invasive Breast Cancer

Exosomes are implicated in physiology such as mammary gland development and lactation but also in pathology, including BC. Growing evidence suggests the potential involvement of EVs in human BC initiation, progression and metastatic spread.

Cancer-derived EVs play a crucial role in the acquisition and transfer of the malignant trait by horizontal propagation of oncogenic molecules. In fact, cancer-derived EVs act on stromal cells within the tumour microenvironment to promote cancer progression by transfering of their oncogenic properties. In this regard, highly metastatic BC cells (*i.e.* 4T1 cells) was found with the ability to transfer the EVs contained microRNA-200 family to non-metastatic BC cells to promote lung metastases [94]. Cancer cells dictate the stromal cell compartment of the primary tumour to permit invasive growth. Cancer cells deliver TGF-β containing exosomes, driving cellular differentiation of fibroblasts, resulting in a myofibroblast phenotype. Functionally active MMPs are also secreted in exosomes to degrade type 1 collagen fibers [95]. Invasive BC cells release exosomes containing HSP-90, a chaperone required for the activation of extracellular proteases, such as MMP-2 [96]. HER ligands, such as Amphiregulin, Epidermal Growth Factor (EGF) and TGF−α, are also released by cancer exosomes [97]. Several studies demonstrated exosome function in angiogenesis, suggesting a role in cancer cell dissemination [98]. Furthermore, proteomic analysis of secreted exosomes identified potent angiogenic factors such as the Delta Like canonical Notch Ligand 4 (DLL4) [99].

Of importance, exosomes were found to move by diffusion to distant organs to prepare the "organotropic pre-metastatic niche" for the settlement and growth of metastatic cancer cells, thus facilitating organ-specific metastatic behaviour [100]. The exosomal proteome of several tumour models (*i.e.,* osteosarcoma, rhabdomyosarcoma, Wilms tumour, melanoma, breast, colorectal, pancreatic and gastric cancers), all of which have a propensity to metastasize to specific sites (*i.e.,* brain, lung or liver), was profiled. The analyses of the biodistribution of tumour-secreted exosomes revealed that exosomal Integrins (ITGs) direct organ-specific colonization by fusing with target cells in a tissue-specific fashion, thereby initiating pre-metastatic niche formation [100]. Importantly, both quantitative mass spectrometry and Western bloting analysis revealed that integrin alpha 6 (ITGα6), and its partner ITGβ1, were present abundantly in lung-tropic exosomes from Breast Cancer cells (including MDA-MB-231, as TNBC cell line) [100].

Remarkably, these tumour-secreted exosomes were found to be sufficient to redirect metastases of tumour cells that normally lack the capacity to metastasize to a specific organ. Finally, clinical data also indicate that integrin expression profiles of circulating plasma exosomes isolated from cancer patients could be used as prognostic factors to predict sites of future metastasis [100].
These findings pave the way for the development of diagnostic tests to predict organ-specific metastasis and therapies to halt metastatic spread.

EVs in the crosstalk between tumorigenic and immune cells

Importantly, exosomes create an immuno-privileged environment within the tumours by modulatung the evasion of cancer cells from immune surveillance through several immunoregulatory molecules (*e.g.,* TGF-β, FasL, NKG2D ligands, Galectin-9, and HSP72) in order to support the immune escape of cancer cells [101]. In fact, cancer cells produce large amounts of exosomes bearing pro-apoptotic molecules such as Fas Ligand and Tumour Necrosis Factor-Related Apoptosis-Inducing (TRAIL) ligand [102]. These induce apoptosis of activated tumor-specific T cells, impairing the ability of effector lymphocytes to exert their cytolytic activity against tumour targets. NK cells lose their cytolytic potential, through the down-modulation of perforin expression, upon encounter with cancer cell-derived exosomes. Further, exosomes produced by BC cells block DCs differentiation by increasing IL-6 expression in myeloid precursor cells [103]. These EVs also induce the differentiation of monocytes into immunosuppressive macrophages in the tumour microenvironment [104]. These macrophages are also capable of producing the EVs that enhance the metastatic properties of cancer cells [105]. Moreover, cancer-derived EVs internalize into macrophages and induce pro-inflammatory cytokines, including IL-6, TNF-a, and CCL2, through activating NF-kB signaling [106]. Thus, EV communications between cancer cells and immune cells seem to provide the advantage of evasion from immune surveillance and cancer progression.
In summary, EVs (*e.g.,* exosomes) may provide novel specific tools or targets for therapeutic intervention. Engineered exosomes are emerging as new and novel avenues for cancer vaccine development, via antigen-presenting cell technology, to prime the immune system to recognize and kill cancer cells. To date, three Phase I clinical trials (China, France, and the United States) have been conducted, involving the application of exosomes to elicit immune responses against established tumors. Dai *et al*., [107] reported that using ascitic cell-derived exosomes in patients with colorectal cancer induces tumor antigen-specific cytotoxic T-cell responses, with none to minimal side effects, and is well tolerated by patients. Escudier *et al*., [108] demonstrated the feasibility of scaling up and purification of clinical grade cell-derived exosomes using good manufacturing practice and restored the number and NKG2D-dependent function of NK cells in patients with melanoma. Furthermore, a

study by Morse *et al*., [109] indicates a Melanoma-Associated Antigens (MAGEs)-specific T cell response and increased NK lytic activity in patients with non-small cell lung carcinoma (NSCLC) with the use of cell-derived exosomes.

2. MATERIALS AND METHODS

Cell culture

Triple-negative murine 4T1 Dual LN P3 (referred to as 4T1; ATCC: #CRL-2539) breast-cancer cell line were grown in PRMI 1640 medium (Euroclone) supplemented with 10% (v/v) fetal bovine serum (FBS) (Invitrogen), 2 mM L-glutamine (Invitrogen), and 1% (v/v) antibiotics (10000 U/ml penicillin, 10 mg/ml streptomycin [Invitrogen]) (Pen/Strep). Murine macrophages J774A.1 (referred to as J774; ATCC: #TIB-67) cells were grown in high-glucose Dulbecco's modified Eagle's medium (DMEM; Euroclone) supplemented with 10% (v/v) FBS, 2 mM L-glutamine, and 1% (v/v) antibiotics (Pen/Strep). Murine macrophages RAW-264.7 referred to as (RAW-264; ATCC: #TIB-71) cells were grown in high-glucose DMEM supplemented with 10% (v/v) FBS, 4 mM L-glutamine, and 1% (v/v) antibiotics (Pen/Strep). The cells were grown at 37 °C in a humidified atmosphere of 95% air, 5% CO_2 (v/v).

Primary murine TNBC cells from the tumours generated by MMTV-Prune1/Wnt1 and MMTV-Wnt1 mice were obtained (after 2 months from the tumour onset) by following the methodology described by DeRose et al., (2013). MMTV-Prune1/Wnt1 and MMTV-Wnt1 mice were grown in high-glucose Dulbecco's modified Eagle's medium (DMEM; Euroclone) supplemented with 10% (v/v) FBS, 2 mM L-glutamine, 1% Non-essential Amino Acid Solution (M7145, Sigma-Aldrich/Merck) and 1% (v/v) antibiotics (Pen/Strep).

Generation of 4T1 stable clones

A construct encoding a fusion protein containing three Flag epitopes (Flag sequence: DYKDDDDK) upstream the Prune-1 protein was generated in the pcDNA3.1 Hygro vector (H-Prune-1-3X-Flag-Hygro plasmid). This construct was transfected to 4T1 cells to generate clones over-expressing Flag-h-Prune-1 fusion protein (referred to as Prune-1 overexpressing 4T1 clones). The pcDNA3.1 Hygro vector was also transfected to generate control clones.

To generate 4T1 clones in which the mouse prune endogenous expression was down-regulated (referred to as Prune-1-silenced 4T1 clones), we transfected the cells with a plasmid containing sh-Prune (Open Biosystems). Similarly control clones were generated transfecting the 4T1 cells with the empty vector plasmid.

One day before transfection, 4T1 cells were plated in 60-mm dish. At the time of transfection, the cell confluence was 50%, and the cells were transfected with 2.4 μg each vector using with TransIT-LT1 Transfection Reagent (Mirus Bio LLC, #MIR2300), according to the manufacturer instructions. Fourty-eight hours after transfection, cells were cultured under the selection pressure of 250 μg/ml

hygromycin B (Invitrogen) for pcDNA3.1 Hygro constructs. After the selection, about 20 clones for each transfected construct were picked up and the expression levels of human and mouse prune proteins were evaluated.

Cell proliferation and migration assays for Cell Index technology

Cell proliferation assays

MMTV-Prune1/Wnt1 and MMTV-Wnt1 cells were harvested, washed with phosphate-buffered saline (PBS), resuspended to 1×10^4 cells/mL in high-glucose Dulbecco's modified Eagle's medium (DMEM; Euroclone) and plated into single wells of the xCELLigence E-plate 16 (Acea Biosciences, #05469830001). The proliferation rate was determined by measuring electrical impedance changes at the bottom of each well, at 2- min intervals over 24 hours.

Cell migration assays

MMTV-Prune1/Wnt1 and MMTV-Wnt1 cells were harvested, washed with phosphate-buffered saline (PBS), resuspended to 2×10^5 cells/mL in high-glucose Dulbecco's modified Eagle's medium (DMEM; Euroclone) without foetal bovine serum (FBS). Each cell suspension was used in a single well of an xCELLigence CIM-plate 16 (Acea Biosciences, #05665817001). Cell migration was driven by a 10% FBS gradient, with 0% FBS used as negative control. Measurements were taken at 2-min intervals, of impedance changes across the electrodes at the bottoms of the wells, over 12 hours.

The effects of conditioned media from Prune-1-overexpressing, Prune-1-silenced and Empty Vector 4T1 cell clones were investigated on J774 cell migration by using the Real-Time XCelligence System Analysis Instrument developed by ACEA Biosciences. Briefly 1 x 10^6 4T1 cells of each clone were resuspended in 10 ml complete RPMI 1640 medium and plated into 10 cm plate. After 24 hours, the conditioned media were collected and put in the lower chamber to be served as the chemoattractant in cell motility assays. Here, 2.5×10^4 J774 cells were seeded into the upper chamber in complete RPMI 1640 medium. Three replicates for each experimental point were used. The cell index was automatically and monitored every 2 min for 12 hours. For each experimental point, the mean ± standard deviation of the cell index were calculated. A total of two independent sets of experiments were performed.

Culture in conditioned medium

The effects of conditioned media from Prune-1-silenced, Empty Vector 4T1 cell clones, MMTV-Prune1/Wnt1 and MMTV-Wnt1 were analyzed on the activation of J774 and/or RAW-264 macrophages. Briefly 1 x 10^6 4T1 cells of each clone were resuspended in 10 ml complete RPMI 1640 medium, plated into 10 cm plate and grown at 37 °C for 24 h. Then the conditioned media were

collected. One day before culture in conditioned medium, J774 and/or RAW-264 macrophages were plated in 100-mm dish. At the time of culture in conditioned medium, the J774 and/or RAW-264 macrophages confluence was 50%, and the macrophages were grown in conditioned medium for 30 minutes (for Western blotting analyses) or 48 hours (for Real-Time PCR analyses) after 6 hours of starvation in serum-free medium. Each experimental point was in duplicate. After culturing in conditioned medium, the immune cells were washed with PBS 1X, collected and used for protein and/or RNA extraction.

Cytokine Antibody Array

The conditioned media from three different Prune-1-overexpressing, Prune-1 silenced or Empty vector 4T1 cell clones were pooled. In the same manner, the sera from three different MMTV-Prune1/Wnt1 and MMTV-Wnt1 were also collected and pooled. The relative levels of cytokines in the pooled conditioned media or murine sera were measured via RayBio Mouse Cytokine Antibody Array C Series 2000 (Prodotti Gianni), according to the manufacturer protocol. Densitometric analysis was conducted using the Quantity One software (BioRad). Expression levels were normalized to the levels of the positive control spots (contained within the membrane). For each cytokine, the mean ±SE was determined.

Immunoblotting

The cells were washed in cold phosphate-buffered saline (PBS) and lysed in cell lysis buffer (20 mM sodium phosphate, pH 7.4, 150 mM NaCl, 10% [v/v] glycerol, 1% [w/v] Nadeoxycholate, 1% [v/v] Triton X-100) supplemented with protease inhibitors (Roche, Basel, Switzerland). Cell lysates were cleared by centrifugation at 16,200Å~ g for 10 min at room temperature, and the supernatants were removed and assayed for protein concentration using the Protein Assay Dye Reagent (Bio-Rad). Cell lysates (50 μg protein lysate) were separated using SDS-PAGE gels of different percentages, depending on the molecular weights of the proteins of interest. The proteins were then electrophoretically transferred to PVDF membranes (Millipore). After 1 h in blocking solution with 5% (w/v) dry milk fat in PBS, or 5% (w/v) bovine serum albumin (Sigma-Aldrich) in Tris-buffered saline (both of which contained 0.02% (v/v) Tween-20), the membranes were incubated with the primary antibody overnight at 4 ÅãC, and then with the secondary antibodies for 1 h at room temperature. Primary and secondary mouse or rabbit horseradish-peroxidase-conjugated antibodies (NC 27606; ImmunoReagents, Inc) were diluted in 5% (w/v) bovine serum albumin in TBS-Tween or in 5% (w/v) milk fat in PBS-Tween, according to the manufacturer instructions. The protein bands were visualised with a chemiluminescence detection system (Pierce-Thermo Fisher Scientific Inc., IL,

USA). Western blotting was performed in triplicate. The densitometry analysis was carried out using the ImageJ software programme. The peak areas of the bands were measured on the densitometry plots, and the percentages were calculated. Then, the density areas of the peaks were normalized with those of the loading controls, and the ratios for the corresponding controls (e.g., empty vector) are presented as fold-changes.

Immunohistochemistry methods on paraffin-embedded tissues

Paraffin sections (thickness, 3 μm) of the tumour specimens were deparaffinised in Bioclear (06-1782D; Bio-Optica) for 30 min, rehydrated in 100%, 90% then 70% ethanol, and washed with PBS and then PBS containing 0.02% Triton-X 100 (215680010; Acros Organics). After incubation in pre-warmed Target Retrieval Solution (S170084; Dako) at 97 ÅãC for 45 min, the sections were washed with PBS and placed in a solution of absolute methanol and 0.3% hydrogen peroxide for 15 min. The tissue sections were then blocked with Antibody Diluent Background Reducing (S302281; Dako) for 1 h at room temperature, and then incubated with the primary antibodies overnight at 4 ° C in a humidified chamber. Tissue sections were washed in PBS and incubated with labelled streptavidin biotin LSAB mouse and rabbit reagents (K0672; Dako). Detection was with the Liquid DAB Substrate Chromogen System (K3468, Dako). All of the slides were counterstained with Gill's haematoxylin (Bio-Optica). The slides were then washed, dehydrated with 70%, 90% and then 100% ethanol, and mounted with cover slips using Eukitt (09-00250; Bio-Optica). Micrographs were taken with a high definition digital microscope camera (ICC50 HD; Leica).

The detection of macro-metastases in lungs derived from MMTV-Prune1/Wnt1 and MMTV-Wnt1 was performed following staining with Bouin's fixative (25% of 37% formaldehyde solution, 70% picric acid, 5% acetic acid) for 24 hours.

Immunofluorescence on paraffin-embedded tissue sections

Paraffin sections of the tumour specimens (thickness, 3 μm) were deparaffinised and rehydrated by immersing the slides in Xylene Substitute (A5597; Sigma) (three washes for 5 min each), then serially in 100%, 95%, 70%, 50%, 30% ethanol (two washes for 10 min, for each), and deionised water (two washes for 5 min each). The washes were then followed by PBS, PBS containing 0.02% Triton-X 100 (215680010; Acros Organics), and PBS (two washes for 5 min, for each). For antigen retrieval, the slides were immersed in boiling 10 mM sodium citrate buffer (pH 6.0) using a microwave oven, and then maintained at sub-boiling temperature for 10 min. The slides were left to cool at room temperature for 30 min. The sections were then washed by immersion in distilled water for 5 min. To block endogenous peroxidase activity, the tissue sections were placed in a solution with 3.0%

hydrogen peroxide in methanol for 15 min. Then to decrease the non-specific background fluorescence, the tissues were digested by treating them with a solution containing 0.2% Trypsin (T2600000; Sigma-Aldrich) and 0.001% CaCl2 for 10 min at 37°C, using a humidified chamber. The slides were then washed in PBS, PBS containing 0.02% Triton-X 100 (215680010; Acros Organics), and PBS (two washes for 5 min, for each). The tissue sections were then blocked with 6% bovine serum albumin (A9418; Sigma), 5% FBS (ECS0180L; Euroclone), 20 mM MgCl2 in PBS containing 0.02% Triton-X 100 for 1 h at room temperature, and incubated overnight with the primary antibodies at 4 ÅãC in a humidified chamber. Tissue sections were washed in PBS and PBS containing 0.02% Triton-X100, and incubated with anti-mouse Alexa Fluor 488 (ab150113; Abcam), anti-rabbit Alexafluor 488 (150077; Abcam) and antirabbit Alexa Fluor 546 (#A10040; ThermoFisher), as the secondary antibodies. DNA was stained with DRAQ5 (#62254; ThermoFisher). The slides were then washed, dehydrated with 70%, 90% and 100% ethanol, and mounted with cover slips using 50% glycerol (G5150; Sigma-Aldrich). Confocal microscopy was carried out using a laser scanning confocal microscope (LSM 510 META, Zeiss), with the 63X-oil immersion objective.

Antibodies used in the study:

The following antibodies were used in this study: anti-Flag (1:5000; Sigma-Aldrich), anti-FLAG (1:200; TA100023, origene), anti-phospho-p44/42 MAPK (ERK1/2) (Thr 202/Tyr 204) (1:500; Cell Signaling Technology), ranti-ERK1/2 (1:500; Santa Cruz Biotechnology), anti-phospho-NF-kB p65 (Ser 311) (1:200; Santa Cruz Biotechnology), anti-NF-kB p65 (1:3000; Abcam), anti-STAT3 (1:5000; Abcam), anti-phospho-STAT3 (Tyr 705) (1:1000; Abcam), anti-phospho-STAT3 (Ser 727) (1:1000; Abcam); anti-Prune-1 (1:500; Abcam), anti-phospho-Ser467-Smad2 (1:1000; Cell Signaling); anti-PTEN (1:1000; 9552, Cell Signaling); anti-phospho-Ser473-Akt (1:500; 4060, Cell Signaling); anti-N-Cadherin (1:1000; 333900, Cell Signaling) anti-E-Cadherin (1:500; 610181, Transduction Laboratories:); anti-GSK (1:500, Transduction Laboratories), anti-Ser9/21-GSK (1:200, Cell Signaling), anti-FAK (1:1000, Abcam), Anti-phospho-Y397-FAK (Abcam), anti-FOXP3 (1:200, Abcam), anti-CD11b (1:150, Abcam), anti-CD68 (1:200, Abcam), anti-CD163 (1:200, SantaCruz), anti-activated-beta-catenin (1:500, Millipore), anti-beta catenin (1:2000, Transduction Laboratories), anti-Wnt3a (1:500, Abcam), anti-cyclin D1 (1:5000, Abcam), anti-S100A4 (1:200, Dako), anti-phospho- ser32/36-iKb-alpha (1:500, SantaCruz), anti-Her2 (1:200, Cell signaling). The following in-house antibodies were produced: rabbit polyclonal anti-Prune-1 (C45; 1:500); rabbit polyclonal anti-phospho-NME1 (pS120-pS122-pS125; 1:500) [117]. These antibodies were detected using horseradish peroxidase–conjugated anti-mouse (1:5000; Amersham) and anti-rabbit (1:3000; Amersham) antibodies. Anti-β-actin antibody (1:5000; Sigma-Aldrich) and anti-α-Tubulin (1:3000; Abcam) were used as controls for equal loading.

Quantitative real-time polymerase chain reaction (qRT-PCR)

Total RNA was isolated from cells using Trizol reagent (Invitrogen) according to the manufacturer protocol. cDNA was synthesized by random hexamers with iScript cDNA synthesis kits (Bio-Rad), according to the protocols supplied by Bio-Rad. After digestion with DNAse RNAse-free, two micrograms of total RNA in 20 µl was used in each reaction. qRT-PCR was performed using the SYBR Green PCR Master Mix (Applied Biosystems) and the Applied Biosystems Model 7900HT sequence detection system, according to the protocols supplied by Applied Biosystems. The primers were designed with the Primer Express 2.1 program (Applied Biosystems). All qRT-PCRs were performed in duplicate, with 50 ng ss-cDNA used in each 10-µl reaction. β-actin mRNA was used to normalize the mRNA concentrations. For statistical analysis of gene expression data, the relative expression $2^{-\Delta Ct} \pm$ SD and the mean fold change = $2^{-(\text{average } \Delta\Delta Ct)} \pm$ SD were calculated using the mean difference in the ΔCt between the genes and the internal control. The ΔCt was calculated using the differences in the mean Ct between the genes and the internal control.

In-vivo mouse experiments

Mice experiments were approved by "The Institutional Animal Care and Ethical Committee of CEINGE–Federico II University of Naples (Protocol 29, September 30, 2012; Dipartimento Sanità Pubblica Veterinaria D.L. 116/92).

Immunocompetent orthotopic xenograft mice models of TNBC using 4T1 cells

Seven-week old female immunocompetent BalbC were anesthetized with Ketamine/Xylazine (87.5 mg/kg, 12.5 mg/kg, respectively), and then had 2.5 x 10^5 4T1 cells of Prune-1 silenced, EV clones or 4T1-LUC cells (stably expressing Firefly luciferase gene) implanted into the VIII right-side mammary gland. Seven days after the implantation of the cells, the mice were imaged, and tumour growth was evaluated by bioluminescence acquisition using an imaging system (IVIS 3D Illumina; Xenogen/ Caliper), as described by Asadzedeh et al., [144]. Briefly, for the acquisitions, the mice were anaesthetised by inhalational of isofluorane, and the D-luciferin (122799; PerkinElmer) (15 mg/mL stock) was injected intraperitoneally (100 µL per 10 g body weight). At 5 min from the luciferin injection, the mice were imaged for 1.5 min. Several acquisitions were made per mouse until each mouse reached its peak of photon emission. Then five total

acquisitions (weekly, over a total of 28 days of analysis) near to the peak value for each mouse were analysed. To quantify the bioluminescence, the integrated fluxes of photons (ph/s) within each area of interest were determined using the Living Images Software Package 3.2 (Xenogen-Perkin Elmer).

For AA7.1 *in-vivo* treatment, starting after 7 days from tumour implantation (i.e., once the tumours were established) the mice (grouped according to their bioluminescence values) were injected intraperitoneally with AA7.1 at 60 mg/kg/day) or with PBS/PEG as the vehicle control, for 5

days/week (2 injections/day) for 4 weeks. The tumour growth was monitored every 7 days by both BLI acquisition. The means ±SE of the photon integrated fluxes were calculated for each experimental point. At the end of the experiments, primary tumours were dissected out and embedded in paraffin for IHC analyses.

Orthotopic xenograft mice models of TNBC in athymic nude mice using MMTV-Prune1/Wnt1 and MMTV-Wnt1 cells

Four-week old female Athymic nude mice were anesthetized with Ketamine/Xylazine (87.5 mg/kg, 12.5 mg/kg, respectively) and 1 x 10^5 MMTV-Prune1/Wnt1 or MMTV-Wnt1 cells were implanted into the VIII right-side mammary gland. Cell implantation was monitored by bioluminescence imaging (BLI) acquisition using an IVIS 3D Illumina Imaging System (Xenogen/Caliper). After 1 month from tumorigenic cells implantation (T0), the xenografted mice were injected with a fluorescent imaging probe (XenoLight RediJect 2-DeoxyGlucosone [DG] 750; or DG-750; Perkin Elmer) for *in vivo/ex vivo* targeting of tumours that typically exhibits elevated glucose uptake rate in comparison to surrounding tissues. The xenografted mice injected with DG-750 were sacrified after 6 hours (in order to achieve maximum glucose targeting and enhanced tumour uptake) to perform *ex vivo* fluorescence imaging in living tissues using an imaging system (IVIS 3D Illumina; Xenogen/Caliper). At the end of the experiments, primary tumours and lungs were dissected out and embedded in paraffin for IHC analyses.

Exosomes isolation

Exosomes were purified from media culture supernatants of MMTV-Prune1/Wnt1 and MMTV-Wnt1 following the methodology described by Thery et al.,(2006).

Briefly, MMTV-Prune1/Wnt1 and MMTV-Wnt1 cells were grown in "exosome-depleted medium" (obtained via via overnight centrifugation at 100,000 x g) until they reached 80% confluency. After 48 hours, the conditioned medium was collected by centrifugation at at 300 × g, for 10 minutes. The supernatant was then pre-cleared to remove cells, dead cells, and cellular debris via centrigufation at 2,000 x g, for 20 minutes. The exosomes were then obtained via ultracentrifugation at Centrifuge 100,000 x g, for 70 minutes. After washing with Phosphate-buffered saline (PBS), exosomes were further purified using ExoQuick Exosome Precipitation Solution (System Biosciences Cat.# EXOQ5A-1) by incubation for 12 hours and centrigugation at 1,500 x g, for 60 minutes.

Generation of MMTV-Prune-1-Flag construct

The pMSG vector (Pharmacia Biotech Sevrage, Uppsala, Sweden) contains the mouse Mammary Tumour Virus Long Terminal Repeat (MMTV-LTR) upstream of a polylinker. The human Prune-1

cDNA, containing the complete protein coding region with the FLAG tag fused in frame at the Carboxyl-Terminus terminal was cloned into polylinker sites of pMSG in sense orientation relative to the MMTV-LTR and the downstream the SV-40 early promoter. The resultant construct was designated pMSG-MMTV-Prune-1-FLAG.

In order to generate MMTV-Prune-1 transgenic animals in FVB background, pronuclear injections of the fertilised oocytes and embryo transfer to the pseudopregnant females was carried out.

Male MMTV-Wnt-1 mice (FVB) were crossed with MMTV-Prune-1 (FVB) to generate the double transgenic MMTV-Prune1/Wnt1 mouse model.

PET/CT imaging

Lung metastases of MMTV-Prune1/Wnt1 mice were also detected by performing X-ray computed tomography (CT) following the methodology described by Gargiulo et al., (2012).

Statistical analysis

The data representative of three independent experiments were analysed using unpaired twotailed t-tests (Student's t-tests). For all Figures, error bars represent standard deviation (SD) of the mean, and $p \leq 0.05$ was considered significant.

In-vivo human experiments

Patients and specimens: From 2003 to 2010, 157 patients who underwent a mastectomy, quadrantectomy or metastectomy at the National Cancer Institute "Giovanni Pascale" of Naples, Italy, were enrolled into this study. In our institution, the percentage of tumors classified as TNBC is approximately 15-19% of the total number of breast cancer surgeries. All cases of TNBC and non-TNBC samples were reviewed according to WHO classification criteria, using standard tissue sections and appropriate IHC slides. Medical records for all cases of TNBC and non-TNBC samples were reviewed for clinical information, including histologic parameters that were determined from the H&E slides. The following clinical and pathological parameters were evaluated for each tumor included in the study: patient age at initial diagnosis, tumor size, histologic subtype, histologic grade, nuclear grade, nodal status, number of positive lymph nodes, tumor stage, tumor recurrence or distant metastasis, and type of surgery (for tumor removal). In addition, all specimens were characterized for all routine diagnostic immunophenotypic parameters.

TMA building: one hundred fifty-seven patients were used for a Tissue Micro-Array (TMA) building, using the most representative areas from each single case. All tumours and controls were reviewed by

two experienced pathologists (MDB/GB). Discrepancies between two pathologists from the same case were resolved in a joint analysis of the cases.

IHC analysis: IHC staining was done on slides from formalin-fixed, paraffin embedded tissues, corresponding to TNBC TMA, to evaluate the expression of Prune-1, ER, PgR, c-Erb B2, Ki67, S100A4, pERK, NF-kB-p65-Ser311, CD68, CD163, CD11b, Granzyme B and FoxP3 markers. Slides were incubated with antibodies against routinely diagnostic markers: mouse anti-human ERα (1:35; DAKO), mouse anti-human PR (1:50; DAKO), rabbit anti-c-Erb B2 (1:300; DAKO), and mouse anti-human Ki67 (1:75; DAKO), and with primary antibodies listed as follow: rabbit anti-prune (1:200; made in home), rabbit anti-S100A4 (1:500; gift from Eugene Lukanidin), rabbit anti-pERK (1:700; Cell Signaling), rabbit anti-NFkB p65 (phospho S311) (1:400; Abcam), mouse anti-CD68 (prediluited, Ventana, Roche), mouse anti-CD163 (1:75; Novocastra), rabbit anti-CD11b (1:100; Abcam), rabbit anti-Granzyme B (prediluited, Cell Marque, Rocklin), mouse anti-FoxP3 (1:50; Abcam). The negative controls omitted the primary antibody. Detection was achieved with the Liquid DAB + Substrate Chromogen System (Dako). Sections were counterstained with hematoxylin and mounted. Results are interpreted using a light microscope.

Evaluation of IHC: antigen expression was evaluated independently by a pathologist using light microscopy. Observer was unaware of the clinical outcome. For each sample, at least five fields (inside the tumor and in the area exhibiting tumor invasion, 400X400) and >500 cells were analyzed. Using a semiquantitative scoring system microscopically and referring to each antigen scoring method in other studies, an observer evaluated the intensity, extent and subcellular distribution of Prune, ER, PgR, c-Erb B2, Ki67, S100A4, pERK, NF-kB p65 Ser311, CD68, CD163, CD11b, Granzyme B and FoxP3 markers. The cutoff used to distinguish "positive" from "negative" cases was ≥ 1% ER/PR positive tumor cells. IHC analyses of c-erbB-2 expression describe the intensity and staining pattern of tumor cells. Only membrane staining intensity and pattern were evaluated using the 0 to 3+ score as illustrated in the HercepTest kit scoring guidelines. The FDA-recognized test, the Herceptest™ (DAKO), describes four categories: no staining, or weak staining in fewer than 10% of the tumor cells (0); weak staining in part of the membrane in more than 10% of the tumor cells (1+); complete staining of the membrane with weak or moderate intensity in more than 10% of the neoplastic cells (2+); and strong staining in more than 10% (3+). Scores of 0 or 1+ were considered negative for *HER-2*/*neu* -expression, 2+ was uncertain, and 3+ was positive. Cases 2 + undergo FISH analysis.

For the proliferative index Ki67 was defined as the percentage of immunoreactive tumour cells out of the total number of cells. The percentage of positive cells per case was scored according to 2 different groups: group 1: ≤14% (low proliferative activity); group 2: >14% (high proliferative activity).

There are not standardized criteria for Prune-1, S100A4, pERK, NF-kB p65 Ser311, CD68, CD163, Granzyme B, CD11b and FoxP3 markers staining evaluation, thus we schematized our score evaluation follow: for nuclear NF-kB p65 Ser311 staining we considered both intensity (high-moderate/low/absent) and cell percentage positivity (0=negative/1=<50%/2=≥50%); for cytoplasmic prune staining we evaluated both intensity of reaction (high-moderate/low/absent) and cell percentage positivity (1=≤60%/2=>60%); we considered cell percentage positivity for nuclear FoxP3 (low=<4%/high=≥4%), for cytoplasmic S100A4 (0=negative/1=<50%/2=≥50%), for cytoplasmic pERK (0=negative/1=≤50%/2=>50%) and for cytoplasmic Granzyme B (low=<8%/high=>8%); we considered cell percentage positivity both in tumor and stromal cells for cytoplasmic CD68 and CD163 (Tumor:0=negative/1=<10%/2=10-50%; Stroma: low=<50%/high=>50%).

Statistical analysis: The association between prune expression with clinic-pathological parameters and the other markers was conducted using the χ^2 or the Spearman correlation test when appropriate. The Pearson χ^2 test was used to determine whether a relationship exists between the variables included in the study. The level of significance was defined as $p<0.05$. Overall survival (OS) and failure-free survival (FFS) curves were calculated using the Kaplan-Meier method. All the statistical analyses were carried out using the Statistical Package for Social Science v. 20 software (SPSS Inc., Chicago, IL, USA). OS was defined as the time from diagnosis (first biopsy) to death by any cause or until the most recent follow-up. FFS was measured as the time from diagnosis to the occurrence of progression, relapse after complete remission, or death from any cause. FFS had a value of zero for patients who did not achieve complete remission. The follow-up duration was five years.

3. RESULTS

3.1 Prune-1 overexpression in Triple Negative Breast Cancer (TNBC)

Prune-1 protein was previously identified as promoter of both tumour invasiveness and metastases in several tumours [23], [24], [36], [45], [110], with these functions being mainly due to its interactions with specific protein partners, including NDPK-A [39, 45], and GSK-3β [36]. Through these interactions, Prune-1 modulates signaling cascades, including canonical WNT and TGF-β pathways [25], [28], which are involved in BC progression and metastases [59] [157], [158].

Here, to better investigate its role in BC, gene-expression data from different public BC datasets were analysed using R2 Genomics Analysis and Visualisation Platform (http://r2.amc.nl). These data show that Prune-1 expression is higher in all BC samples compared to normal epithelium (n=1779, $p=3.0e^{-169}$; Figure 10), thus confirming the overexpression of Prune-1 in BC. Interestingly, the highest expression of Prune-1 is found in the public TNBC dataset (*i.e.,* Brown [111], n=198; as shown within the red dotted line in Figure 10), thus suggesting a potential role in this highly metastatic BC subgroup with the worst prognosis.

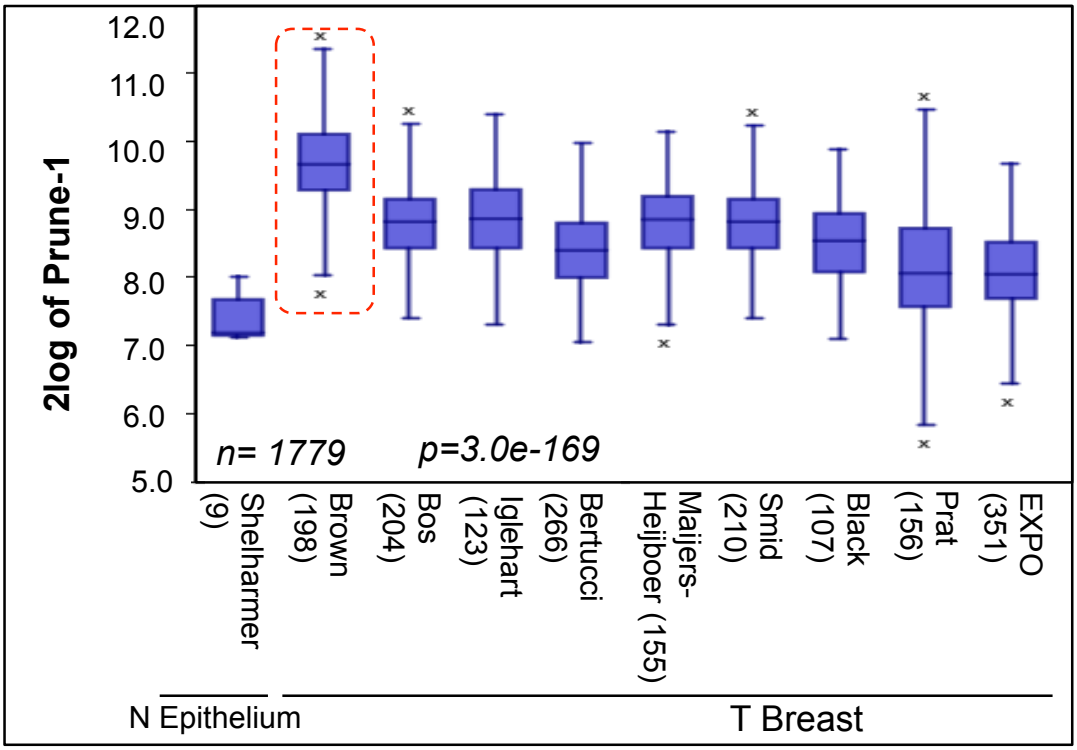

Figure 10: Prune-1 overexpression in Triple Negative Breast Cancer. RNA log2 expression analysis of Prune-1 levels of primary BC samples across different publically available datasets, compared with normal Epithelium (N Epithelium; Shelharmer dataset). Data from 10 independent public-domain BC gene-expression datasets are shown. Overexpression of Prune-1 in all BC samples compared to normal epithelium is shown. Higher Prune-1 expression levels are found in Triple Negative Breast Cancer (TNBC) samples (*i.e.,* Brown; Burstein *et al.,* 2015), as shown within the red dashed line (n=1779; p=3.0e-169).

The peculiarity of TNBC is its association with the negativity of ER/PgR/HER2 status [112], as confirmed in Figure 11.

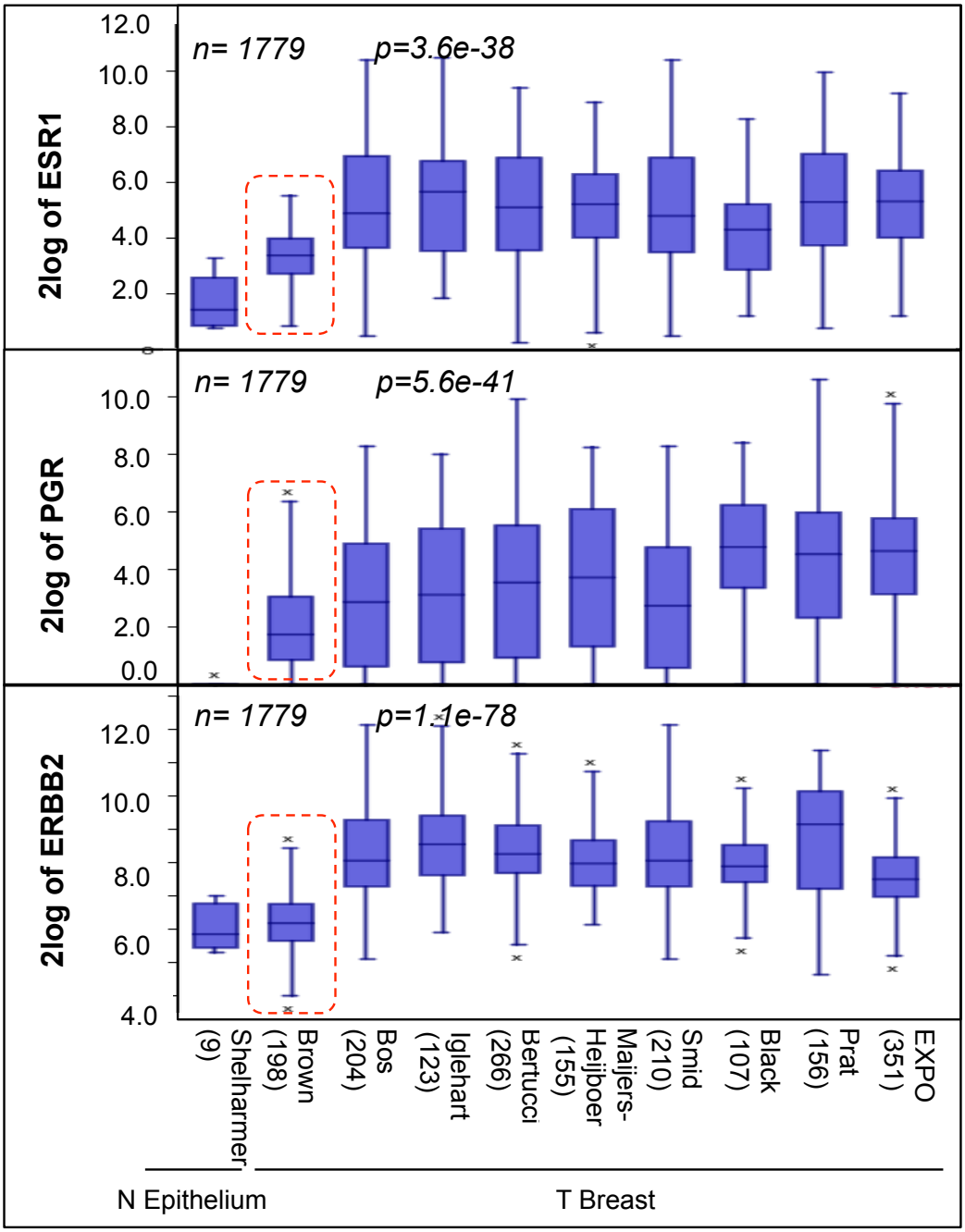

Figure 11: Lower expression levels of PR, PgR and HER2 in Triple Negative Breast Cancer. RNA log2 expression analysis of ER (ESR1), PgR and HER2 (ERBB2) levels of primary BC samples across different publically available datasets, compared with normal Epithelium (N Epithelium). Data from 10 independent public-domain BC gene-expression datasets are shown. Lower ER, PgR and HER2 expression levels are found in Triple Negative Breast Cancer (TNBC) samples (*i.e.,* Brown; Burstein *et al.,* 2015) as shown within the red dashed lines (n=1779; ER: p=3.6e-38; PgR: p=5.6e-41). HER2: p=1.1e-78. ER, Estrogen receptor; PgR: Progesteron receptor; HER2, Human epidermal growth factor.

In order to provide deep insights into the role of Prune-1 in TNBC, its potential association with the Estrogens/Progesteron Receptors status (*i.e.,* ER/PgR/HER2) was investigated. For this purpose, we

used the publicly accessible dataset of "Tumor Breast Invasive Carcinoma" with gene expression data acquired from Cancer Genome Atlas (TCGA) of BC cohort (n=1097). For this analysis, BC samples were stratified according to their ER, PgR, or HER2 score (as evaluated by immunohistochemistry, IHC), which ranges from 0 to 3^{+}, with 0 score indicating negativity. These data show higher expression levels of Prune-1 in BC samples with negative score for both ER and PR, and in those with score ranging from 0 to 1^{+} for HER2 status (as shown within the red dotted line in Figure 12). This further suggest the involvement of Prune-1 in TNBC.

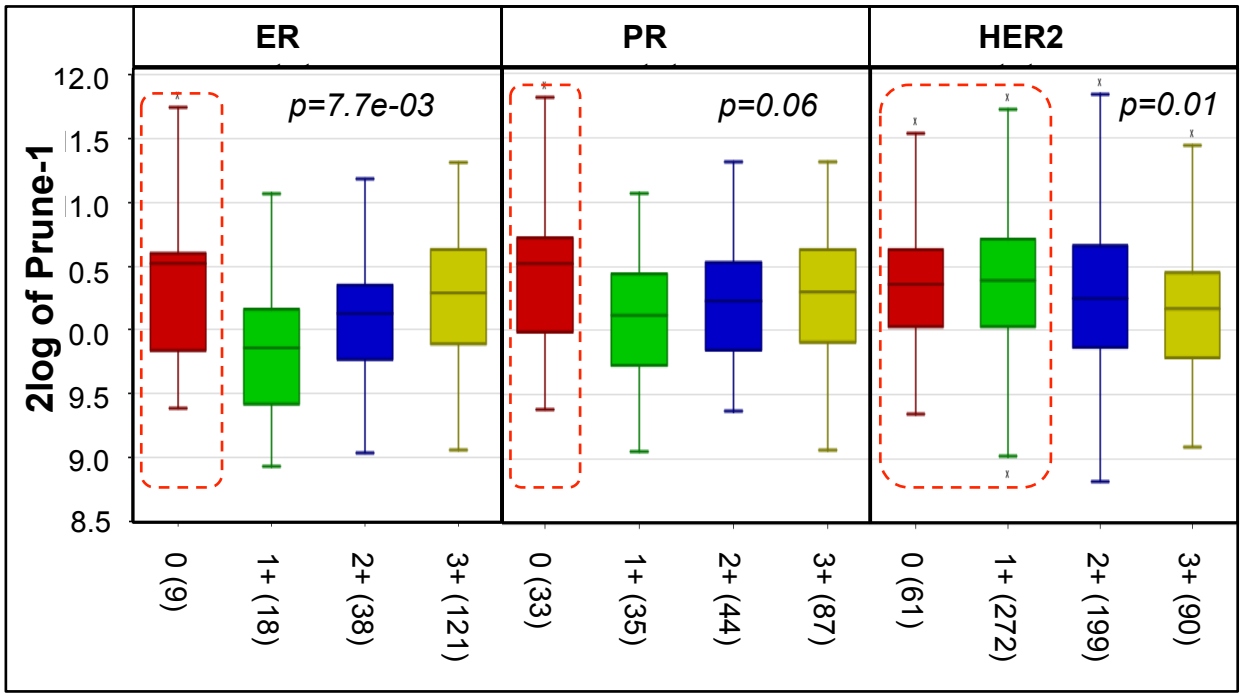

Figure 12: Prune-1 overexpression in ER^{-}/PgR^{-}/HER2^{-} Breast Cancer. RNA log2 expression of Prune-1 across primary BC grouped according to their Estrogens/Progesteron receptors (*i.e.,* ER, PrG, HER2) in the publically available dataset of "Tumor Breast Invasive Carcinoma" with gene expression data acquired from Cancer Genome Atlas (TCGA). Higher expression levels of Prune-1 in BC samples with negative score for both ER and PR, and in those with score ranging from 0 to 1+ for HER2 status. ER, Estrogen receptor; PgR, Progesterone receptor; HER2, human epidermal growth factor receptor 2.

To further support these data, Prune-1 protein expression was analyzed in human TNBC by performing IHC on Tissue Micro-Array (TMA), using a collection cohort of primary TNBC samples (n=157) derived from patients who underwent a mastectomy, quadrantectomy or metastectomy at the National Cancer Institute "Giovanni Pascale" of Naples (Italy) from 2003 to 2010 (in collaboration with Prof. Maurizio Di Bonito, Prof. Gerardo Botti, Dr. Monica Cantile and Dr. Francesca Collina; Istituto Tumori Napoli Fondazione G. Pascale, Naples). In our casuistry, 157 TNBC samples were included (11 lobular, 4 ductal-lobular, 9 medullary, 1 mucinous, 1 metaplastic, 128 invasive ductal breast carcinomas and 3 TNBC metastases). The age of patients ranged from 24–93 years, with an

average age of 57 years. Tumours larger than 2 cm were present in 53% (83/157) of patients and metastatic lymph nodes were found in 42.8% (66/154) of patients at surgery. Here are the percentages of tumor gradings: 86.6% (136/157) were grade 3; 12.1% (19/157) were grade 2; 1.3% (2/157) were grade 1. The expression of proliferation marker Ki67 was high (>14%) in 121/139 cases, and low (≤ 14%) in 18/139 cases.

Prune-1 protein expression was detected in 141/157 samples of our tissue cohort bank, excluding the samples that could not be assessed. In 14/141 samples (9.93%) there was a negative Prune-1 expression, in 54/141 samples (38.3%) there was a low Prune-1 expression, while in 73/141 specimens (51.77%) there was a moderate/high Prune-1 expression (Figure 13).

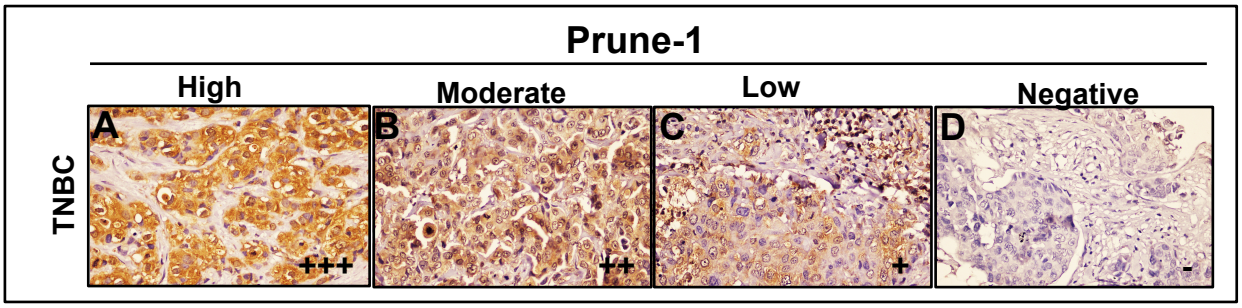

Figure 13: Prune-1 protein expression on human Triple Negative Breast Cancer (TNBC). Representative Prune-1 immunostaining from our TNBC tissue cohort (n=141) derived from patients who underwent a mastectomy, quadrantectomy or metastectomy at the National Cancer Institute "Giovanni Pascale" of Naples (Italy) from 2003 to 2010. **(A)** High immunopositivity (+++) for Prune-1 in TNBC cells (magnification 40X). **(B)** Moderate immunopositivity (++) for Prune-1 in TNBC cells (40X). **(C)** Low immunopositivity (+) for Prune-1 in TNBC cells (40X). **(D)** Immunonegativity (-) for Prune -1 in TNBC cells (40X). A moderate/high expression of Prune-1 protein levels is found in 73/141 specimens (51.77%), while a low Prune-1 expression is detected in 54/141 samples (38.3%). Only 14/141 samples (9.93%) presented undetectable levels of Prune-1.

These findings indicate that more than 50% of TNBC (*i.e.,* 51.77%) samples show overexpression of Prune-1, thus further confirming its involvement in this aggressive BC subgroup.

To better investigate and validate the role of Prune-1 in TNBC, its expression level was correlated to the clinic-pathological parameters of the patients from our cohort and to the expression protein levels of Ki-67 proliferation marker (Table 6). The statistical elaboration of Prune-1 protein expression analyses (based on the intensity of expression) with the other clinico-pathological parameters in our TNBC tissue cohort, indicates that Prune-1 is significantly associated with lymph node metastases (p=0.004) and with the proliferative index Ki67 (p=0.019). These data further support the overexpression of Prune-1 can predict those tumours with metastatic behavior pattern also in TNBC.

Table 6: The association between Prune-1 expression and the tumour characteristics of TNBC patients. The clinic-pathological parameters of the patients from our TNBC cohort gouped according to their Prune-1 protein expression levels are shown.

Clinic-pathological parameters		Prune-1*		P value
		Low	High	
Age	<40	8 (42,1%)	11 (57,9%)	0.834
	>40≤60	27 (48,2%)	29 (51,8%)	
	>60	31 (50%)	31 (50%)	
Histotype	IDC	51 (49,5%)	52 (50,5%)	0.610
	ILC	3 (37,5%)	5 (62,5%)	
	MC	4 (44,4%)	5 (55,6%)	
	MetC	0 (0%)	1 (100%)	
	MuC	1 (100%)	0 (0%)	
	MDLC	3 (75%)	1 (25%)	
Size	≤2 cm	30 (46,9%)	34 (53,1%)	0.961
	>2≤5	28 (49,1%)	29 (50,9%)	
	>5	6 (50%)	6 (50%)	
LMN**	Negative	44 (58,8%)	31 (41,2%)	0.004
	Positive	18 (34,5%)	36 (65,5%)	
Metastases	Negative	61 (49,2%)	63 (50,8%)	0.835
	Positive	6 (46,2%)	7 (53,8%)	
Grading	G1	1 (50%)	1 (50%)	0.138
	G2	9 (75%)	3 (25%)	
	G3	53 (44,9%)	65 (55,1%)	
Ki67**	<14%	11 (73,4%)	4 (26,6%)	0.019
	≥14%	44 (41,1%)	63 (58,9%)	

LMN, lymph node metastases; IDC, Invasive ductal carcinoma; ILC, invasive lobular carcinoma; MC, mucinous carcinoma; MetC, Metaplastic Carcinoma; MDLC, mixed IDC and ILC; G1, Grade 1 or low grade (sometimes also called well differentiated); G2, Grade 2 or intermediate/moderate grade (moderately differentiated); Grade 3 or high grade (poorly differentiated). '*' Prune-1 protein expression is based on the intensity of expression. '**' indicates statistical significant association (*i.e.,* $p<0.05$)

Furthermore, in order to gain insight into the function of Prune-1 in metastatic TNBC, the potential relationships between the protein and tumorigenic signaling pathways responsible for the aggressive behaviour of TNBC were also evaluated. For this purpose, we took into account the nuclear localization of MAPK and NF-kB effectors, due to their prognostic significance and their corrrelation with poor prognosis in TNBC [113], [114]. Our correlation studies show a statistically significant relationship between Prune-1 and both phosphorylated-ERK1/2 (phospho-[Thr202/Tyr204]-ERK1 and phospho-[Thr185/Tyr187]-ERK2; $p=0.029$) and phosphorylated-p65 (phospho-[Ser311]-p65; $p<0.00001$) as shown in Figure 14 and in Table 7. Furthermore, since a pro-metastatic role for S100 calcium-binding protein A4 (S100A4) has been described in TNBC [115], we also evaluated its potential correlation with Prune-1 protein levels in our patient tissue cohort. Moreover, a trend of

statistical correlation was found also between Prune-1 and S100A4 (p=0.084; Figure 14 and in Table 7).

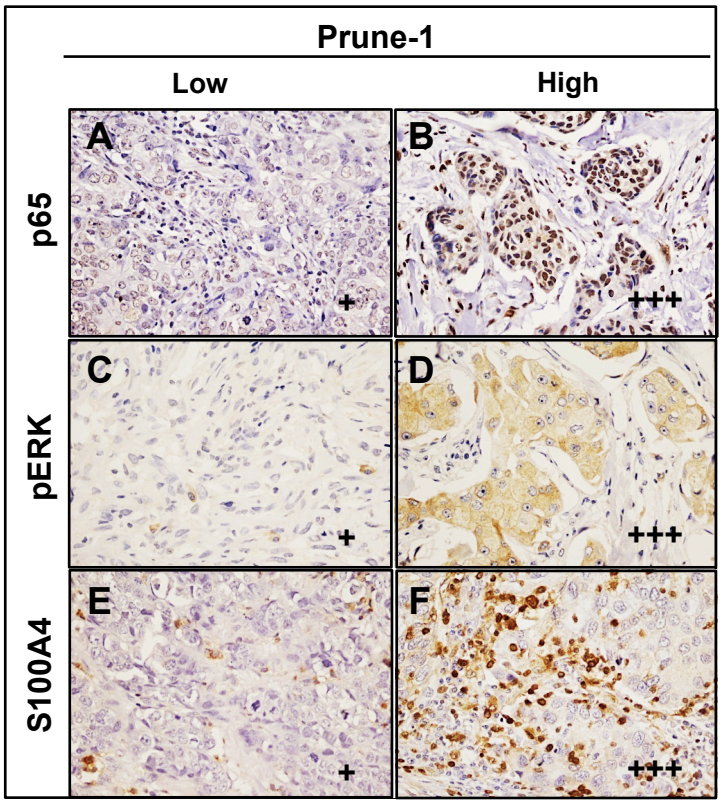

Figure 14: Activated MAPK and NF-kB signaling and overexpression of S100A4 in human TNBC with high expression of Prune-1. Representative immunostaining for phosphorylated-(Ser311)-p65 **(A-B)**, phosphorylated-ERK1/2 *(i.e.,* phospho-[Thr202/Tyr204]-ERK1 and phospho-[Thr185/Tyr187]-ERK2) **(C-D)** and S100A4 **(E-F)** from our TNBC tissue cohort grouped according to Prune-1 expression levels **(A)** High immunopositivity *(+++)* for phospho-p65 **(B)**, phospho-ERK1/2 **(D)** and S100A4 **(F)** is observed in TNBC samples with higher Prune-1 expression (magnification 40X). In contrast, low immunopositivity (+) for the same markers (*i.e.,* phospho-p65 in **[A]**, phospho-ERK1/2 in **[B]** and S100A4 in **[F])** is shown in TNBC specimens with lower Prune-1 expression (magnification 40X).

Table 7: Correlation analyses between Prune-1, nuclear effectors of MAPK and NF-kB signaling pathways, and pro-metastatic S100A4 in TNBC.

Signalling pathways		Prune-1*		P value
		Low	High	
Phospho-p65§	Negative Low High	20 (83,3%) 22 (56,4%) 21 (29,5%)	4 (16,7%) 17 (43,6%) 50 (70,5%)	<0,00001
Phospho-ERK1/2#	Negative Low High	39 (51,6%) 11 (68,8%) 14 (32,6%)	38 (49,4%) 5 (31,2%) 29 (67,4%)	0,029
S100A4	Negative Low High	37(39,4%) 7 (38,9%) 0 (0%)	57 (60,6%) 11 (61,1%) 8 (100%)	0,084

MAPK, mitogen-activated protein kinase; NF-kB, nuclear factor kappa-light-chain-enhancer of activated B cells; S100A4, S100 calcium-binding protein A4. '§' phosphorylated-(Ser311)-p65. '#' phosphorylated-(Thr202/Tyr204)-ERK1 and phosphorylated-(Thr185/Tyr187)-ERK2

These results highlight the involvement of Prune-1 in TNBC progression and metastases by activating MAPK signaling cascade, inflammatory pathways, such as NF-kB, and S100A4 signaling.

Because of the positive association between Prune-1 expression and inflammatory tumour environment (*i.e.,* activated NF-kB signaling as shown by phospho-p65 levels in Figure 20 and Table 10) in TNBC, we explored the potential correlation of Prune-1 expression with immune cell infiltration. For this purpose, we investigated the presence of immunosuppressive pro-tumorigenic M2-TAMs (*i.e.,* $CD68^+$, $CD163^+$), Tregs (*i.e.,* $FOXP3^+$) and Myeloid-Derived Suppressor Cells (MDSCs; *i.e.,* $Cd11b^+$). Our analyses, show that TNBC patients with higher Prune-1 protein levels are also characterized by an higher number of tumour infiltrating pro-tumorigenic M2-TAMs (*i.e.,* $CD68^+$, $CD163^+$), Tregs ($FOXP3^+$) and MDSCs ($CD11b^+$) than those with lower Prune-1 expression (CD68: p=0.02; CD163: p=0.08; FOXP3: p=0.08; CD11b: p=0.05; as shown in Figure 15).

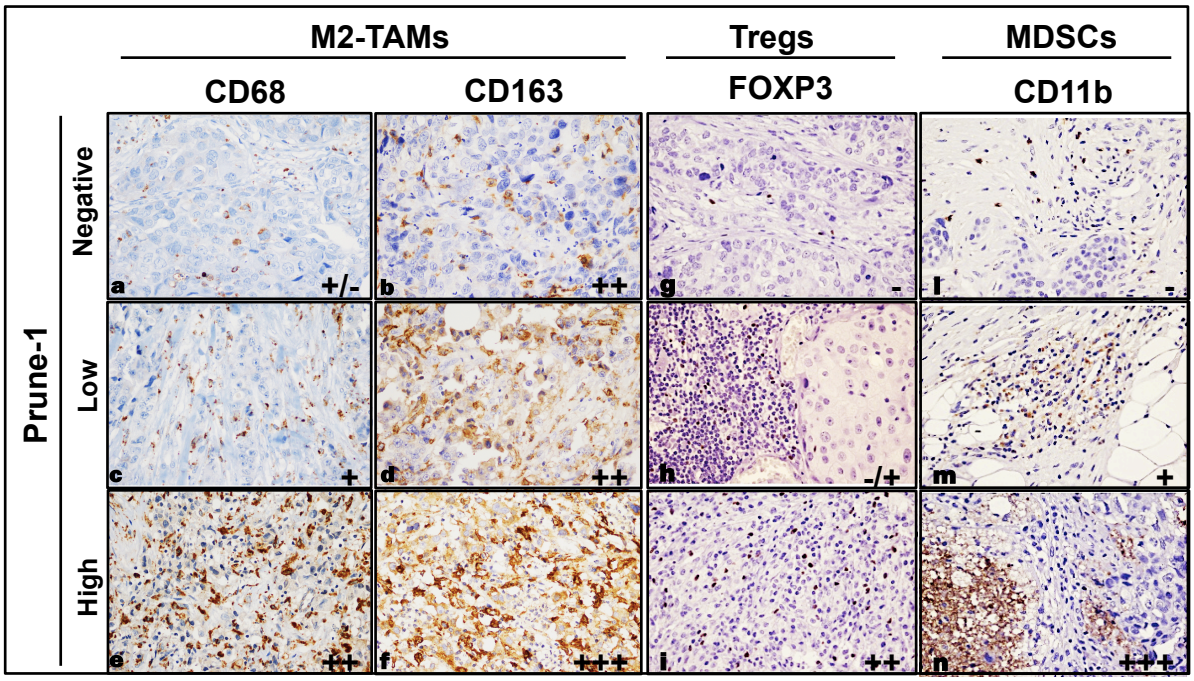

Figure 15: Increased number of infiltrating immunosuppressive M2-Tumour-Associated Macrophages (M2-TAMs), Regulatory-T cells (Tregs) and Myeloid-Derived Suppressor Cells (MDSCs) in human TNBC with high expression of Prune-1. Representative immunostaining for CD68 **(A-C-E)** and CD163 (as markers used for M2-TAMs; **[B, D, F]**, FOXP3 (as marker for Treg population and CD11b (a marker for MDSCs). **[G, H, I]**) from our TNBC tissue cohort grouped according to Prune-1 expression levels (*i.e.,* negative, low and high expression levels). Negative/Low immunopositivity for CD68 **(A)**, CD163 **(B)**, FOXP3 **(G)** and CD11b **(L)** was observed in those TNBC samples negative for Prune-1 expression (magnification 40X). Low/moderate immunopositivity for CD68 **(C)**, CD163 **(D),** FOXP3 **(H)** and CD11b **(M)** is found in those TNBC samples with low Prune-1 expression (magnification 40X). High immunopositivity for CD68 **(E)**, CD163 **(F)**, FOXP3 **(I)** and CD11b **(N)** was observed in those TNBC samples with higher Prune-1 expression (magnification 40X).

Altogether, these immunopathological clinical correlation data strongly indicate that Prune-1 is significantly associated with metastatic behaviour and proliferative index in TNBC patients by activating inflammatory pathways and recruiting immunesuppressive cells with anti-tumorigenic role within the tumour microenvironment.

For this purpose, we decided to focus on TAMs because, among the immune infiltrating cells, they have a strong prognostic significance in the subgroup of TNBC patients with the worst prognosis [72].

3.2 Canonical TGF-β signaling cascade in TNBC is enhanced by Prune-1

We have defined a novel role for Prune-1 as a promoter of the SMAD-mediated canonical TGF-β pathway in metastatic Medulloblastoma Group 3 [28]. In details, the activation levels of SMAD2 and SMAD3 were analyzed in terms of their phosphorylation status and subcellular distribution upon

Prune-1 overexpression in Medulloblastoma Group 3 cells (D283-Med cells). We found phosphorylated-Ser467-SMAD2 and phosphorylated-Ser423/425-SMAD3 protein levels increased with full-length Prune-1 in transfected D283-Med cells (Figure 16A, [28]). These findings suggested that this regulation occurs at the carboxyl-terminus region of Prune-1, that is responsible for the binding to NDPK-A. Then we used immunofluorescence microscopy to show that transient overexpression of Prune-1 increased the levels of the nuclear SMAD2/3 protein complex in HEK-293T cells, thus inducing their nuclear accumulation (positive control: SMAD2-transfected cells; Figure 16B; [28]). Overall, these data supported the concept that Prune-1 participates in the canonical TGF-β signalling cascade through nuclearization of the SMAD2/3 protein complex, as an action mediated by the carboxyl-terminal region of Prune-1, as the region of interaction with NDPK-A [46].

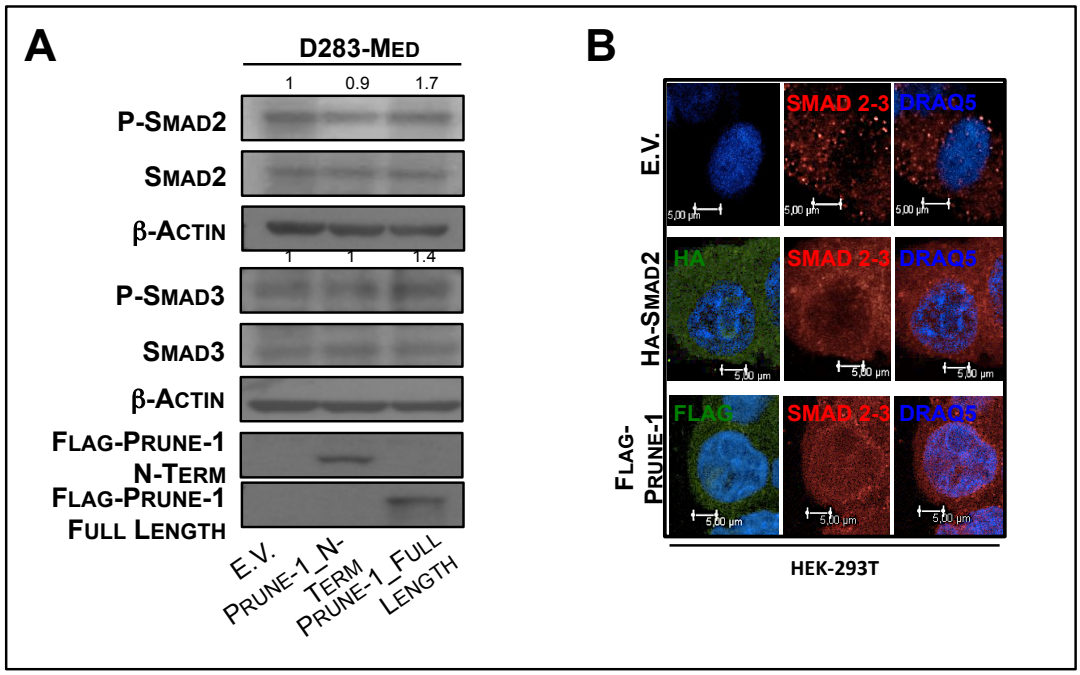

Figure 16: Prune-1 enhances canonical TGF-β pathway inducing phosphorylation and nuclearization of SMAD2/3 complex. (A) Representative immunoblot on cell lysates from Medulloblastoma$_{Group3}$ D283-Med cells transiently transfected with plasmids containing FLAG-tagged amino-terminus-Prune-1 (Prune-1_N-Term: 1-333 amino-acid residues), FLAG-tagged full-length Prune-1 (Prune-1_Full-Length; 1-453 amino-acid residues), and empty vector (E.V.) as negative control. The phosphorylated-Ser467-SMAD2 (1.7-fold) and phosphorylated-Ser423/425-SMAD3 (1.4-fold) protein levels increased in cells overexpressing full-length Prune-1 compared to those transfected with Prune-1_N-Term and empty vector (E.V.) plasmids. β-Actin levels were used as loading control. **(E)** Confocal immunofluorescence analysis showing subcellular distribution of R-SMADs (i.e., SMAD2/3; red) in HEK-293T cells transiently transfected with FLAG-tagged full-length Prune-1 (Prune-1_Full-Length; green), and the HA-SMAD2 (green), and empty vector (E.V.) plasmids (positive and negative controls, respectively). Similar nuclear staining for SMAD2/3 complex was shown in HEK-293T cells overexpressing Prune-1 and SMAD2, in comparison to empty vector control plasmid, which showed cytoplasmic distribution for R-SMADs. This thus indicated that Prune-1 can promote activation of the SMAD2/3-mediated TGF-β signalling cascade. Nuclei were stained with DRAQ5 (as blue staining). Scale bars, 5 mm. Assays were performed as independent triplicates, with photographs taken as representative of all of these experiments. From Ferrucci V *et al.,* Brain. 2018. *In press*.

We investigated further the role of Prune-1 on transcriptional activation through the Smad binding elements (SBEs) using HEK-293T cells, because of their negligible levels of endogenous PRUNE-1 expression [25]). These data indicated that PRUNE-1 enhances SMAD-transactivation induced by SMAD3 and SMAD4 (as positive controls; 1.3-fold; $p<0.0003$; Figure 17A; [28]). In summary, we defined a novel role for Prune-1 as a promoter of the SMAD2/3-mediated canonical TGF-β pathway in Medulloblastoma. Of note, NDPK-A has been reported to negatively regulate TGF-β signalling through a physical association with Serine/threonine kinase receptor associated protein (STRAP), which is known to prevent activation of SMAD effector proteins [28]. To gain insight into the mechanisms of PRUNE-1/ TGF-β axis regulation, we investigated the effects of NDPK-A on negative regulation of TGF-β signalling in Medulloblastoma. We found NDPK-A overexpression impaired the canonical TGF-β pathway, with reduction of SMAD transactivation (0.64-fold; $p<0.01$; Figure 17A; [28]) in HEK-293T cells. Furthermore, this overexpression also resulted in decreased levels of phosphorylated-Ser467-SMAD2 (Figure 17B; [28]),which thus confirmed the inhibitory effects of NDPK-A on the TGF-β canonical pathway also in a tumorigenic MBGroup3 cell line.

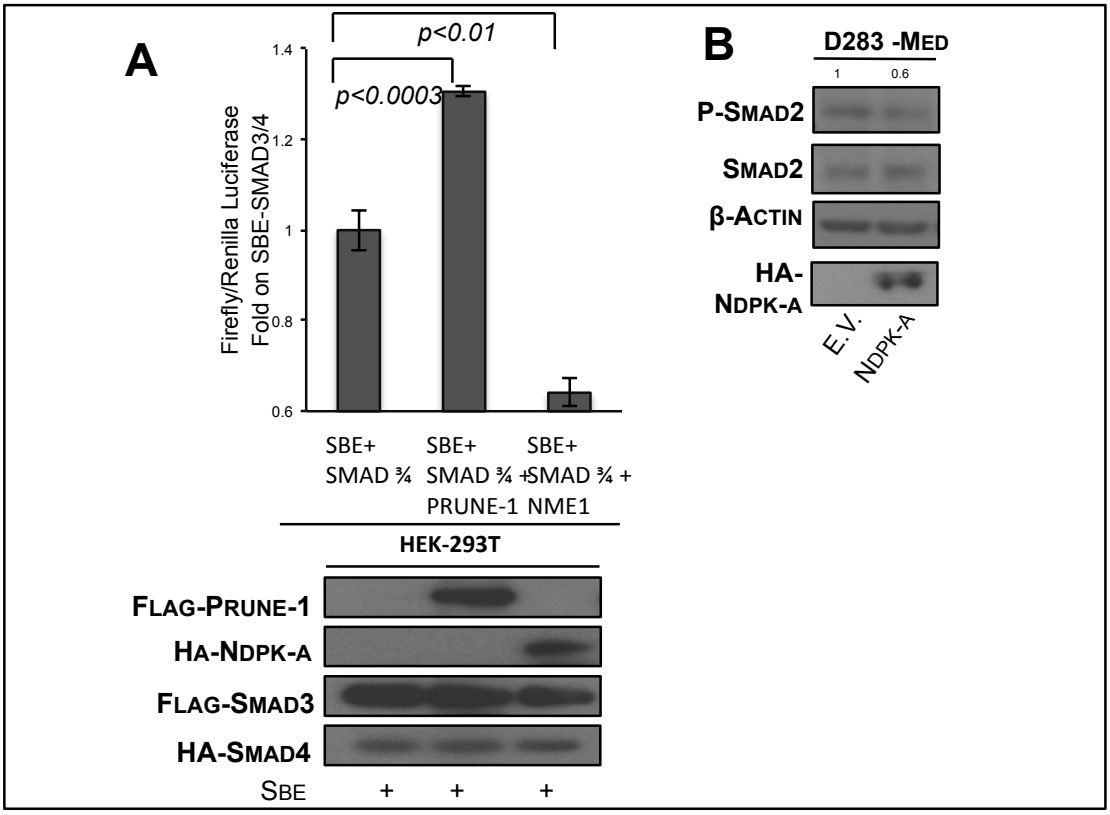

Figure 17: Prune-1 enhances canonical TGF-β pathway via NDPK-A binding (A) Transactivation assays in transiently transfected HEK-293T cells using firefly luciferase constructs that contained Smad binding elements (4× SBE, composed of the sequence 5'-CAGACA-3') in the backbone of the PGL4.14 plasmid, together with plasmid containing FLAG-tagged-SMAD3 and HA-tagged-SMAD4 in combination with FLAG-tagged full-length Prune-1 or HA-tagged-NDPK-A, as indicated. Firefly luciferase (Luc) activity is shown as fold of positive control. Prune-1 enhanced the TGF-β signalling cascade, as an increase in Luc activity (1.3-fold; $p<0.0003$). In contrast, NDPK-A inhibited TGF-β signalling activation, as seen here (0.6-fold; $p<0.01$). Bottom panel: Representative Western blots with indicated antibodies. Cell protein lysates from HEK-293T transfected with plasmids containing SMAD3 and SMAD4 in combination with PRUNE-1 or NDPK-A. **(B)** Cell protein lysates from $Medulloblastoma_{Group3}$ D283-Med cells transiently transfected with the NDPK-A plasmid. Protein levels of phospho-SMAD2 were decreased (0.6-fold) in D283-Med cells transfected with NDPK-A compared to empty vector (E.V.) as control. From Ferrucci V *et al.,* Brain. 2018. *In press.*

Overall our data showed that, Prune-1, through its binding to NDPK-A, impaired NDPK-A-inhibitory activity on TGF-β pathway, thus enhancing TGF-β signaling cascade, as defining a new signaling axis of metastatic behaviour of Medulloblastoma Group 3 (as shown in Figures 2-16-17; [28]).

Since TGF-β cascade has a crucial role in tumour invasion and metastasis also by modulating the cellular components of the tumour microenvironment, we investigated the expression levels of its downstream effectors (*i.e.,* SMAD2 and SMAD4; see additionaly [50]) in BC using gene-expression data from different public BC datasets. These analyses show that both SMAD2 and SMAD4

expression levels are higher in TNBC dataset (*i.e.,* Brown [111]; as shown within the red dotted line in Figure 18; SMAD2: p= $5.6e^{-230}$; SMAD4: p=$2.1e^{-86}$).

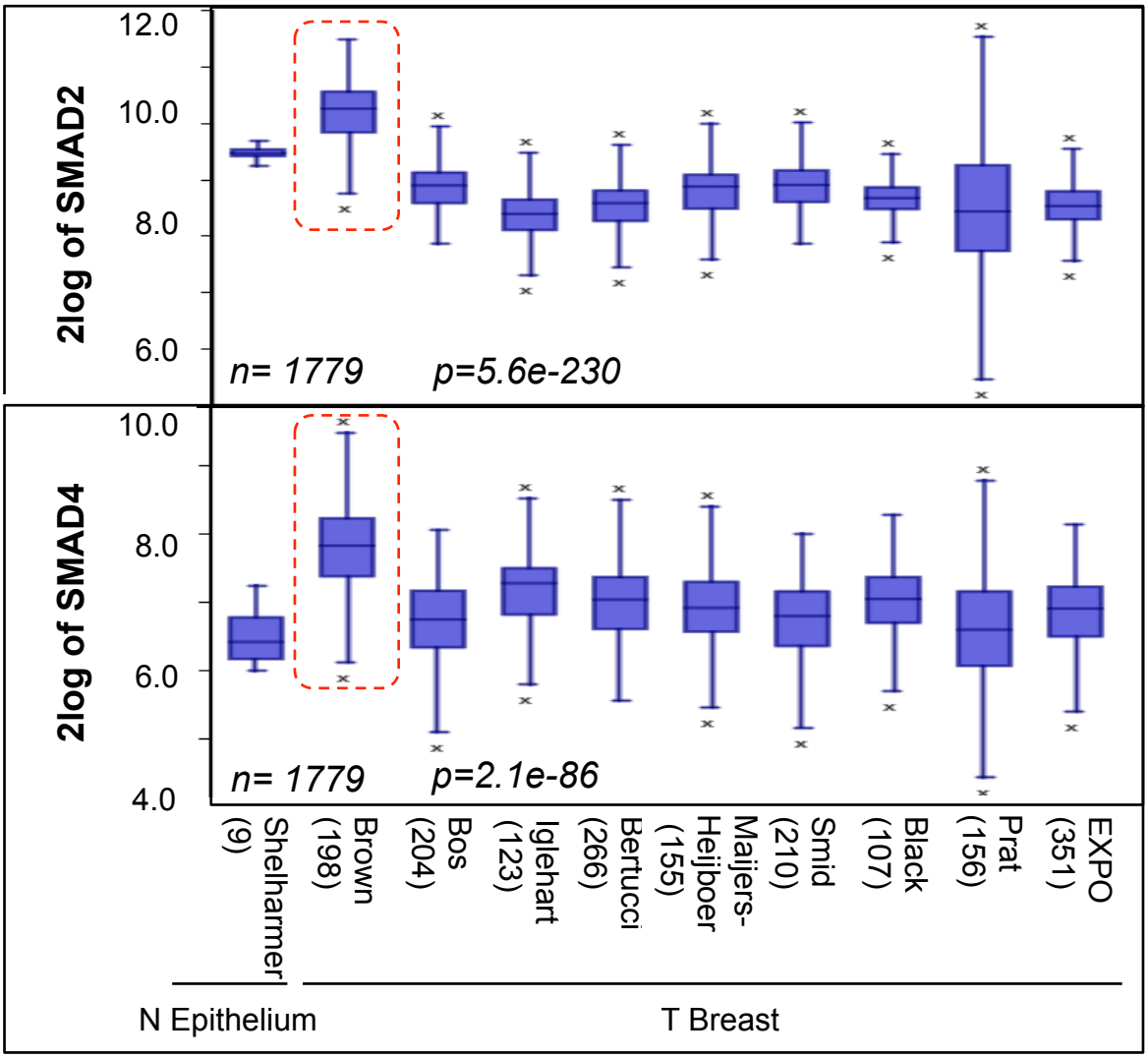

Figure 18: Overexpression of SMAD2 and SMAD4 in Triple Negative Breast Cancer. RNA log2 expression analysis of SMAD2 **(Upper panel)** and SMAD4 **(Bottom panel)** levels of primary BC samples across different publically available datasets, compared with normal Epithelium (N Epithelium). Data from 10 independent public-domain BC gene-expression datasets are shown. Overexpression of both SMAD2 and SMAD4 is found in Triple negative Breast Cancer (TNBC) samples (*i.e.,* Brown; Burstein *et al.,* 2015) n=1779; SMAD2: p=5.6e-230; SMAD4: p= 2.1e-86.

These data altogether are indicating a potential action of Prune-1 in TNBC occurring thought TGF-β canonical signaling pathways (*i.e.,* SMAD2 and SMAD4).

To better dissect this hypothesis, further correlation analyses between Prune-1, SMAD2 and SMAD4 in BC samples stratified according to their Estrogens/Progesteron receptor status were performed using gene expression data acquired from publicly accessible cohort of BC samples (n=1097) logged in TCGA (as shown in Table 8).

Table 8: Gene expression correlation analyses between Prune-1, SMAD2 and SMAD4 in Breast Cancer samples stratified according to their Estrogens/ Progesteron receptor status.

PgR, ER, HER2 status	Variable 1	Variable 2	r-value	p-value
PgR negative (n=344)	PRUNE-1	SMAD2	0.35	$2.3e^{-11}$
		SMAD4	0.328	$4.6e^{-10}$
ER negative (n=238)	PRUNE-1	SMAD2	0.35	$2.8e^{-08}$
		SMAD4	0.308	$1.3e^{-06}$
HER2 negative (n=563)	PRUNE-1	SMAD2	0.209	$5.3e^{-07}$
		SMAD4	0.193	$4.1e^{-06}$

PgR, Progesteron receptor; ER, Estrogen receptor; HER2, Human epidermal growth factor 2. The data were obtained from "R2-Genomic and Visualization Platform" using "Tumor Breast Invasive Carcinoma" dataset containing gene expression data acquired from publicly accessible Cancer Genome Atlas (TCGA) breast cancer cohort (n=1097 breast cancer samples logged in TCGA).

In summary, our analyses show that Prune-1 positively correlated to both SMAD2 and SMAD4 in those BC with PgR, ER and HER2 negative status (r-value ranging from 0.19 to 0.35, as reported in Table 9). Overall, Prune-1 positively correlated to TGF-β downstream effectors in TNBC. These findings provide sufficient evidences that Prune-1 may act via canonical TGF-β cascade also in TNBC. Prune-1/NDPK-A protein complex is involved in metastatic dissemination in several tumours, including BC [101, 105, 123, 125].

To determine whether Prune-1 takes part to TGF-β signaling through NDPK-A, we investigated the gene expression of both Prune-1 and NDPK-A (or NME1) in TNBC dataset (*i.e.,* Brown). For this purpose, TNBC samples were grouped according to their subtypes (*i.e.,* immune-activated, immune-suppressed, Luminal Androgen Receptor and Mesenchymal). Among TNBC samples, both genes are found overxpressed in immune-activated, followed by immune-suppressed TNBC subtype (n=198; Prune-1, $p=1.2e^{-07}$; NDPK-A, $p=4.4e^{-05}$; as reported in Figure 19).

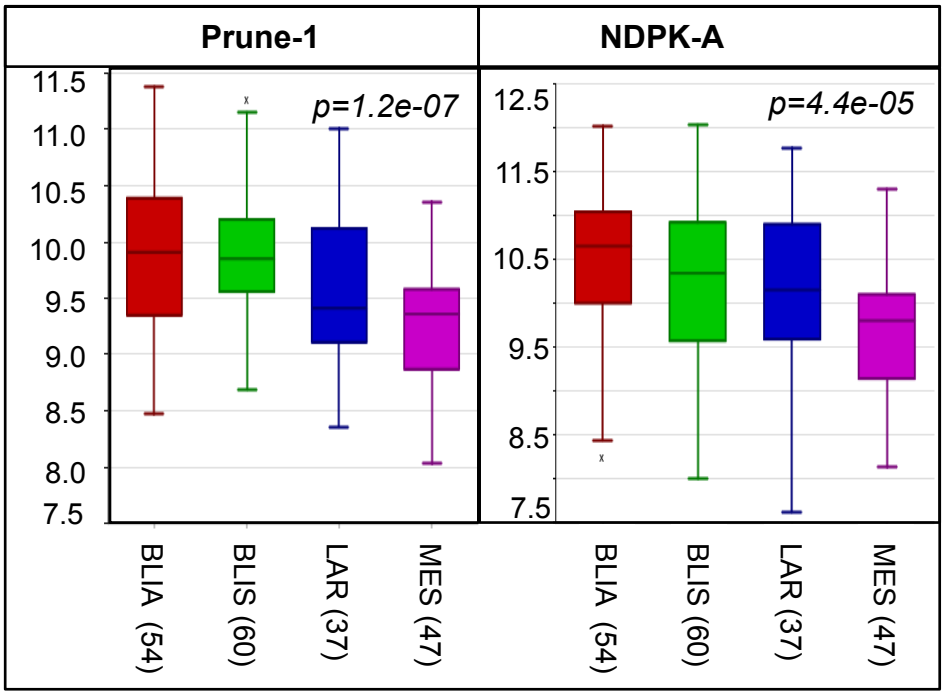

Figure 19: Prune-1 and NDPK-A are overexpressed in "immune-activated" and "immune-suppressed" TNBC subtype. RNA log2 expression of Prune-1 and NDPK-A (or NME1) across primary TNBC grouped according to their subtype in the public available Brown dataset. Higher expression levels of Prune-1 and NDPK-A are found within "immune-activated" (*i.e.,* BLIA; red box) and "immune-suppressed" (*i.e.,* BLIS; Green box) Triple Negative Breast Cancer subtype compared to those belonging to Luminal (*i.e.,* LAR; Blue box) or Mesenchymal (*i.e.,* MES; Purple box) subtype. Prune-1, $p=1.2e^{-07}$; NDPK-A, $p=4.4e^{-05}$. BLIA, Basal-like_immune-activated; BLIS, Basal-like_immune-suppressed; LAR, Luminal-Androgen receptor; MES, Mesenchymal.

These findings indicate a potential involvement of both Prune-1 and NDPK-A in the tumour microenvironment, in terms of immune infiltrating cells.

These results, further support the hypothesis that Prune-1 can act in concert with NDPK-A, to enhance the canonical TGF-β signaling cascade (mainly via SMAD2/4) in order to generate an immune-suppressive tumour environment, thus enhancing tumour progression and metastatic spread in TNBC.

For the above reasons, we then investigated whether Prune-1 influences TGF-β axis in TNBC cells. For this purpose, we used murine 4T1 cell lines, as cellular model of metastatic TNBC, to generate both Prune-1-overexpressing- and Prune-1-silenced- stable clones [116]. The reason of creating Prune-1-overexpressing cell clones is related to avoid feedback loops due to the regulatory actions of other transcription factors on Prune-1 endogenous promoter. As such, Prune-1 cDNA was driven by a CMV promoter.

We analyzed by Western blotting the potential Prune-1-induced perturbations of TGF-β signaling pathways in these 4T1 clones. For this purpose, the expression levels and the phosphorylation status of SMAD2 (on Serine 467 amino acid residue), which is the main effectors of canonical TGF-β cascade, were investigated. As shown in Figure 20A, decreased levels of phosphorylated-Ser467-SMAD2

(phospho-Ser467-SMAD2) was found in Prune-1-silenced 4T1 clones; In the same manner, an increase of pospho-Ser467-SMAD2 was observed in Prune-1-overexpressing 4T1 clones (Figure 20B) as compared to control clones (*i.e.,* Empty vector [E.V.] clones**)**.

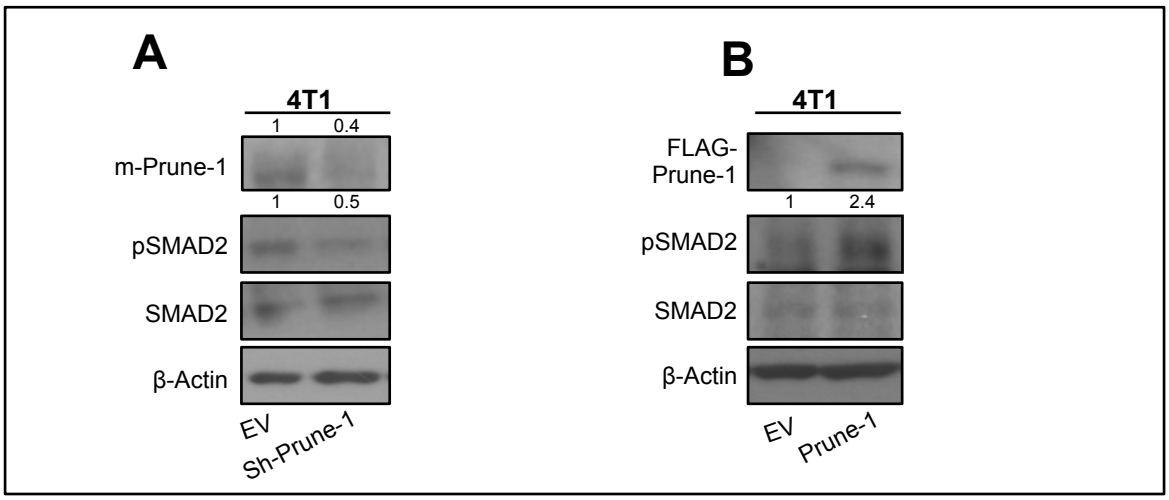

Figure 20: Prune-1 promotes TGF-β signaling pathway in TNBC 4T1 cells *in vitro*. Immunoblotting for the indicated proteins in Prune-1 silenced **(A)** and Prune-1-overexpressing **(B)** 4T1 stable clones. Empty vector (EV) 4T1 clones were used as negative control. Down- and up-regulation of phospho-Ser467-SMAD2 was shown in Prune-1 silenced (0.5-fold) **(A)** and Prune-1-overexpressing (2.4-fold) **(B)** 4T1 cells, respectively. The densitometer analyses for the proteins were also shown. β-Actin levels were used as loading control.

Overall, these results confirm that Prune-1 is responsible for the enhancement of canonical TGF-β pathways (SMAD2-mediated) also in this TNBC cellular model (*i.e.,* 4T1 cells).

Previous reports have shown that Prune-1 binds GSK-3β [36], the major regulator of Wnt canonical signaling pathway, and its minimal region of interaction was also identified by NMR studies [46]. Moreover, Prune-1 was found to enhance the canonical Wnt signaling pathway activation in NSCLC [25].

For the above reasons, we decided to verify if Wnt cascade is also affected by Prune-1 in TNBC. For this purpose, we investigated the β-catenin protein levels in our 4T1 stable clones by Western blotting analyses (as reported in Figure 21). Our data show reduced actived-β-catenin (*i.e.,* dephosphorylated on Serine 37 and/or Threonine 41 amino acid residues) protein levels in Prune-1-silenced 4T1 clones (Figure 19A); In contrast, increased levels of actived-β-catenin was found in Prune-1 overexpressing 4T1 cell clones (Figure 19B). These results thus confirm the ability of Prune-1 to enhance canonical Wnt signaling cascade also in TNBC cells.

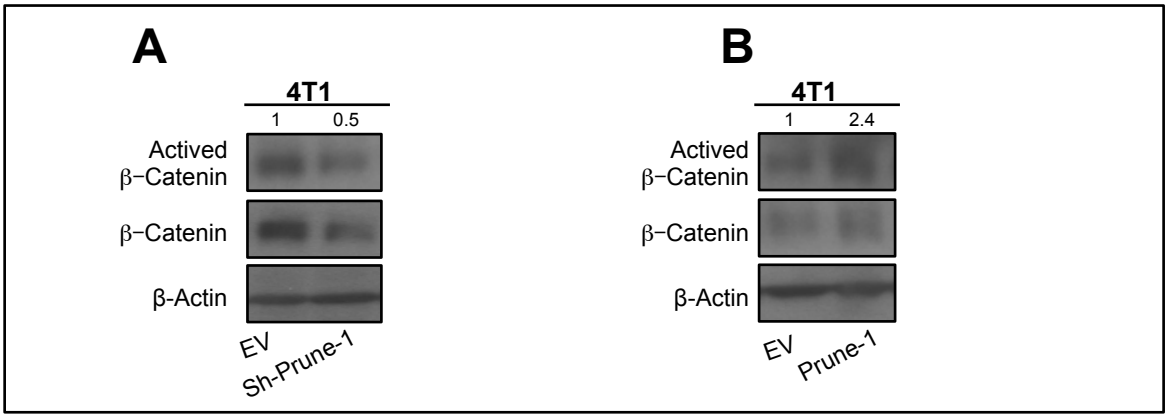

Figure 21: Prune-1 promotes canonical Wnt signaling pathways in TNBC 4T1 cells *in vitro*. Immunoblotting for the indicated proteins in Prune-1 silenced **(A)** and Prune-1-overexpressing **(B)** 4T1 stable clones. Empty vector (EV) 4T1 clones were used as negative control. Down- and up-regulation of actived-β-catenin was shown in Prune-1 silenced (0.5-fold) **(A)** and Prune-1-overexpressing (2.4-fold) **(B)** 4T1 cells, respectively. The densitometer analyses for the proteins were also shown. β-Actin levels were used as loading control.

In summary, these results showed that Prune-1 enhances TGF-β and Wnt signaling pathways activation *in vitro* using 4T1 cells as model of metastatic TNBC.

3.3 Prune-1 takes part to the communication between TNBC cells and macrophages *in vitro*

It is well established that the tumorigenic cells and immune cells within the tumor microenvironment communicate with each other, through extracellular mediators (*e.g.,* cytokines and exosomes). In fact, cancer cells in the tumour microenvironment secrete chemoattractant factors for immune cells.

Of note, Prune-1 was reported with the ability to induce Wnt signaling in paracrine manner via Wnt3a cytokine secretion, thus suggesting a potential role in entracellular environment [25]. Of importance, we found Prune-1 to be positively correlated with infiltrating immune cells (mainly M2-TAMs) in our TNBC samples cohort.

In order to assess if Prune-1 overexpression is responsible for the intratumoural increase of M2-TAMs, we investigated the potential involvement of Prune-1 in the crosstalk between TNBC cells and macrophages *in vitro* (in terms of activation and recruitment of these immune cells) using 4T1 stable cell clones (as cellular model for TNBC) and murine macrophages J774A.1 (*i.e.,* J774; #ATCC-TIB-67; [117]) and/or RAW-264.7 (*i.e.,* RAW-264; #ATCC-TIB-71; [118]). For this purpose, the conditioned media from 4T1 cell clones (collected after 24 hours) were used to treat macrophages *in vitro* and their subsequent activation was evaluated by verifying the phosphorilation status of STAT3 because of its prominent role during macrophages activation and M1-M2 polarization [119]. More in details, J774 or RAW-264 were starved for 6 hours in serum free media and then grown for 30 minutes

in conditioned media previously collected (after 24 hours) from Prune-1-silenced and control (Empty Vector, EV) 4T1 clones, as summarized in Figure 22A. Untreated macrophages were used as negative control. After 30 minutes of culture in those conditioned media, the expression levels and the phosphorylation status of STAT3 protein from macrophages (J774 and RAW-264) were assessed. STAT3 activation was analysed by immunoblotting for phosphorylation of STAT3 at Tyrosine 705 (*i.e.,* pY705-STAT3, required for dimerization and nuclear translocation, [120]), and Serine 727 (*i.e.,* pS727-STAT3, linked to increased STAT3 transactivation, [121]) amino acid residues. As shown in Figure 22B, a significantly decreased phospho-STAT3/STAT3 ratio was observed for both phosphorylations in both macrophage types cultured in media from Prune-1-silenced 4T1 clones compared to those cultured in media from control clones or untreated macrophages.

These results suggest that the overexpression of Prune-1 in TNBC cells has a role in the intercellular communication between tumorigenic cells and macrophages to induce activation and polarization of macrophages via STAT3 signaling.

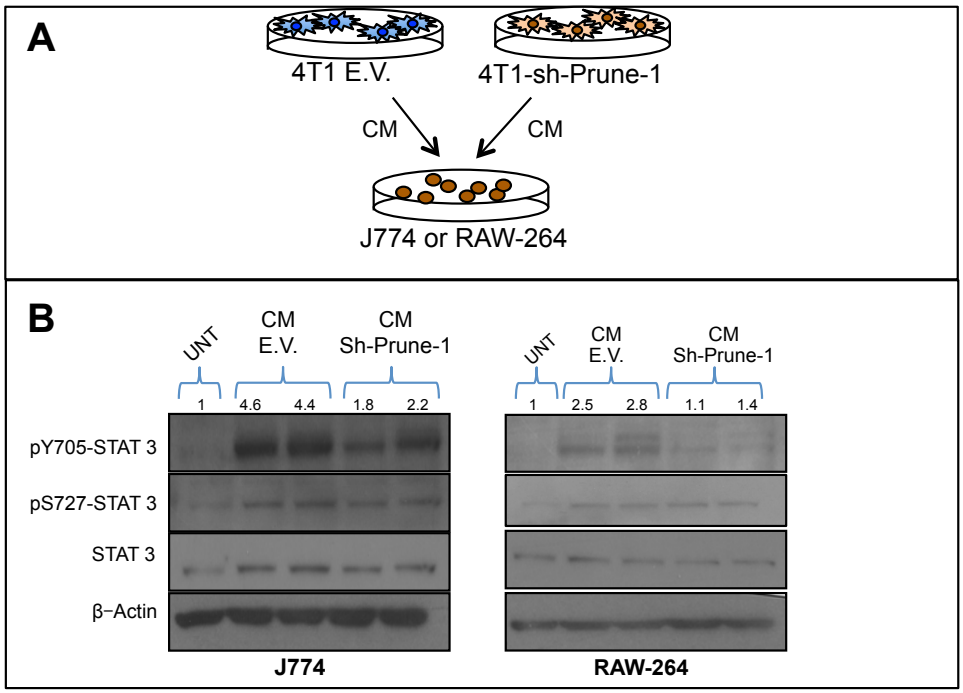

Figure 22: Prune-1 in TNBC cells activates macrophages in a paracrine manner *in vitro*. (A) Representative scheme for the experiment using Prune-1-silenced 4T1 cell clones. Conditioned media (CM) from 4T1 clones were collected after 24 hours. Macrophages (J774 or RAW-264) were starved for 6 hours in serum free media and then grown for 30 minutes in the conditioned media previously collected from 4T1. Empty Vector (E.V.) 4T1 clones and untreated (UNT) macrophages were used as negative controls. **(B)** Immunoblotting for the indicated proteins in J774 macrophages grown for 30 minutes in CM) from Prune-1-silenced and control 4T1 clones. Those macrophages grown in the conditioned media collected from Prune-1-silenced 4T1 cell clones show decreased phosphorylated-STAT3 protein compare to those grown in the media from EV clones. The densitometer analyses for the proteins were shown. β-Actin levels were used as loading control.

Therefore, in another set of experiments, we investigated whether Prune-1 overexpression in 4T1 cellular model modulated the migration ability of murine J774 macrophages. For this purpose, the

conditioned media from Prune-1-overexpressing, Prune-1-silenced and control 4T1 cell clones were used as chemoattractant in cell motility assays performed with J774 macrophages *in vitro*. As shown in Figure 23, the conditioned media from Prune-1-overexpressing 4T1 cell clones increased the migration rate of J774 macrophages (red line), while the media supernatant from Prune-1-silenced 4T1 cell clones reduced their migratory properties (green line) in comparison with to those from control clones (black line), as measured by variation of cell impedance (*i.e.,* Cell Index) using X-CELLigence technology (Roche).

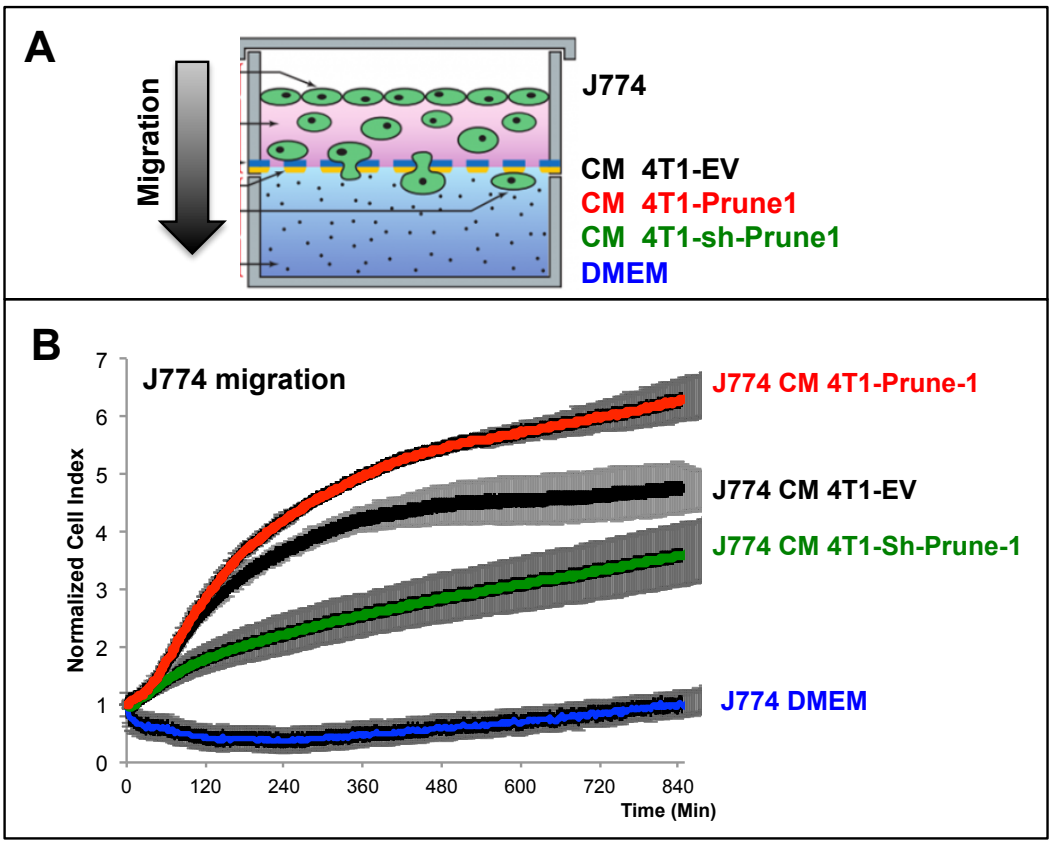

Figure 23: Overexpression of Prune-1 in TNBC cells enhances macrophages chemotaxis *in vitro*. (A) Representative scheme for the experiment monitoring the migration rate (chemotaxis) of J774 macrophages towards the conditioned media (CM) collected from Prune-1-overexpressing, Prune-1-silenced or Empty Vector (EV) 4T1 cell clones, used as chemoattractants. CM from 4T1 stable clones were collected after 24 hours. DMEM was used as negative control. **(B)** Normalized Cell Index as measure of cell migration/chemotaxis of macrophages (J774) as generated by xCELLigence RTCA software. Migration kinetics were monitored in response to conditioned media collected from Prune-1-overexpressing (red), Prune-1-silenced (green) or E.V. (black) 4T1 cell clones, used as chemoattractants. DMEM was used as negative control (blue). Macrophages grown toward the CM from Prune-1-overexpressing clones show increased migration rate. In contrast, those grown toward CM from Prune-1-silenced 4T1 cells show decreased cell migration compared to macrophages grown toward CM from E.V. 4T1 cell clones. Data are means of triplicate samples. EV, empty vector; CM, conditioned media

Overall these findings are suggesting that Prune-1 in TNBC cells takes part to the crosstalk between tumorigenic and immune cells (*i.e.,* macrophages) to enhance the recruitment, the activation (via STAT3), the migratory ability of macrophages *in vitro*, thus confirming the statistically significant association between higher Prune-1 protein levels and the presence of M2-TAMs observed in TNBC primary samples of our tissue cohort.

3.4 Immune-modulating cytokines secretion in TNBC is induced by Prune-1

Prune-1 has been previously shown with a role in extracellular environment by inducing Wnt pathway in a paracrine manner via Wnt3a cytokine secretion [25], thus indicating its potential involvement into the mechanisms of intercellular communication.

In an effort to identify potential entracellular mediators (cytokines and/or chemokines) differentially secreted from Prune-1 overexpressing TNBC cells, the conditioned media from three different Prune-1 overexpressing and control clones were pooled and incubated with the mouse cytokine antibody array nitrocellulose membranes (RayBio® Cytokine Antibody Arrays, from Raybiotech), as shown in Figure 24A. The cytokines expression profile of conditioned media from 4T1 prune clones compared with conditioned media from control clones showed n.17 cytokines significantly differentially secreted (n.14 up-regulated: fold > 2; and n.3 down-regulated: fold < 0.5; as shown in Figure 22B-C). In particular the levels of CD30T, lungkine/CXCL15 and E-cadherin were decreased in the pooled conditioned media from 4T1 prune clones compared with conditioned media from control clones. In contrast the levels of LIX/CXCL5, Thymus CK-1/CXCL7, thymic stromal lymphopoietin (TSLP), 6Ckine, ALK1, amphiregulin (Areg), CD36, CD40 ligand/CD154, galectin 1, IL-17F, IL-28, JAM-A/F11R, IL-20 and Regulated Upon Activation, Normal T-Cell Expressed And Secreted (RANTES) were increased in the pooled conditioned media from Prune-1-overexpressing 4T1 clones compared with conditioned media from control clones (Figure 24B-C).

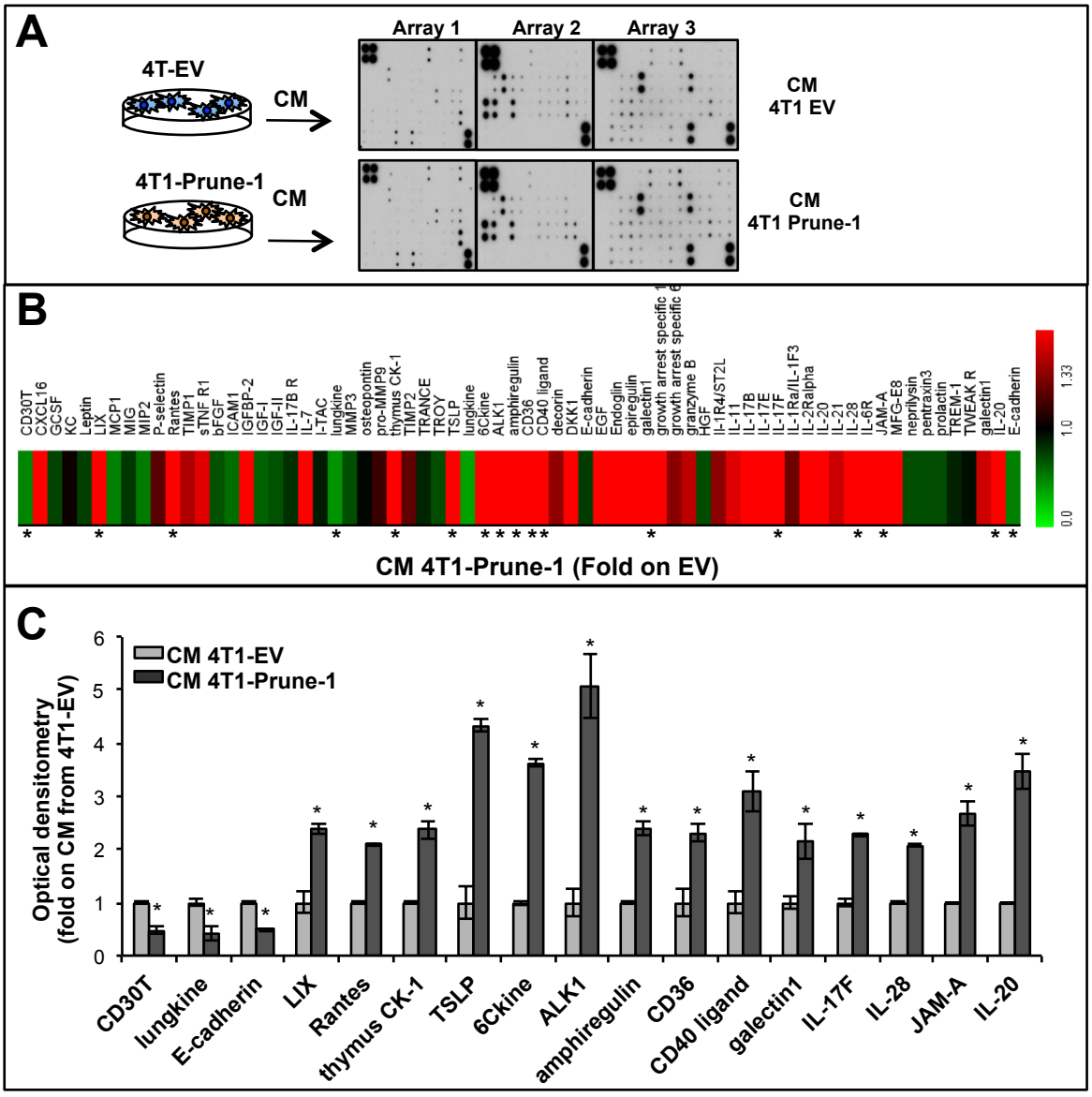

Figure 24: Prune-1 promotes the secretion of inflammatory cytokines in TNBC cells *in vitro*. (A) A Mouse cytokine antibody arrays incubated with pooled conditioned media (CM) from Prune-1-overexpressing and Empty Vector (EV) 4T1 cell clones. The densitometer analyses for the cytokines from **(A)** were performed with MultiExperiment Viewer (MeV; http://www.tm4.org/mev.html) in **(B)**. The cytokines found significantly up-regulated in CM from Prune-1-overexpressing 4T1 cell clones compared to EV clones are shown in red and marked with an asterisk. The fold of induction of Prune-1 induced cytokines on those of CM from EV clones was presented in **(C)**. Data are mean ± SD. "*" $p \leq 0.05$.

Then, in order to dissect how Prune-1 modulates the immune cells through the secretion of these extracelullar mediators, we selected the n.14 cytokines that had been found up-regulated in conditioned media collected from Prune-1-overexpressing 4T1 clones to generate a protein interaction network via STRING (Search Tool for the Retrieval of INteracting Genes/proteins) database together with SMAD2, whose phosphorylation levels were found increased in 4T1 cell clones due to PRUNE-1

overexpression. As described in Figure 25, a protein network consisting of 31 nodes representing proteins connected via 119 edges by virtue of protein-protein interaction (PPI) was obtained (PPI enrichment p-value< $1.0e^{-16}$) by setting the interaction score as "medium confidence" (*i.e.,* 0.4). All the proteins used as input (*i.e.,* Prune-1-increased cytokines and SMAD2) take part to this network, excluding Areg.

Further analyses using the KEGG (Kyoto Encyclopedia of Genes and Genomes) pathway database, showed that the proteins taking part to the network were mainly involved in JAK/STAT (ID:04630), NF-kB (ID:04064) and TGF-β (ID#04350) signaling pathways, as shown in Figure 25 within the boxes with the dotted lines (red, blue and green, respectively). Of importance, these proteins are involved in inflammatory response (GO:0006954) by positively regulating immune system processes (GO:0002684), such as cell migration (GO:0030335) and leucocyte chemotaxis (GO:0030595). Furthermore, the same proteins have also a role in positive regulation of NF-kB (GO:0043123) and MAPK (GO:0043410) cascades, thus confirming the enhancement of cell migration in those macrophages grown in the conditioned media collected from Prune-1-overexpressing 4T1 cell clones (see Figure 27 for cell migration). Most importantly, some cytokines of the network were found with the ability to phosphorylate STAT on Tyrosine residues (GO:0042531) and to enhance the cytokine production by macrophages (GO:0010935), thus further supporting the Prune-1-driven activation/polarization of macrophages via STAT3.

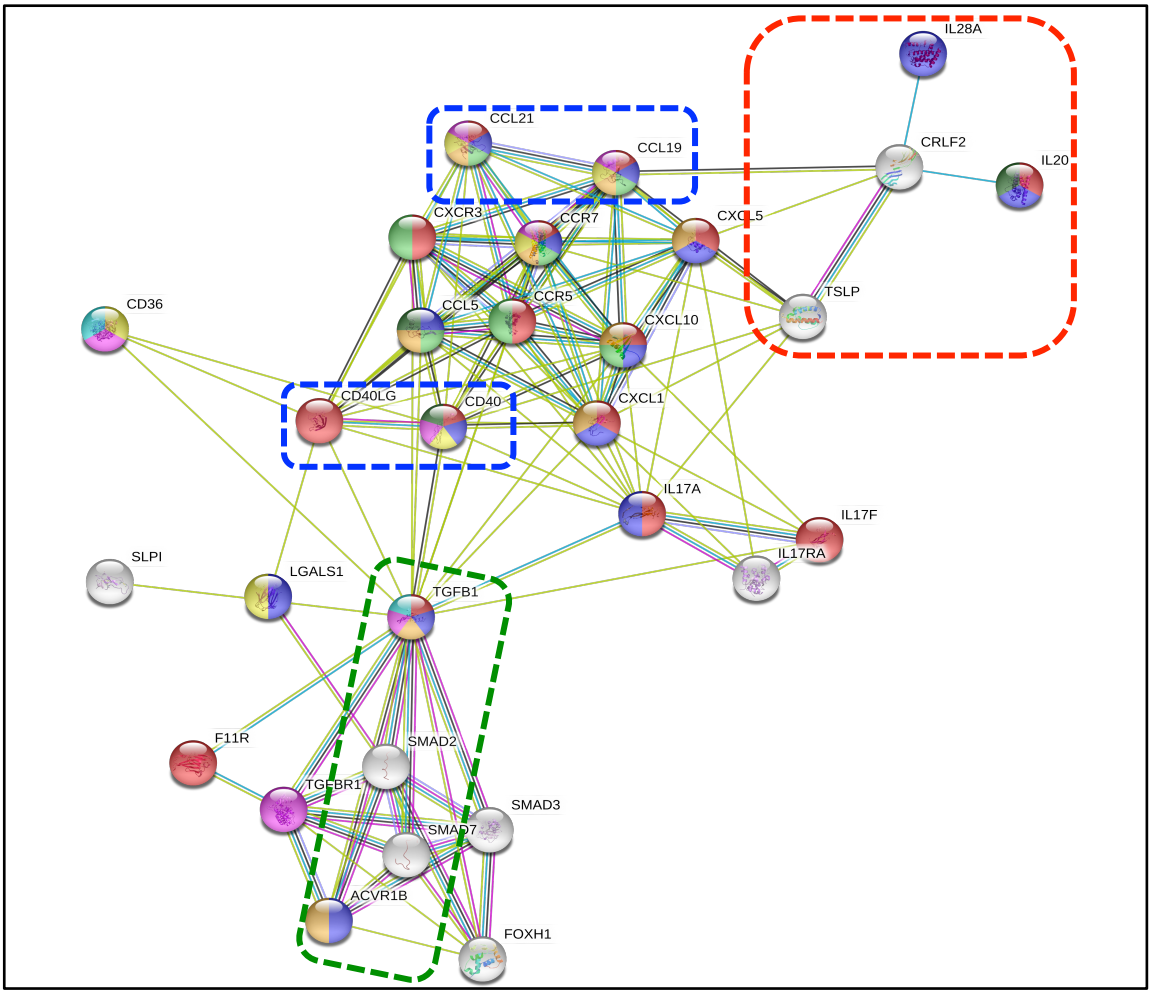

Figure 25: Prune-1 induces a network of "inflammatory" soluble proteins secreted by TNBC cells. The cytokines found up-regulated in the conditioned media (CM) derived from Prune-1-overexpressing 4T1 clones (n.14) were selected to generate a protein interaction network via STRING (Search Tool for the Retrieval of INteracting Genes/proteins) database together with SMAD2, whose phosphorylation levels were found increased in 4T1 cell clones due to PRUNE-1 overexpression. A protein network consisting of 31 nodes (representing proteins) connected via 119 edges (by virtue of protein-protein interaction [PPI]) was obtained (PPI enrichment, p-value< 1.0e-16) by setting the interaction score as "medium confidence" (i.e., 0.4). All the proteins used as input (*i.e.*, Prune-1-induced cytokines and SMAD2) take part to this network, excluding Areg. **Boxes with dotted lines represent signalling pathways as follow:** Red, Jak/Stat pathway (#04630); Blue, NF-kB pathway (#04064); Green, TGF-b pathway (#04350). **Nodes represent proteins as follow:** Red, Inflammatory response (GO:0006954); Blue, positive regulation of immune system process (GO:0002684); Green, leucocyte chemotaxis (GO: 0030595); Yellow, positive regulation of NF-kB (GO:0043123); Pink, positive regulation of MAPK (GO:0043410); Dark Green, positive regulation of Tyrosine phosphorilation of STAT (GO:0042531); Light Blue, positive regulation of macrophage cytokine production (GO:0010935); Orange: positive regulation of cell migration (GO:0030335).

In summary, these results showed that in 4T1 cells (as cellular model for TNBC), Prune-1 promotes *in vitro* the activation of macrophages in terms of migration and activated-STAT3 signaling, through the increased secretion of immune-modulating cytokines that are involved in immune system response via TGF-β, STAT3 and NF-kB pathways.

Subsequently, a similar experiment using a mouse cytokine antibody array was performed to detect the expression levels of the selected Prune-1-modulated cytokines (n.17) in the conditioned media from Prune-1-silenced 4T1 cell clones (Figure 26A). The data revealed that, among the n.17 cytokines analyzed, the levels of IL-17F and IL-28 were significantly decreased, while those of soluble E-Cadherin and Lungkine (or CXCL-15) were increased in the conditioned media collected from from Prune-1-silenced 4T1 cells, thus following an opposite trend compared to those found in conditioned media from Prune-1-overexpressing 4T1 cell clones (Figure 26B-C and Table 9). These findings strongly indicate that the secretion of IL-17F and IL-28 (also known as Type III Interferon-λ2; *i.e.,* INFλ2) cytokines is directly regulated by Prune-1 expression in TNBC cells.

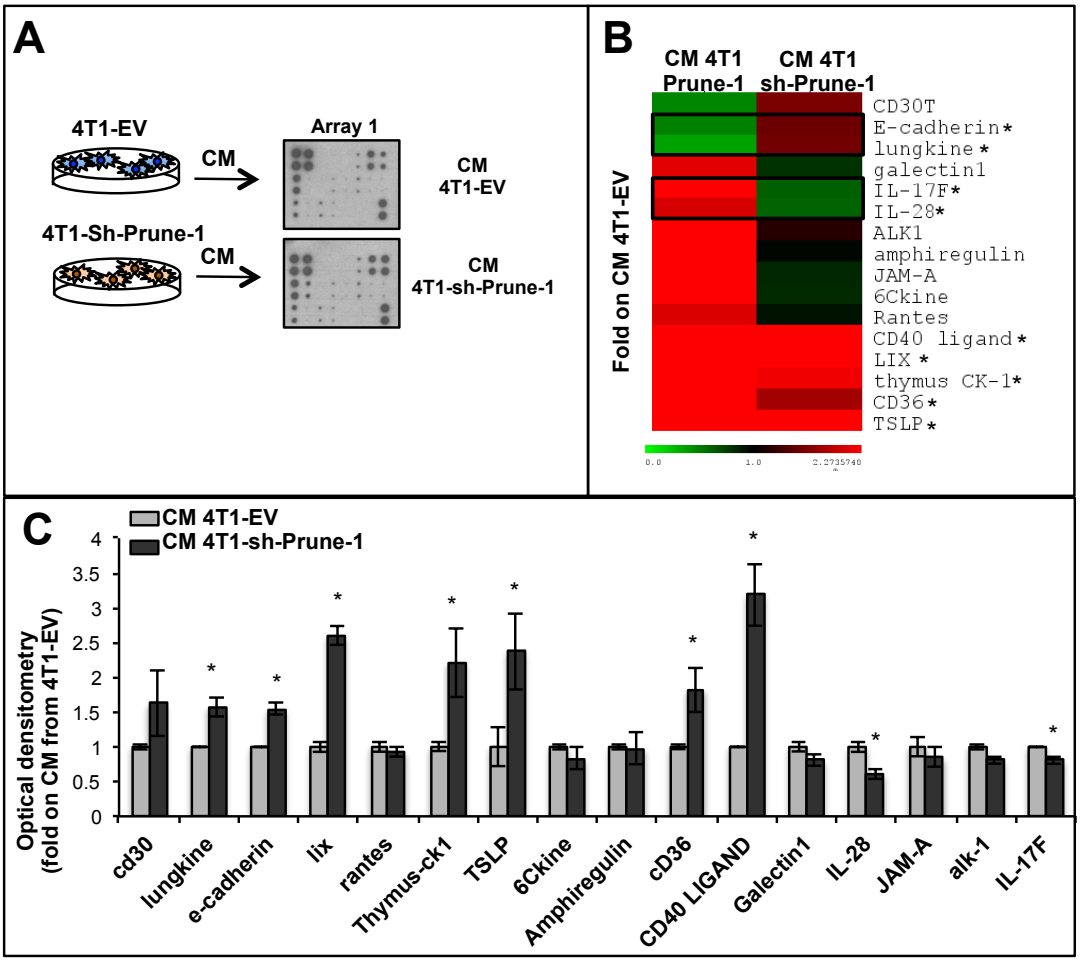

Figure 26: Prune-1 induces IL17-F and IL-28 in TNBC cells *in vitro*. (A) A mouse cytokine antibody array was performed to detect the expression levels of 17 cytokines (previously found up- or down-regulated by Prune-1) in conditioned media (CM) from Prune-1-silenced 4T1 cell clones. **(B-C)** The densitometer analyses for the cytokines from **(A)** were evaluated with MultiExperiment Viewer (MeV; http://www.tm4.org/mev.html) in **(B)**. Among the n.17 cytokines modulated by Prune-1, we found n.6 and n.2 cytokines as up-regulated and down-regulated in CM from Prune-1-silenced 4T1 clones, respectively **(C)**. The significant down-regulation of IL-17F and IL-28, and the up-regulation of soluble E-Cadherin and Lungkine was found with an opposite trend in comparison to the cytokines in the CM of Prune-1-overexpressing 4T1 cells **(B)**. Data are mean ± SD. "*" $p \leq 0.05$.

Table 9: Cytokines whose levels were found directly regulated by Prune-1 in the conditioned media from Prune-1-overexpressing and Prune-1-silenced 4T1 cell slones.

Cytokines/ Chemokine	Function	References
Soluble E-Cadherin	Cancer progression, invasion, metastasis (including Breast Cancer)	Hu *et al.*, Int J Cancer. 2016 15;138(12):2804-12
Lungkine (CXCL15)	Neutrophils recruitment	Zhou *et al.* Carcinogen. 2014;35:597–605
IL-17F	lymphocytes and macrophages infiltration in lung; Induction of IL-2, TGF-b, and monocyte chemoattractant protein-1 (MCP1)	Yang *et al.*, J Exp Med. 2008. 12; 205(5): 1063–1075; Starnes *et al.*, J Immunol. 2001. 15;167(8):4137-40.
IL-28	monocytes to macrophages differentiation cascade; Promoting Jak-STAT and MAPK signaling cascades	Dumoutier *et al.*, Biochem J, 2003. **370** (Pt 2): p. 391-6 Zhou *et al.,* J Virol, 2007. **81**(14): p. 7749-58.

These data further highlight the role of Prune-1 in the recruitment and activation of macrophages through the secretion of immuno-modulatory cytokines from TNBC cells. In this regard, IL-17F has been reported to promote a pro-inflammatory response also through macrophages recruitment [122], [123], and to induce the expression of TGF-β1 and monocyte chemoattractant protein-1 (MCP1) in endothelial cells [124]. IL-28 was reported to influence the differentiation cascade of monocytes to macrophages [125] and to induce cellular responses through Jak-STAT and MAPK signaling cascades [126]. The potential function of IL-17F and IL-28, as driven by Prune-1, in macrophages recrutiment and polarization in TNBC will be dissected in future studies, together with the role of soluble E-Cadherin and Lungkine.

3.5 Prune-1 affects *in vivo* primary tumor growth modulating the tumor microenvironment

The role of Prune-1 in TNBC was further investigated *in vivo* using TNBC xenograft orthotopic mouse model with 4T1 cells engineered to stably express the Firefly Luciferase (4T1-LUC) gene through lentiviral particles (RediFect Red-Fluc-Puromycin; CLS960002, Perkin Elmer, Waltham, MA, USA) as previously described [127]. To determine the effects of Prune-1 on primary tumour growth, Prune-1-silenced and control 4T1-LUC clones (2.5 x 10^5) were orthotopically implanted into the mammary fat pads of Balb/c syngeneic mice (4-weeks old; grouped according to weight). Tumorigenesis was followed for up to 21 days after tumour implantation using a non-invasive approach with *in vivo* bioluminescent imaging (BLI; [127]). The mice were imaged weekly with BLI system (IVIS Spectrum In-Vivo Imaging System) to monitor tumour growth. The BLI signals were then quantified according to the photon/emission (Photon/Sec) from the Region Of Interest (ROI). The differences in total flux from the two groups of mice showed impairment of tumour growth *in vivo* in the mice implanted with Prune-1-silenced compared to those implanted with control 4T1-LUC clones at day 14 and 21 post-implantation (T14: p=0.001; T21: p=0.022; Figure 27).

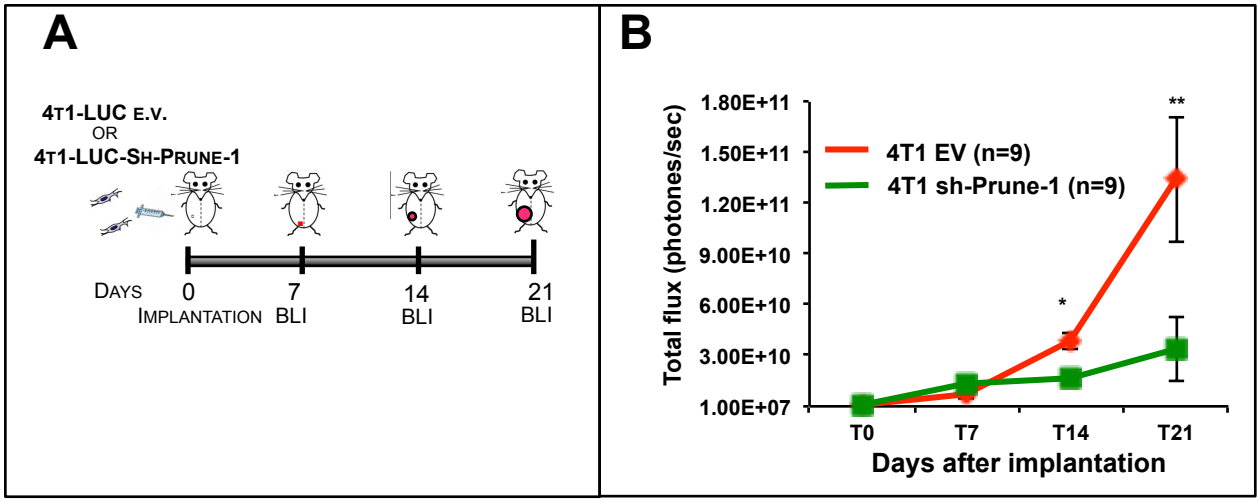

Figure 27: Prune-1 affects *in vivo* primary tumor growth in TNBC. (A) Representative orthotopic xenograft experiment using Prune-1-silenced 4T1 cells stably expressing firefly luciferase gene (4T1-LUC cells) and EV as control, and then implanted into mammary fat pad of 18 immunocompetent BalbC mice (n.9 mice for each group). The mice were imaged every 7 days via *in-vivo* bioluminescent imaging (IVIS Spectrum In-Vivo Imaging System) to monitor tumour growth from time of implantation (T0) to 21 days after tumour implantation. **(B)** Tumour growth according to quantified photon emission (photones/sec) from the region of interest (ROI) of mice orthotopically injected with 4T1-LUC stable clones. The differences in total flux from the two groups of mice at 21 days showed impairment of tumour growth *in vivo* in the mice implanted with Prune-1-silenced 4T1-LUC cell clones ($p<0.05$).

Given the important role played by tumour infiltrating immune cells in promoting TNBC growth and the role of Prune-1 in modulating the communication between the tumorigenic cells and the immune cells (*i.e.,* macrophages), we analyzed the presence of tumour infiltrating macrophages together with their polarization status into the tumor microenvironment *in vivo* by performing IHC analyses of TAMs on paraffin-embedded tissue sections of primary tumours obtained from TNBC xenograft mice. The infiltration of TAMs ($CD68^+$) into the tumor microenvironment was significantly decreased by Prune-1 silencing (Figure 28). Most importantly, their polarization toward an immunosuppressive pro-tumorigenic phenotype (*i.e.,* M2 status; $CD163^+$) was also reduced in the microenvironment of those tumours generated by Prune-1-silenced 4T1-LUC cells. In contrast, in tumours from mice implanted with control 4T1-LUC cells, the M2-TAMs staining ($CD68^+$ and $CD163^+$) showed a massive infiltration among the tumour cells.

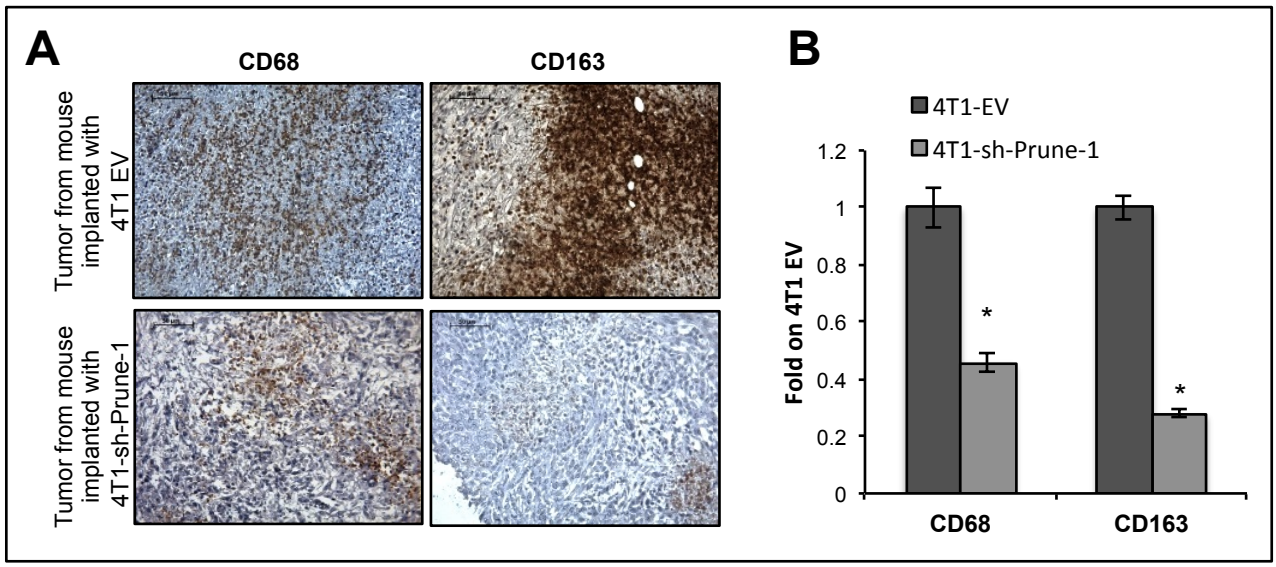

Figure 28: Prune-1 affects *in vivo* TAMs recruitment and polarization. (A) Representative immunohistochemistry with indicated antibodies of paraffin-embedded tumours generated by implanting 4T1-LUC cells into mammary fat pad of BalbC mice (magnification 40X). **(B)** Histograms showing the number of the cells positive for surface staining for CD68 and CD163 expression within primary tumours from mice implanted with Prune-1-silenced or Empty Vector (EV) 4T1 cell clones. The fold on $CD163^+$ and $CD68^+$ cells infiltrating the tumours generated from EV-4T1 cell clones is shown. The number of inlfiltrating M2-polarized TAMs ($CD68^+$ and $CD163^+$) was evaluated. "*" $p<0.05$.

In summary our *in vivo* results on TNBC xenograft models demonstrate that a decreased expression of Prune-1 in TNBC cells affects the recruitment and the polarization of TAMs within the tumour microenvironment, thus impairing the tumor growth.

3.6 Pharmacological inhibition of Prune-1 impairs TNBC growth *in vivo* by inhibiting TAMs recruitment and polarization.

We recently identified a small molecule pyrimido-pyrimidine derivative (AA7.1; [128], whose chemical structure is shown in Figure 29A) with the ability to enhance Prune-1 degradation [28]. This molecule was also found to decrease Prune-1 protein levels in different Medulloblastoma Group3 cells (as shown in Figure 29B; [28]) and to inhibit primary tumour growth and metastases *in vivo* by imparing TGF-β activation and EMT driven by Prune-1 in Medulloblastoma Group 3 [28]. Of importance, we also demonstrated that AA7.1 is not toxic *in vivo* in terms of hepatotoxicity and nephrotoxicity, as previously shown by evaluating hematological and biochemical parameters in mice treated with ecalating doses of the drug [28]. Here, we investigated the potential ability of AA7.1 to inhibit Prune-1 protein levels and to decrease the recruitment and the polarization of M2-TAMs also in TNBC. For this purpose, 4T1-LUC cells were treated with 100 μM AA7.1 or PBS/PEG (as vehicle control) and Prune-1 protein levels were evaluated through Western blotting analysis. Our data show that AA7.1 reduces Prune-1 protein levels (Figure 29C) also in 4T1, as cellular model of TNBC.

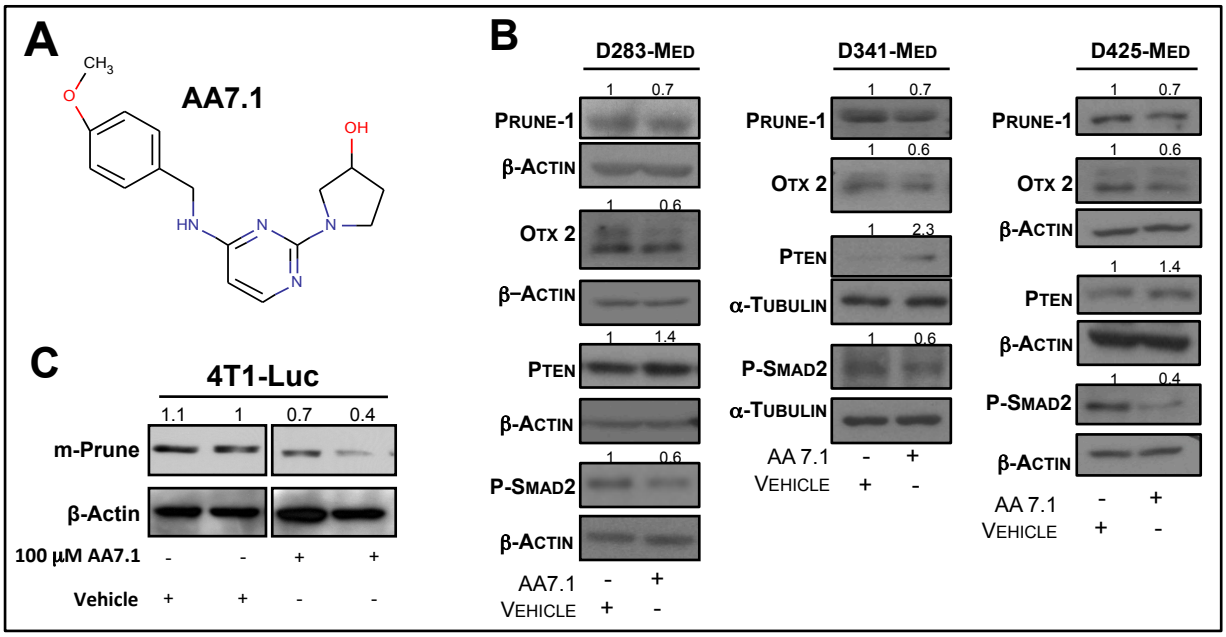

Figure 29: Pharmacological inhibition of Prune-1. (A) The chemical structure of AA7.1 is shown. **(B)** Representative Western blots using protein lysates from indicated different Medulloblastoma Group3 cell lines treated with 100 μM AA7.1 for 6 h (AA7.1 replacement every 3 h), or PBS as vehicle control. Densitometric values given showed down-regulation of Prune-1 (0.7-fold), similar in all AA7.1-treated MB cells, compared to vehicle. AA7.1-treated MBGroup3 cells also showed decrease in phospho-Ser467-SMAD2 and OTX2 (overall, impairing TGF-β activation) and up-regulation of PTEN. Data are representative of three independent assays. From Ferrucci V *et al.,* Brain. 2018. *In press.*
(C) Representative immunoblotting indicated antibodies using protein lysates from 4T1 TNBC cell lines treated with 100 μM AA7.1 for 24 h or PBS/PEG as vehicle control. Densitometric values given showed down-regulation of Prune-1 in AA7.1-treated TNBC cells, compared to vehicle.

Then the anti-tumorigenic action of AA7.1 drug was further investigated *in vivo* using xenograft orthotopic mouse model of TNBC with 4T1-LUC cells. For this purpose, 4T1-LUC cells (1×10^5) were orthotopically implanted into the mammary fat pads of Balb/c syngeneic mice. After tumours were etabilished (7 days after tumour implantation), intraperitoneal administration of AA7.1 (60 mg/kg for 5 days/week) or PBS-PEG (as vehicle control) was started (Figure 30A). Tumorigenesis was follow *in vivo* using BLI techology, as previously described. Importantly, mice treated *in vivo* with AA7.1 showed a significant reduction in the primary tumour growth (Figure 30B) on day 35 post-implantation, as compared to the control (p=0.0128).

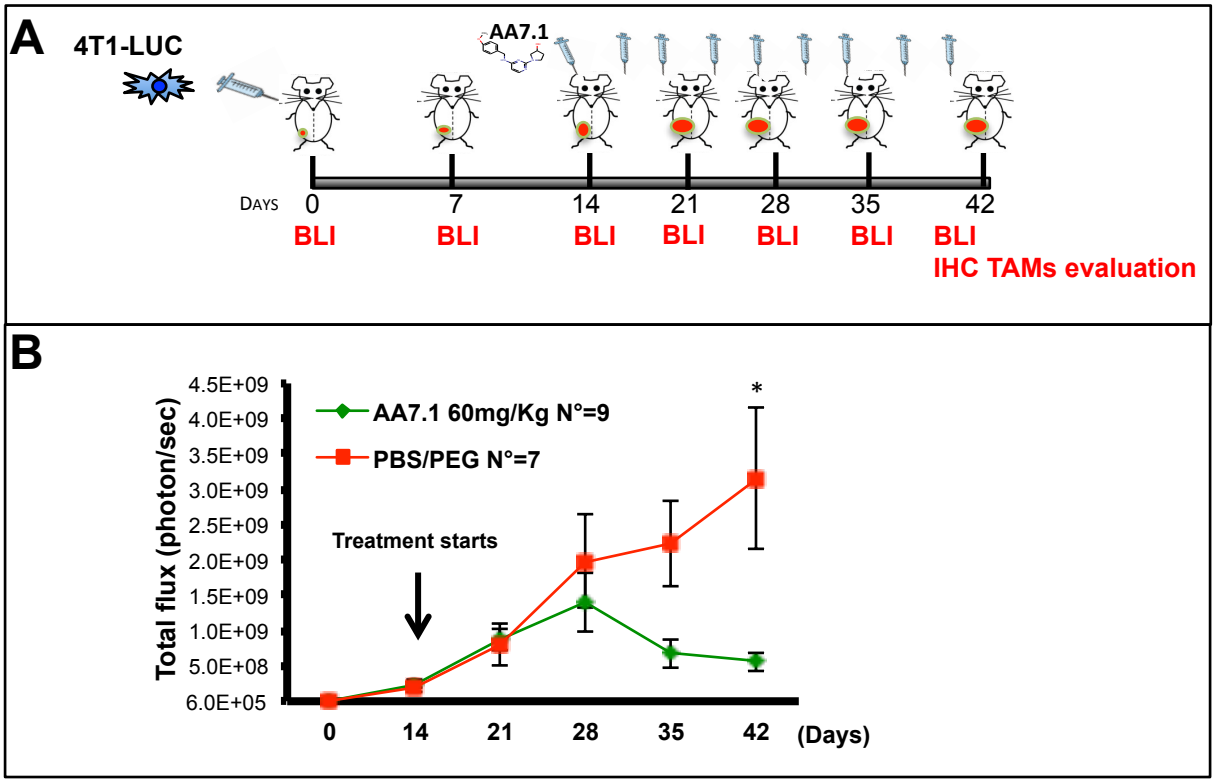

Figure 30: Prune-1 affects *in vivo* primary tumor growth in TNBC. (A) Representative orthotopic xenograft experiment using 4T1 cells stably expressing firefly luciferase gene (4T1-LUC cells), and then implanted into mammary fat pad of 16 immunocompetent BalbC mice. After tumours were etabilished (7 days after tumour implantation), intraperitoneal administration of AA7.1 (60 mg/kg for 5 days/week) or PBS-PEG (as vehicle control) was started. Tumorigenesis was follow *in vivo* using BLI techology, as previously described. from time of implantation (T0) to 42 days after tumour implantation. **(B)** Tumour growth according to quantified photon emission (photones/sec) from the region of interest (ROI) of mice orthotopically injected with 4T1-LUC stable clones. The differences in total flux from the two groups of mice at 35 days from treatment showed a significant impairment of tumour growth *in vivo* in the mice treated with AA7.1 (p=0.0128).

To determine the effects of pharmacological inhibition of Prune-1 (using AA7.1 drug) treatment on immune-cell infiltration into the tumour microenvironment, IHC analyses of TAMs and MDSCs were conducted on paraffin-embedded tissue sections of primary tumours from the TNBC xenograft mice

implanted with 4T1-LUC cells into the mammary fat pad that had been treated with vehicle (PBS-PEG) or 60 mg/kg/day AA7.1 (5 days per week), as shown in Figure 31. Our data show that AA7.1 treatment decreased the number of infiltrating M2-polarized TAMs ($CD163^+$ cells; p=0.0182) and MDSCs (Gr-1+, CD11b+; p=0.0005 and p<0.0001, respectively) into the tumor microenvironment, as compared to vehicle treatment.

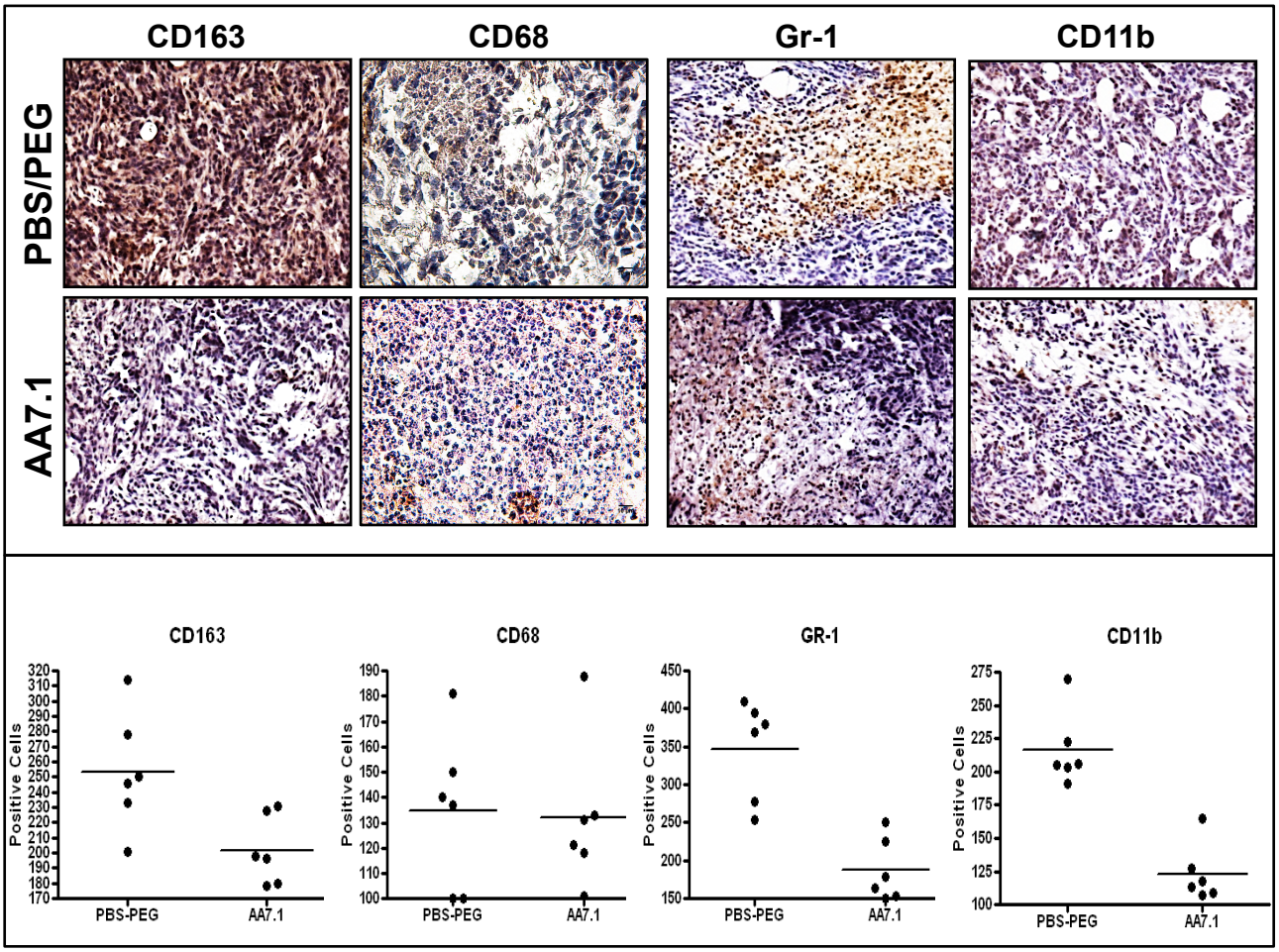

Figure 31: Prune-1 affects *in vivo* immune cells in TNBC microenvironment. (A) Representative immunohistochemistry with indicated antibodies of paraffin-embedded tumours generated by implanting 4T1-LUC cells into mammary fat pad of BalbC mice (magnification 40X). The number of inlfiltrating M2-polarized TAMs (CD68+, CD163+) and MDSCs (Gr1+, CD11b+) was evaluated. A significantly decrease of M2-polarized-TAMs (*i.e.,* CD163+) and MDSCs was shown in the microenvironment of the tumour from AA7.1 treated mice (after 35 days of treatment). CD163: p=0.0182; CD68: p=0.8822 [N.S.]; Gr1: p=0.0005; CD11b: p<0.0001.

Overall, these data are indicating that the anti-tumorigenic drug AA7.1 also possesses immuno-modulatory activity, by impairing both the polarization of TAMs toward an M2-phenotype and the recruitment of MDSCs within TNBC microenvironment. These effects may occurr through the inhibition of Prune-1-induced TGF-β activation in the tumour microenvironment.

In conclusion, the inhibition of Prune-1 by AA7.1 treatment has *in vivo* effects on both tumour cells and the tumor microenvironment, which result in negative regulation of the inflammatory response and tumour growth. The potential action of Prune-1 on recruitment and/or activation of MDSCs will be investigated in future studies.

In order to deep insight the role of Prune-1 in modulating the tumour microenvironment, we generated a Genetically Engineered Mouse Model (GEMM) overexpressing Prune-1 in mammary gland. This GEMM represents a useful source to study the function of Prune-1 in recruiting and polarizing the infiltrating immune cells in the tumour microenvironment *in vivo*.

3.7 A Genetically Engineered Mouse Model driven by Prune-1 resembles metastatic Triple Negative Breast Cancer with high infiltrating M2-TAMs

During the last years, several different experimental models for mammary cancer are being applied in an effort to distinguish gene mutations responsible for early events in malignant transformation from those leading to malignant progression and metastases. In this regard, Mouse Mammary Tumour Virus [MMTV] represents an inherited biological carcinogen that induces, by insertional mutagenesis, premalignant lesions and malignant tumours of the mammary glands [129]. In fact, the study of the MMTV has provided important insights into the mechanisms of neoplastic transformation in the mammary gland.

In an effort to analyze the phenotype and to better characterize the effects of Prune-1 overexpression in mammary oncogenesis, a Genetically Engineered Mouse Model (GEMM) overexpressing Prune-1 in mammay glands was generated using a vector construct containing the human Prune-1 cDNAs under the control of Mouse Mammary Tumour Virus [MMTV] promoter (as reported in Figure 32; the transgenic model was made by Dr. Natascia Marino).

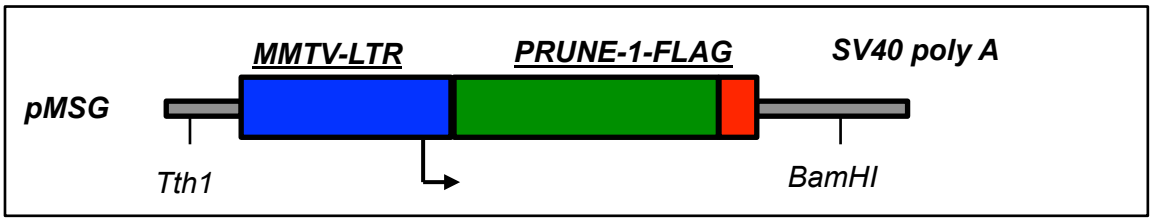

Figure 32: Schematic diagram of plasmid pMSG-MMTV-LTR-Prune-1-FLAG. The pMSG vector (Pharmacia Biotech Sevrage, Uppsala, Sweden) contains the mouse Mammary Tumour Virus Long Terminal Repeat (MMTV-LTR) upstream of a polylinker. The human Prune-1 cDNA, containing the complete protein coding region with the FLAG tag fused in frame at the Carboxyl-Terminus terminal was cloned into polylinker sites of pMSG in sense orientation relative to the MMTV-LTR and the downstream the SV-40 early promoter. The resultant construct was designated pMSG-MMTV-Prune-1-FLAG.

Female mice harboring human Prune-1 overexpressed in mammary gland (*i.e.,* MMTV-Prune-1) develop extensive mammary hyperplasia early in life (by 80-days of age), as shown in Figure 33. MMTV-Prune-1 mice were monitored for 12 months. While benign mammary lesions, usually hyperplasia, were found in female mice with 100% penetrance, none developed tumours in mammary gland.

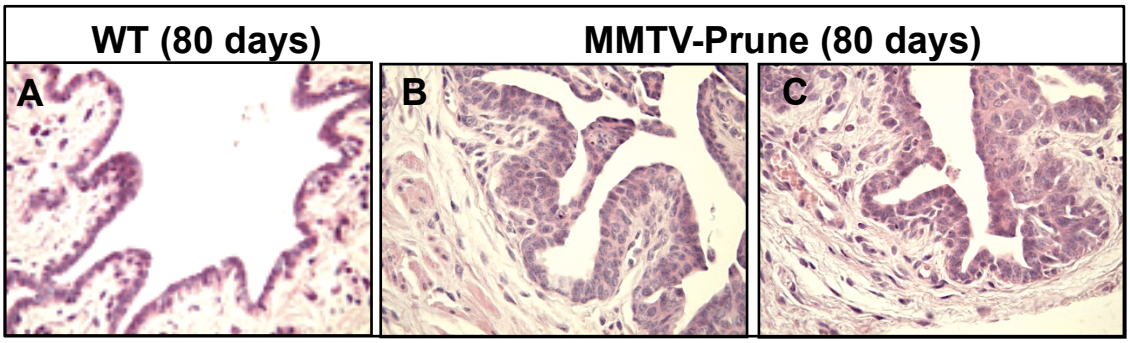

Figure 33: MMTV-Prune-1 mice develop mammary hyperplasia. Representative Hematoxylin-Eosin sections of mammary hyperplasia from females of the MMTV-Prune-1 **(B-C)** compared to normal gland **(A)**.

Furthermore, Western blotting analyses were performed on tissue lysates of normal breast from wild-type (FVB strain) or mammary hyperplastic tissues from MMTV-Prune-1 to dissect the signaling pathways affected by the overexpression of Prune-1 in mammary gland. The data show hyperplastic lesions in MMTV-Prune-1 tissues with increased AKT, Jak/STAT, NF-kB and MAPK cascades and S100A4 signaling, as shown by the up-regulation of phospho-(Ser473)-AKT, the increase of phospho-STAT3, the reduction of phospho-Ik-Bα and augmented phospho-ERK1/2 levels presented in Figure 34. Importantly, activation of canonical Wnt-1 pathway was also observed in those mammary hyperplastic tissues from MMTV-Prune-1 mice with increased activated-β-catenin (as reported in Figure 32), thus confirming the ability of Prune-1 to induce Wnt pathway also in mammary cells.

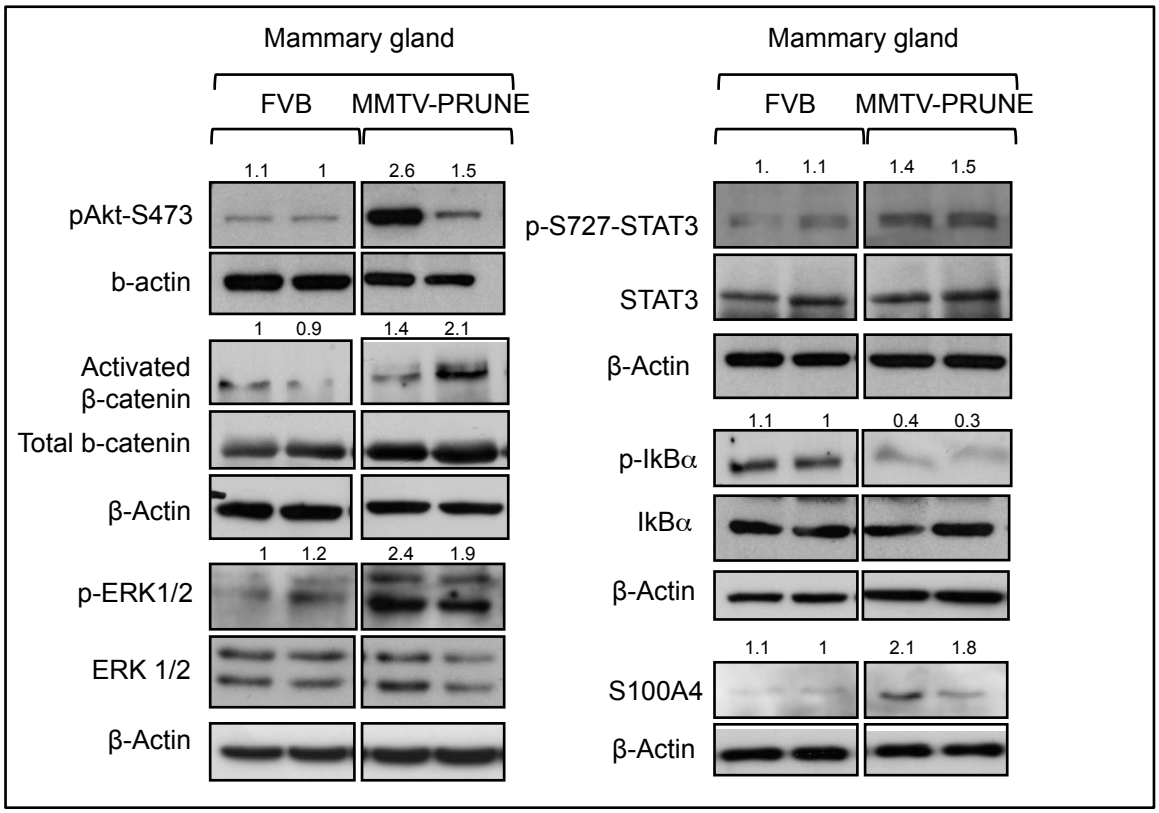

Figure 34: Prune-1 induces proliferative and inflammatory pathways *in vivo* responsible for mammary hyperplasia. Representative immunoblotting from tissue lysate from primary sections of mammary hyperplasia from MMTV-Prune-1 mice and normal mammary gland from FVB female mice (as negative control). Densitometer analyses show increased AKT, Wnt, MAPK, JAK/STAT3 and NF-kB pathways, as shown by increased levels of phospho-AKT, actived-β-catenin, phospho-ERK1/2, phospho-STAT3 and S100A4 and decreased phospho-Ikbα, respectively.

For all the above reasons, females MMTV-Prune-1 were crossed with MMTV-Wnt-1 mice, a well estabilished GEMM of TNBC [130]. The transgenic overexpression of Wnt-1 in mammary gland (under the control of MMTV-LTR promoter) causes extensive ductal hyperlasia in prepubertal ages and mammary adenocarcinomas in approximately 50% of the female mice by 6 months of age; the rest succumb to tumours by 1 year [130]. Spontaneous metastases to the lung and proximal lymph nodes are rare at the time tumours are detected but more frequent after the surgical removal of the primary neoplasm [130], [131]. Of importance, it is noteworthy that the murine MMTV-Wnt-1 model of BC shares transcriptional patterns with, and exhibits hallmarks of, human TNBC/Basal-like BC, such as the expression of Keratin-5 [132], [133], [134]. In addition, hyperactive Wnt signaling, with nuclear β-catenin and overexpression of Cyclin-D1 (as Wnt target), is found in TNBC or Basal-like types [132]. Furthermore, Wnt-1 does not require Estrogen signaling for stimulating proliferation and inducing tumours. Infact hyperplastic ductal growth in MMTV-Wnt-1 mice persisted despite estradiol deprivation due to ovariectomy or in ER knockout backgroung [135]. Nevertheless, some studies

reported both ER and PR positivity (*i.e.,* ER^+, PR^+) in tumours arising from MMTV-Wnt-1 [136]. This dual function of ER signaling in MMTV-Wnt-1 could be ascribed to the progenitor/stem cells from which these neoplasms arise that can differentiate into both ER^- and ER^+ tumorigenic cells. This hypothesis is strengthened by the expression of putative progenitor cell markers (*e.g.,* Sca-1 and Keratin-6) and both myoepithelial and epithelial markers (i.e., Keratin-5 for basal and Keratin-18 for luminal lineage, respectively) in the MMTV-Wnt-1 neoplastic lesions, thus implying that they arise from a progenitor/stem cell population that gives rise to both lineages [131], [133].

The resulting double transgenic MMTV-Prune-1/Wnt-1 (*i.e.,* MMTV-Prune1/Wnt1) mouse model developed BC with 100% penetrance with breeding females developing tumours slightly earlier than virgin mice. This acceleration may be caused by either hormonal influence on cell growth or the increased mass of the mammary epithelium attribuited to pregnancies and lactation. Because of the extensive ductal hyperplasia, female MMTV-Prune1/Wnt1 mice can not deliver milk to their pups, a phenomenon already presented with MMTV-Wnt-1 mice. Interestingly, Prune-1 overexpression in mammary gland of virgin MMTV-Wnt-1 mice did not alter the breast tumour onset compared to MMTV-Wnt-1 mice. These data were obtained by monitoring n.31 MMTV-Prune1/Wnt1 and n. 44 MMTV-Wnt1 mice. Since breeding females developed BC earlier than virgin mice, female MMTV-Prune1/Wnt1 and MMTV-Wnt1 mice (3-months old) were mated, the pregnancy was observed and the mice (n.11 MMTV-Prune1/Wnt1 and n.18 MMTV-Wnt1 mice) were then monitored. We found any differences in the breast tumour onset in pregnant female MMTV-Prune1/Wnt1 mice compared to pregnant MMTV-Wnt-1.

After 2 months from the tumour onset, the mice were sacrificed and both the primary tumour and lungs were removed. While MMTV-Wnt1 mice did not develop lung metastases, the presence of both macro- and micro-metastases in lungs from MMTV-Prune1/Wnt1 was observed with 97% penetrance, as shown in Table 10 and in Figure 35.

Table 10: Incidence of lung metastases in MMTV-Prune1/Wnt1 and MMTV-Wnt1 mice

Genotype	Genetic background	ID	Tumour growth timing	Lung metastases
MMTV-Wnt1	FVB	432	2 months	NO
MMTV-Wnt1	FVB	446	2 months	NO
MMTV-Wnt1	FVB	Z1-C21	2 months	NO
MMTV-Wnt1	FVB	573	2 months	NO
MMTV-Wnt1	FVB	502	2 months	NO
MMTV-Wnt1	FVB	Z1-C226	2 months	NO
MMTV-Wnt1	FVB	43	2 months	NO
MMTV-Wnt1	FVB	19	2 months	NO
MMTV-Prune1/Wnt1	FVB	409	2 months	**YES**
MMTV-Prune1/Wnt1	FVB	389	2 months	NO
MMTV-Prune1/Wnt1	FVB	444	2 months	**YES**
MMTV-Prune1/Wnt1	FVB	428	1 month 20 days	**YES**
MMTV-Prune1/Wnt1	FVB	521	2 months	NO
MMTV-Prune1/Wnt1	FVB	476	2 months	**YES**
MMTV-Prune1/Wnt1	FVB	493	2 months	**YES**
MMTV-Prune1/Wnt1	FVB	Z1-C231	3 months	**YES**
MMTV-Prune1/Wnt1	FVB	772	2 months	**YES**
MMTV-Prune1/Wnt1	FVB	821	2 months	**YES**
MMTV-Prune1/Wnt1	FVB	Z1-802	2 months	**YES**

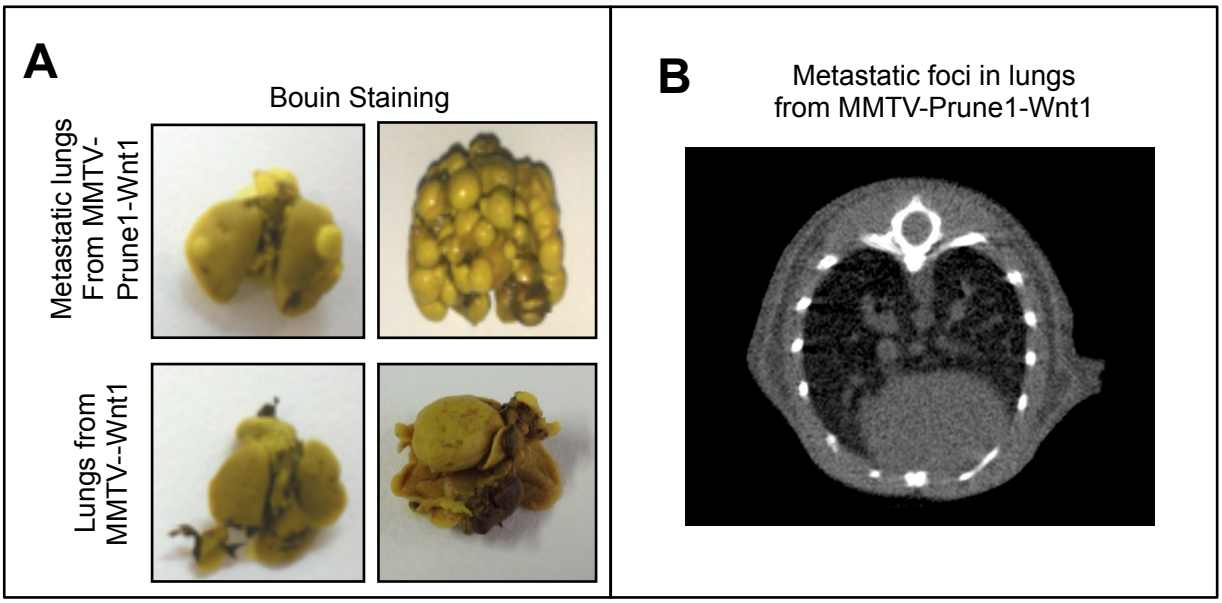

Figure 35: MMTV-Prune1/Wnt1 mice develop pulmonary metastases. (A) Representative lung pictures from MMTV-Prune1/Wnt1 and MMTV-Wnt1 mice fixed by Bouin's solution. Metastatic foci on the gross tissue are visible in lungs from MMTV-Prune1/Wnt1 mice. **(B)** 100 micron Micro CT of lungs of MMTV-Prune1/Wnt1 mouse model. Multiple metastases are evident.

In order to gain insights into the role of Prune-1 in BC, we characterized and compared the primary tumours generated by MMTV-Prune1/Wnt1 with those generated by MMTV-Wnt1 mice by performing anatomopathological analyses through IHC and Immunofluorescence (IF) approaches.

As shown in Figure 36, the overexpression of human FLAG-tagged Prune-1 in MMTV-Prune1/Wnt1 primary tumours was confirmed by both IHC and IF analyses.

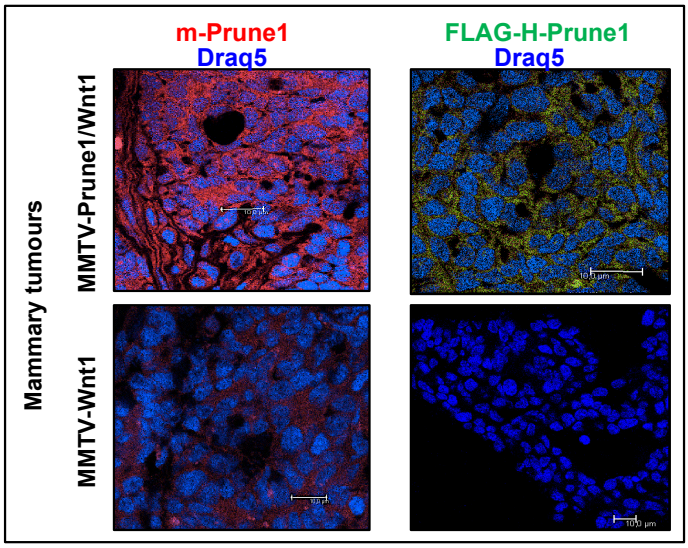

Figure 36: Overexpression of human Prune-1 transgene in breast tumour from MMTV-Prune1/Wnt1 mice. Representative immunofluorescence (IF) staining for antibodies as indicated. Endogenous Prune-1 (red) in overexpressed in mammary tumours from MMTV-Prune1/Wnt1 mice compared to MMTV-Wnt1 mice. The expression of FLAG-tagged-human Prune-1 is also shown (Green). Draq5 is used for nuclear staining (Blue), magnification 63X.

Since MMTV-Wnt1 breast tumours have been reported to share common feature with human Basal-like/TNBC, we investigated the BC subgroups of both GEMM models by analyzing ER, PgR and HER2 status via IHC. The data reported in Figure 37 showed undetectable levels of both Estrogens and Progesteron Receptors. These findings confirm that MMTV-Wnt1 mouse model belongs to TNBC subgroups, but most importantly show that MMTV-Prune1/Wnt1 model resembles metastatic TNBC.

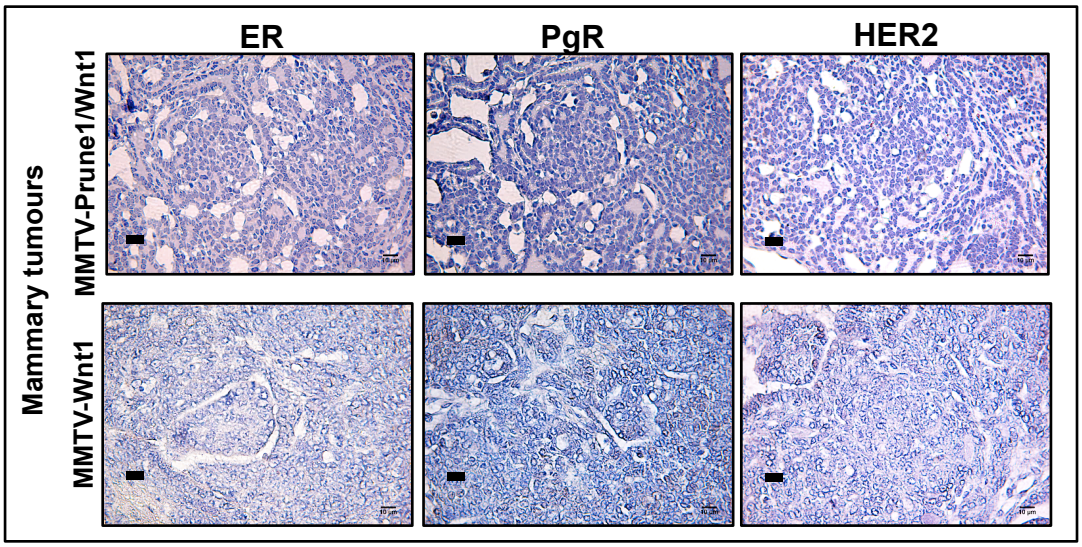

Figure 37: MMTV-Prune1/Wnt1 and MMTV-Wnt1 are GEMM of TNBC. Representative immunohistochemistry (IHC) staining for antibodies as indicated. Undetectable levels of both Estrogens/Progesteron Receptor (*i.e.,* ER^-, PgR^- and $HER2^-$; magnification 40X). This confirms MMTV-Wnt1 as GEMM for Basal-Like/TNBC, and indicates that MMTV-Prune1/Wnt1 represents a model for metastatic TNBC.

Then, to better understand the role of Prune-1 in metastatic TNBC, we investigated its functions on the activation of TGF-β signaling and induction of EMT *in vivo* in this new GEMM model of metastatic TNBC. Our data reported higher nuclear SMAD2/3 levels in primary tumours derived from the double transgenic, compared to those from MMTV-Wnt1 mice (as shown in Figure 38).

The activation of canonical TGF-β cascade (via SMAD2) was then corroborated by the induction of EMT processes with undetectable E-Cadherin and higher N-Cadherin levels in BC from MMTV-Prune1/Wnt1. In contrast, MMTV-Wnt1 primary tumours showed higher E-Cadherin and lower N-Cadherin levels. These data confirm the ability of Prune-1 to activate TGF-β and EMT processes, thus enhancing the metastatic spread in this GEMM model of metastatic TNBC (Figure 38).

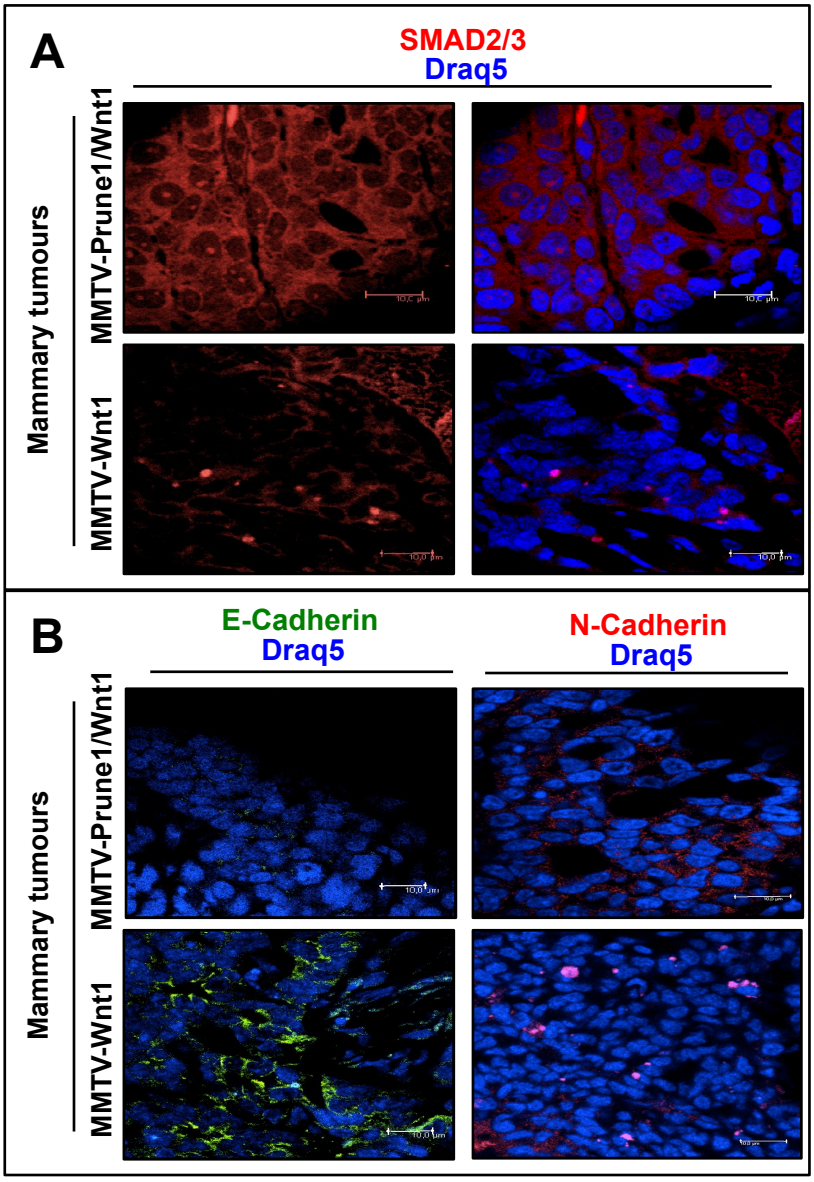

Figure 38: Prune-1 promotes canonical TGF-β cascade and induces EMT in breast tumour from MMTV-Prune1/Wnt1 mice. Representative immunofluorescence (IF) staining for antibodies as indicated. The overexpression of Prune-1 in mammary tumours from MMTV-Prune1/Wnt1 mice enhances canonical TGF-β cascade through nuclearization of SMAD2/3 (red) (**A**), thus resulting in promoting EMT process **(B)** with E-Cadherin loss (green) and increased N-Cadherin (red), in comparison with MMTV-Wnt1 tumours. Draq5 is used for nuclear staining (Blue). Megnification 63X.

Furthermore, the presence of TAMs and their polarization status was also evaluated in the tumour microenvironment of MMTV-Prune1/Wnt1 mice and compared to MMTV-Wnt1 model. As presented in Figure 39A-C, we found a statistically significant increase of M2-TAMs (*i.e.,* $CD68^+$, $CD163^+$) within the tumour mass of MMTV-Prune1/Wnt1 when compared to MMTV-Wnt1, thus confirming *in vivo* the role of Prune-1 in modulating the immune cells (*i.e.,* macrophages) infiltrating in the tumour microenvironment of TNBC.

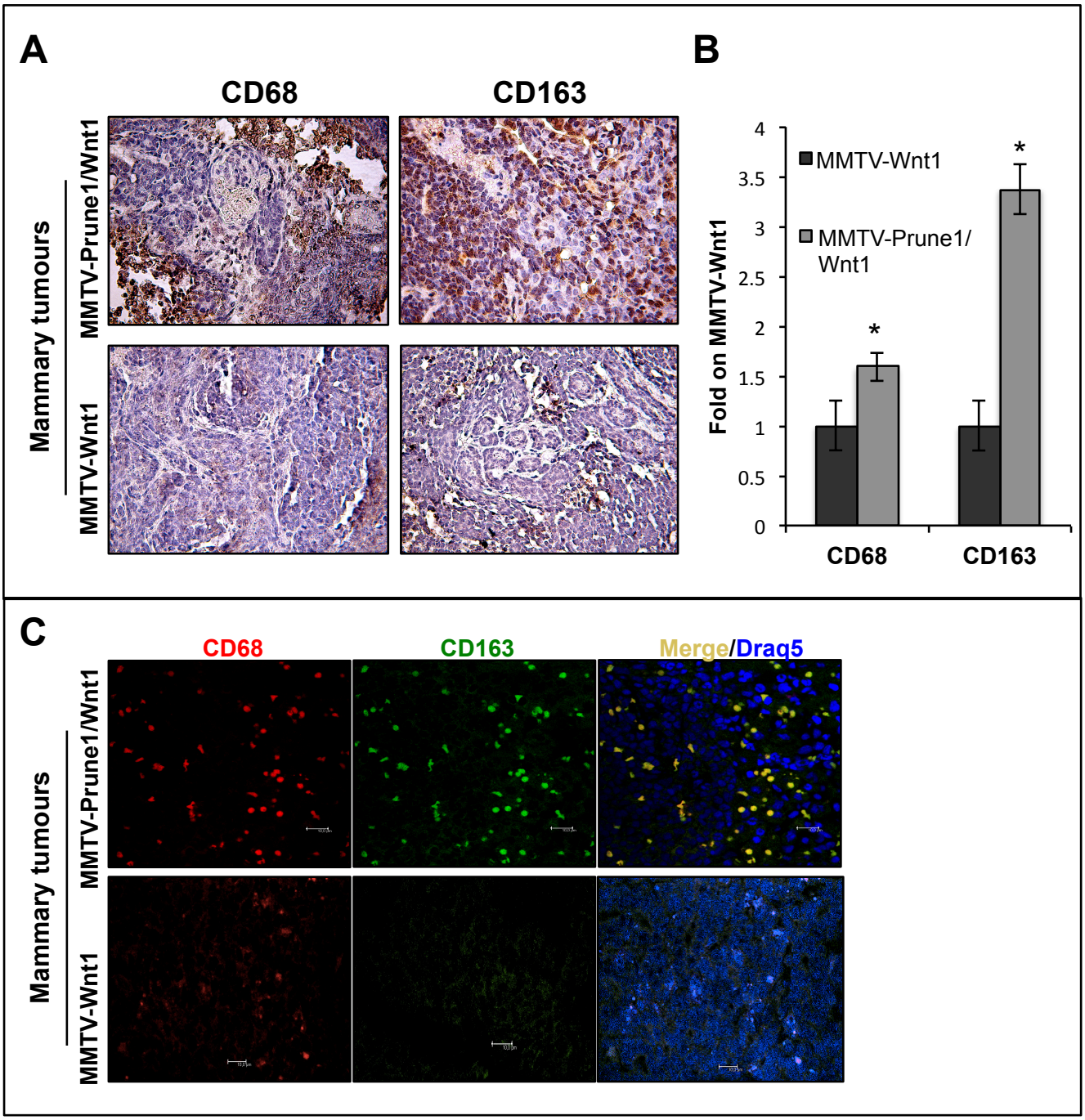

Figure 39: Prune-1 induces M2-polarization of TAMs in TNBC microenvironment. Representative immunohistochemistry (IHC) **(A)** and immunofluorescence (IF) **(C)** staining for antibodies as indicated. CD68 (red) and CD163 (green) mark M2-polarized TAMs (Yellow the overlay). On the right, histograms shows the number of the cells positive for surface staining for CD68 and CD163 expression within primary tumours generated from MMTV-Prune1/Wnt1 or MMTV-Wnt1. The fold on $CD163^+$ and $CD68^+$ cells infiltrating the tumours of MMTV-Wnt1 is shown. Data were calculated from 4 independent tumours. A statistically significant increase of M2-TAMs (i.e., CD68+, CD163+) within the tumour mass of MMTV-Prune1/Wnt1 when compared to MMTV-Wnt1 is shown **(B)**, thus confirming *in vivo* the role of Prune-1 in modulating macrophages polarization toward an M2-phenotype in the tumour microenvironment of metastatic TNBC. IHC, magnification 40X; IF: magnification 63X. "*" $p<0.05$.

Of note, the presence of M2-TAMs ($CD68^+$, $CD163^+$) was also found in metastatic lungs from MMTV-Prune1/Wnt1 mice (Figure 40), thus suggesting that Prune-1 has the ability to recruit and polarize macrophages in TNBC microenvironment to prepare the lung pre-metastatic niche.

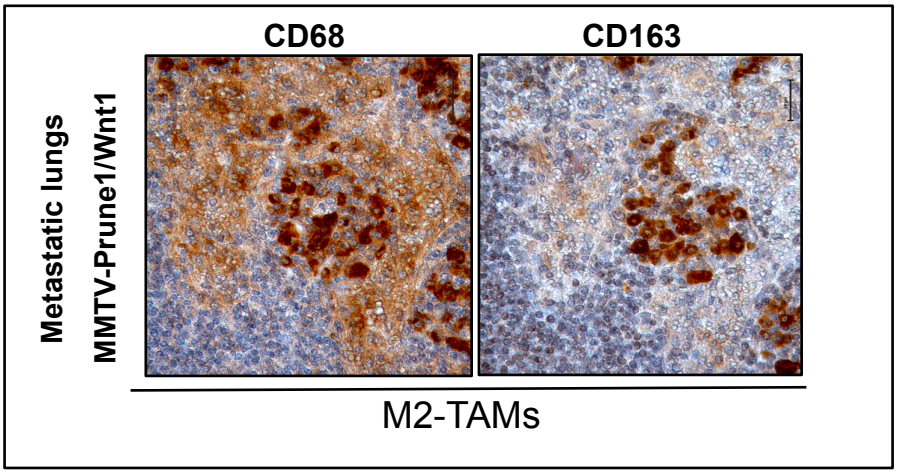

Figure 40: Prune-1 promotes M2-polarization of TAMs in metastatic lung microenvironment. Representative immunohistochemistry (IHC) staining for antibodies as indicated. CD68 and CD163 mark M2-polarized TAMs. 40X.

This hypothesis was also confirmed by the up-regulation of some pro-inflammatory cytokines in the sera of MMTV-Prune1/Wnt1 as compared to MMTV-Wnt1 mice. Of importance, among the Prune-1-modulated cytokines (n.17) evaluated, IL17-F and IL-28 were found statistically increased (Figure 41) in the sera from MMTV-Prune1/Wnt1 compared to MMTV-Wnt1 mice, thus confirming the ability of Prune to modulate TAMs recruitment, activation and polarization mainly through the secretion of these two cytokines.

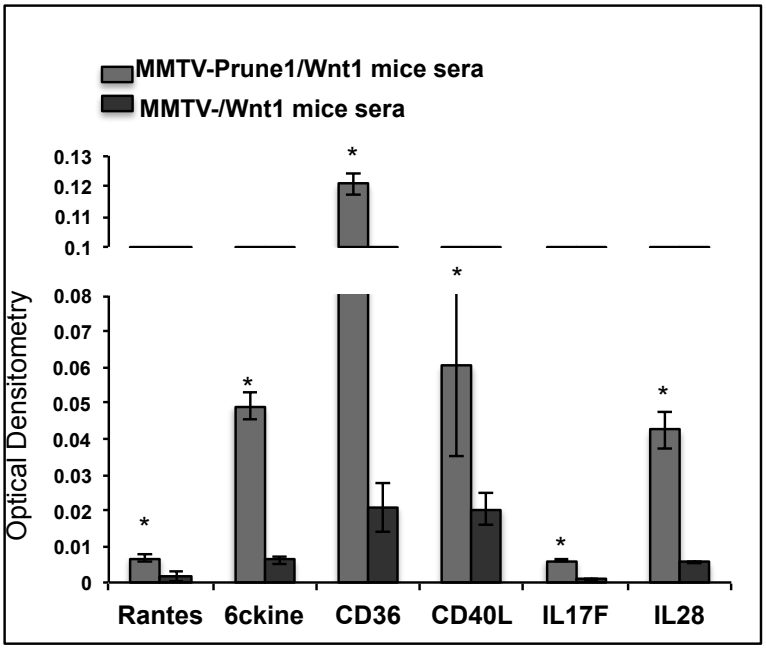

Figure 41: Prune-1 induces IL17-F and IL-28 inflammatory cytokines also *in vivo*. A mouse cytokine antibody array was performed to detect the expression levels of 17 cytokines (previously found up- or down-regulated by Prune-1) in sera collected from MMTV-Prune1/ Wnt1 and MMTV-Wnt1 mice. Among the n.17 cytokines modulated by Prune-1, we found n.6 cytokines significantly up-regulated in sera from MMTV-Prune1/Wnt1 mice compared to MMTV-Wnt1. Among those, a significant up-regulation of IL-17F and IL-28, was found with an opposite trend in comparison to the cytokines in the CM of Prune-1-silenced 4T1 cells. Data are mean ± SD. "*" $p \leq 0.05$.

3.8 Prune-1 activates metastatic pathways and enhances migratory phenotype in murine TNBC primary cells

In order to further dissect the function of Prune-1 in TNBC, in terms of intracellular pathways activation and extracellular communication with macrophages, primary cell lines from the tumours generated by MMTV-Prune1/Wnt1 and MMTV-Wnt1 mice were obtained (after 2 months from the tumour onset), as represented in Figure 42.

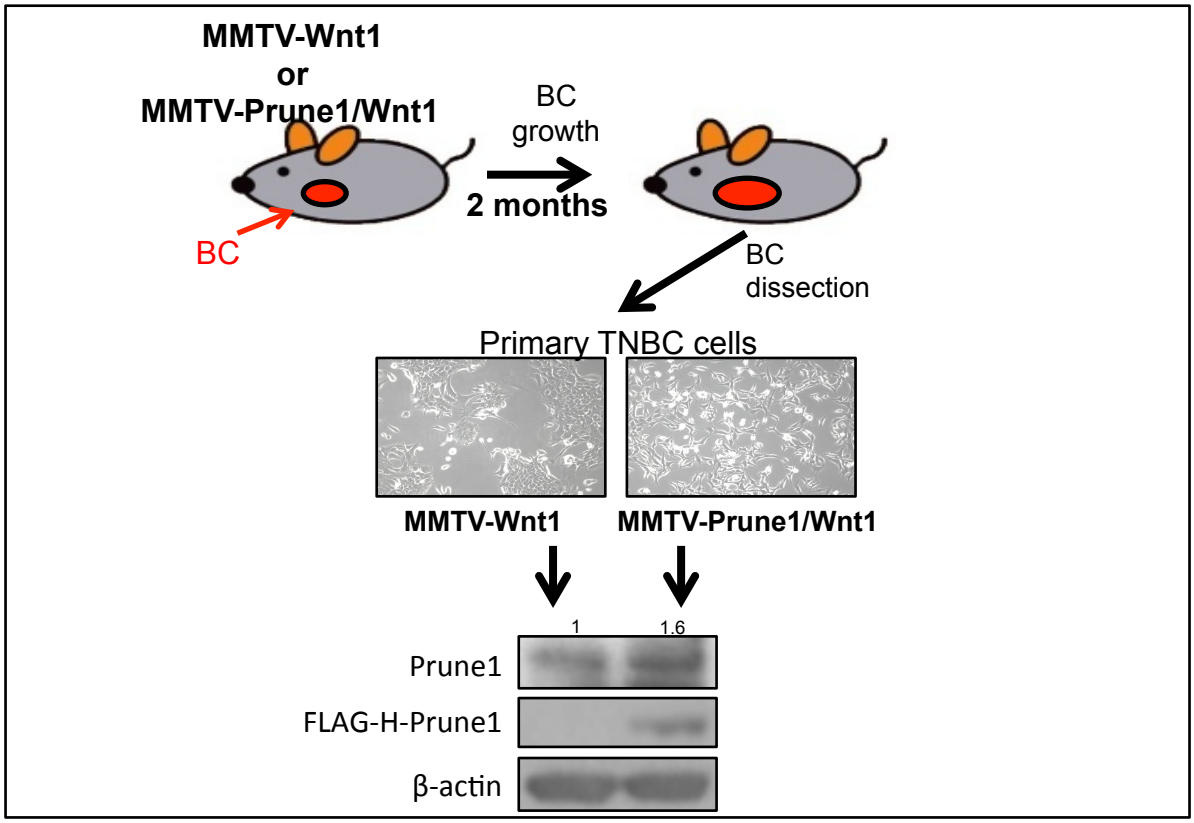

Figure 42: Schematic representation of the experimental design. After 2 months from the mammary tumours (Breast Cancer, BC) onset, the mice were sacrified, the primary tumours were removed and dissected to obtain primary TNBC cells. Bright field images showing murine primary MMTV-Prune1/Wnt1 and MMTV-Wnt1 TNBC cells (magnification 20X). Representative Western blotting analysis on total lysate from primary murine MMTV-Prune1/Wnt1 and MMTV-Wnt1 cells showing increased Prune-1 protein levels and expression of FLAG-Tagged human Prune-1 transgene

Furthermore, Western blotting analyses performed on these primary TNBC cells confirmed the activation of Wnt and TGF-β signaling (shown by increased levels of phospho-(Ser9/21)-GSK and phospho-SMAD2, respectively) in MMTV-Prune1/Wnt1 cells due to overexpression of Prune-1 when compared to MMTV-Wnt1 cells (Figure 43). Importantly, the same analyses also show induction of EMT in MMTV-Prune1/Wnt1 with undetectable E-Cadherin and higher N-Cadherin protein levels when compared to MMTV-Wnt1 cells (Figure 43), thus validating the data obtained *in vivo* with IF analyses. Furthermore, major phosphorilation levels of (Ser-473)-AKT, togher with decreased expression of its repressor PTEN in MMTV-Prune1/Wnt1 cells also suggest activation of PI3K-AKT signaling cascade due to Prune-1 overexpression (Figure 43).

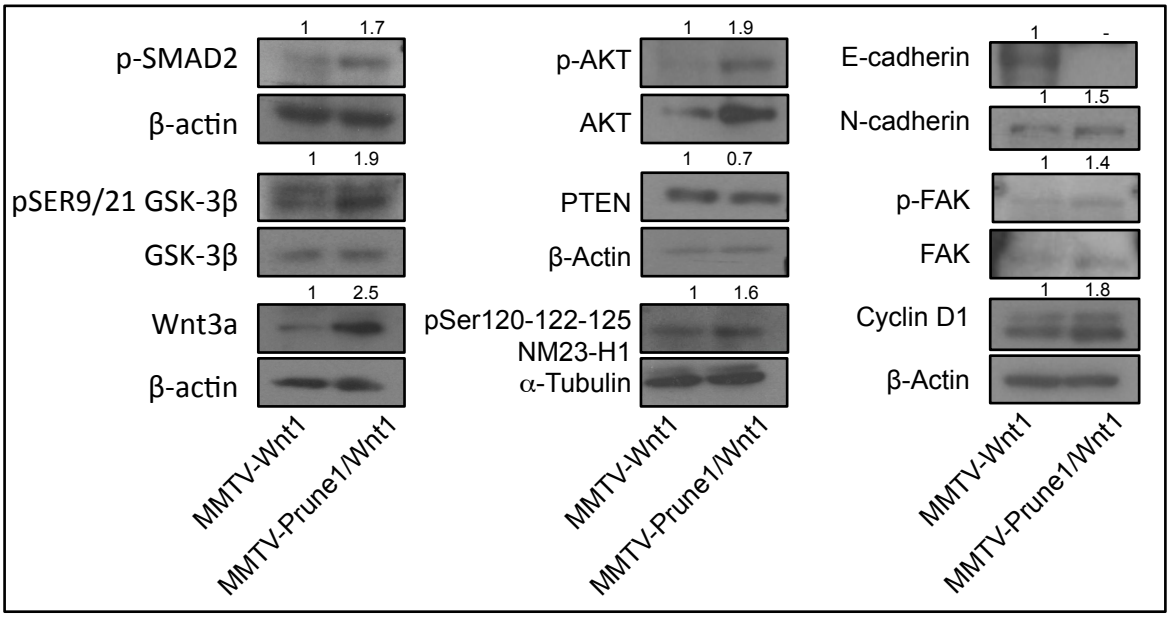

Figure 43: Prune-1 induces tumorigenic pathways activation in primary cells derived from MMTV-Prune1/Wnt1 model. Representative immunoblotting from tissue lysate from primary sections of BC (Breast cancer) obtained from females MMTV-Prune-1/Wnt1 and MMTV-Wny1. Densitometer analyses show increased TGF-β, Wnt, AKT pathways in MMTV-Prune1/Wnt1 cells compared to MMTV-Wnt1, as shown by increased levels of phospho-SMAD2, phospho-Ser9/21-GSK-3β and Wnt3a, phospho-AKT and reduction of PTEN, respectively. EMT markers were also evaluated showing E-Cadherin loss and N-Cadherin up-regulation in MMTV-Prune1/ Wnt1 cells. Increased levels of phospho-FAK and Cyclin-D1 in the same cells suggest enhancement of migration and proliferation, respectively, compaerd to MMTV-Wnt1 cells. The increase of phospho-Ser120-122-125-NDPK-A suggests that the "metastatic axis" involving Prune-1/NDPK-A complex, enhanced TGF-b signalling, reduction of PTEN and EMT (Ferrucci *et al.,* Under revision), is conserved also in metastatic TNBC cells.

This is of importance due to the role of PI3K/AKT signaling activation and PTEN loss in TNBC, as previously reported [3], [17], and here validated using gene-expression data from different public BC datasets showing that PTEN expression levels are lower in TNBC dataset (*i.e.,* Brown) than other BC datasets (n=1779, p= $7.3e^{-116}$; Figure 44).

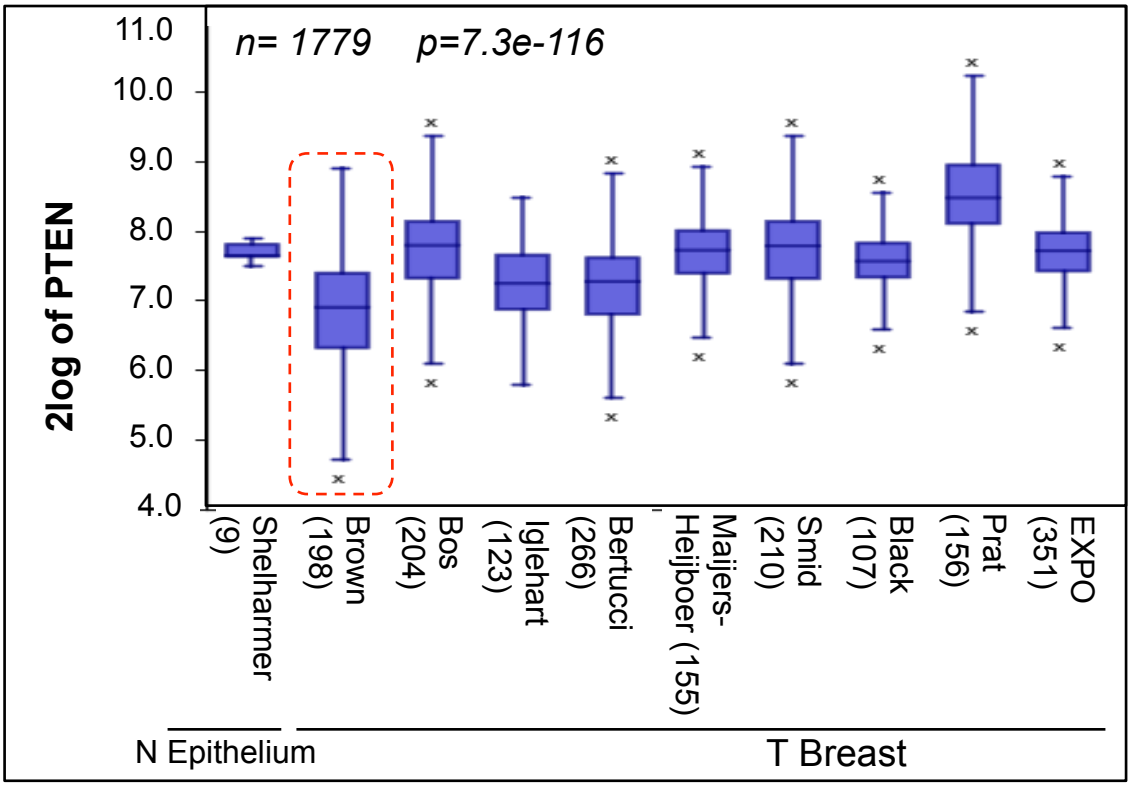

Figure 44: Low expression levels of PTEN in Triple Negative Breast Cancer. RNA log2 expression analysis of PTEN levels of primary BC samples across different publically available datasets, compared with normal Epithelium (N Epithelium). Data from 10 independent public-domain BC gene-expression datasets are shown. Overexpression of Prune-1 in all BC samples compater to normal epithelium is shown. Higher Prune-1 expression levels are found in Triple Negative Breast Cancer (TNBC) samples (*i.e.,* Brown; Burstein *et al.,* 2015) n=1779; p=7.3e-116

Furthermore, PTEN loss was also reported to anticipate the tumour onset by accelerating mammary oncogenesis when introduced in MMTV-Wnt1 GEMM models [137]. Of note, as already discussed, a novel Prune-1-driven metastatic axis in Medulloblastoma Group 3 which results in PTEN down-regulation [28]. This newly identified axis is driven by Prune-1/NDPK-A protein formation complex and was inhibited by a small cell permeable competitive peptide (CPP) that have the ability to inhibit the protein complex formation [47]. Prune-1 has the ability to bind NDPK-A when phosphorylated in Serine (120-122-125) amino acid residues [39]. For the above reasons, we investigated the phosphorylation levels of NDPK-A in our primary TNBC cells. As expected, we found higher phospho-(Ser-120-122-125)-NDPK-A levels in MMTV-Prune1/Wnt1 than MMTV-Wnt1 (Figure 43). Altogether these findings further validated the ability to Prune-1 to bind NDPK-A and subsequently to enhance canonical TGF-β cascade (via SMAD2), thus resulting in EMT (with E-Cadherin loss and N-Cadherin up-regulation) and down-regulation of PTEN. This confirm the Prune-1-driven metastatic axis also in metastatic TNBC primary cells (*i.e.,* MMTV-Prune1/Wnt1).

Furthermore, our Western blotting analyses also show increased levels of Cyclin-D1 and activated Focal adhesion kinase (FAK), as shown by higher levels of phospho-(Tyr397)-FAK in MMTV-Prune1/Wnt1 compared to MMTV-Wnt1 cells, (Figure 43) thus suggesting increased proliferative and migratory properties in these primary Prune-1-overexpressing TNBC cells.

These findings were further validated *in vitro* through proliferation and migration assays performed using X-Celligence technology. Our data show primary MMTV-Prune1/Wnt1 cells with higher proliferation and migration rates (Figure 45A-B,respectively) compared to MMTV-Wnt1 cells.

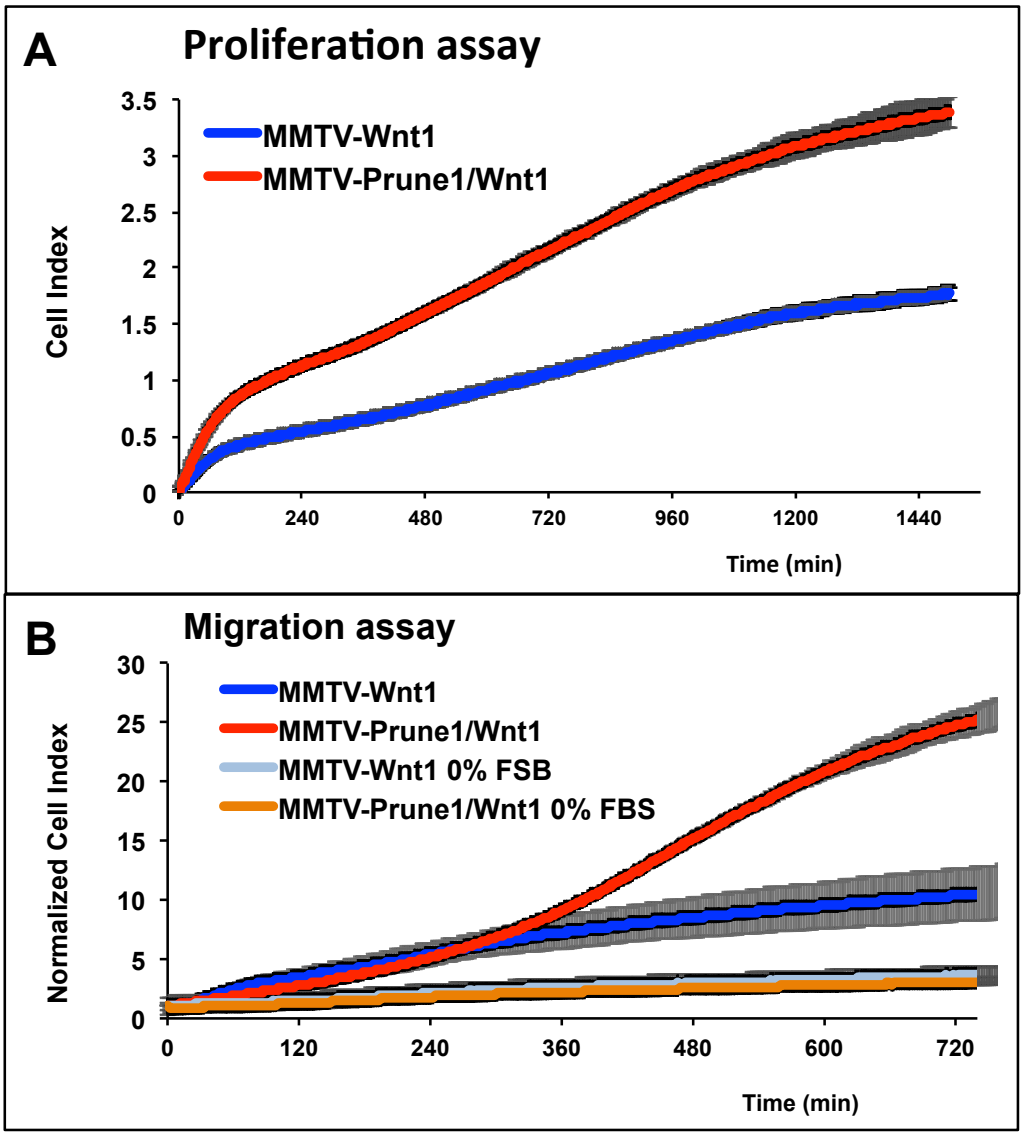

Figure 45: Prune-1 enhances proliferation and migration of TNBC *in vitro*. Cell Index as measure of cell proliferation **(A)** and migration **(B)** of MMTV-Prune1/Wnt1 (red) and MMTV-Wnt1 (blue), as generated by xCELLigence RTCA software. Migration kinetics were monitored in response to 10% FBS (red, blue) and to 0% FBS (brown, light blue) as negative controls. MMTV-Prune1/Wnt1 cells (red) showed increased proliferative **(A)** and migratory properties in response to 10% FBS Gradient (**B**), in comparison with MMTV-Wnt1 cells (blue). Data are means +/- SD of triplicate samples.

These results were further validated *in vivo* by performing xenograft orthotopic implantation of our primary TNBC cells in athymic Nude-Foxn1^{nu} female mice (4-weeks old). In details, MMTV-Prune1/Wnt1 and MMTV-Wnt1 cells (1 x 10^5) were injected into mammary fat pad of two groups of mice (n=2 for each group) as shown in Figure 46A. After 1 month from tumorigenic cells implantation (T0), the xenografted mice was injected with a fluorescent imaging probe (XenoLight RediJect 2-DeoxyGlucosone [DG] 750; or DG-750; Perkin Elmer) for *in vivo/ex vivo* targeting of tumours that typically exhibits elevated glucose uptake rate in comparison to surrounding tissues. The xenografted mice were injected with DG-750 and sacrified after 6 hours (in order to achieve maximum glucose targeting and enhanced tumour uptake) to perform *ex vivo* fluorescence imaging in living tissues using an imaging system (IVIS 3D Illumina; Xenogen/Caliper).

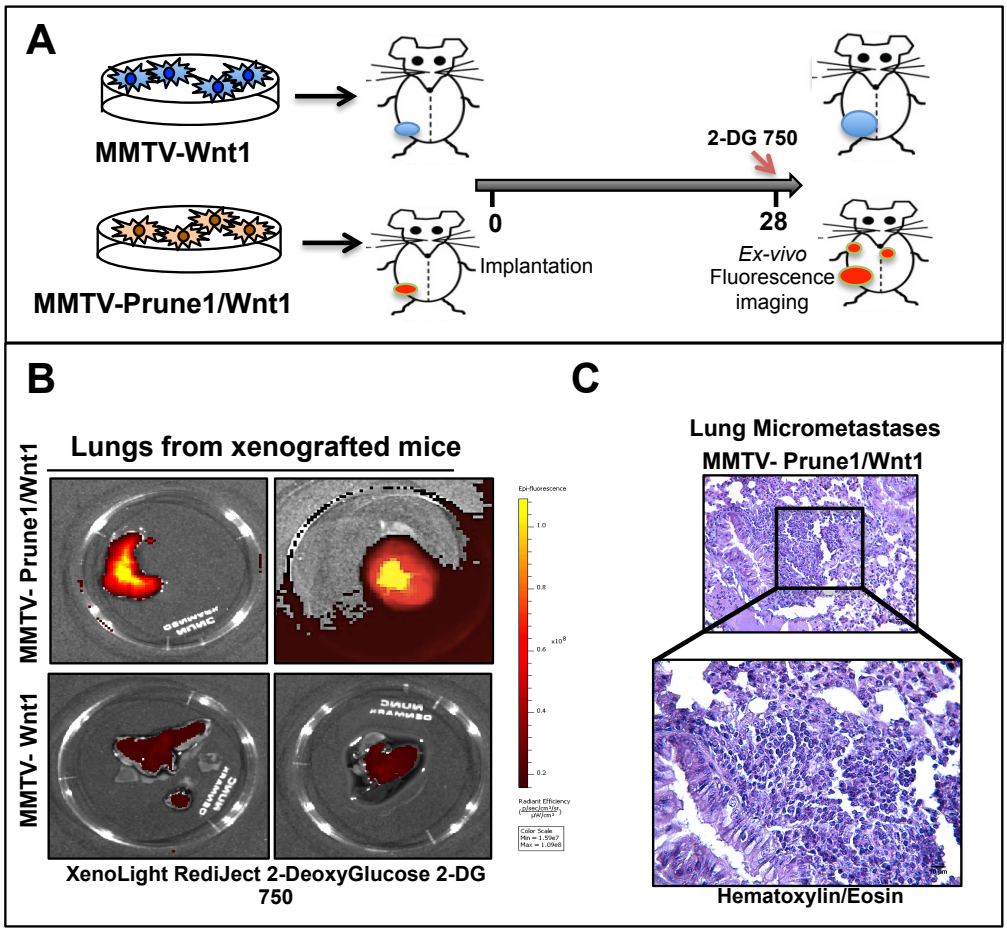

Figure 46: MMTV-Prune1/Wnt1 cells are able to metastatize lungs in orthotopic xenograft mice models. (A) Schematic representation of the experimental design. MMTV-Prune1/Wnt1 or MMTV-Wnt1 cells (1 x 10^5) were orthotopically implanted into mammary fat pad of athymic Nude-Foxn1^{nu} female mice (4-weeks old; 2 mice for each group). **(B)** *Ex vivo* fluorescent images of the dissected lungs from mice implanted with MMTV-Prune1/Wnt1 or with MMTV-Wnt1 cells after 28 days from implantation (T0) and 6 hours post-injection of XenoLight RediJect 2-DeoxyGlucose 2-DG 750. Lungs from mice implanted with MMTV-Prune1/Wnt1 cells tissues strong fluorescence signals, indicating the presence of metastatic foci. **(C)** Micrometastases in lungs from MMTV-Prune1/Wnt1 mice were detected through haematoxylin and eosin staining. Magnification, 20X, 40X.

We detected positive fluorescence signals (due to DG-750 uptake) in the lungs derived from the xenografted mice implanted with MMTV-Prune1/Wnt1 cells, but not in those from mice implanted with MMTV-Wnt1 cells (Figure 46B), thus showing the presence of metastatic foci driven by Prune-1-overexpressing primary TNBC cells. The presence of micrometastases in lung from MMTV-Prune1/Wnt1-implantedmice was also confirmed through Hematoxylin/Eosin staining, as shown in Figure 46C. Moreover, these data further confirm the migratory properties of MMTV-Prune1/Wnt1 TNBC cells also *in vivo*.

3.9 Prune-1 activates metastatic pathways and enhances migratory phenotype in murine TNBC primary cells

Whether Prune-1 is responsible for the activation of TAMs in these primary Wnt1-overexpressing TNBC cells was also investigated. For this purpose, the conditioned media from MMTV-Prune1/Wnt1 and MMTV-Wnt1 primary cells (collected after 24 hours) were used to treat macrophages (*i.e.,* J774) *in vitro* and their subsequent activation was evaluated by performing Western blotting analyses (Figure 47A). Untreated macrophages were used as negative control. Our data show higher phospho-STAT3 levels in J774 macrophages treated for 30 minutes with the conditioned media from MMTV-Prune1/Wnt1 compared to those treated with media from MMTV-Wnt1 cells (Figure 47B).

These data further confirm the role of Prune-1 in TNBC cells to activate macrophages toward a pro-inflammatory M2-phenotype.

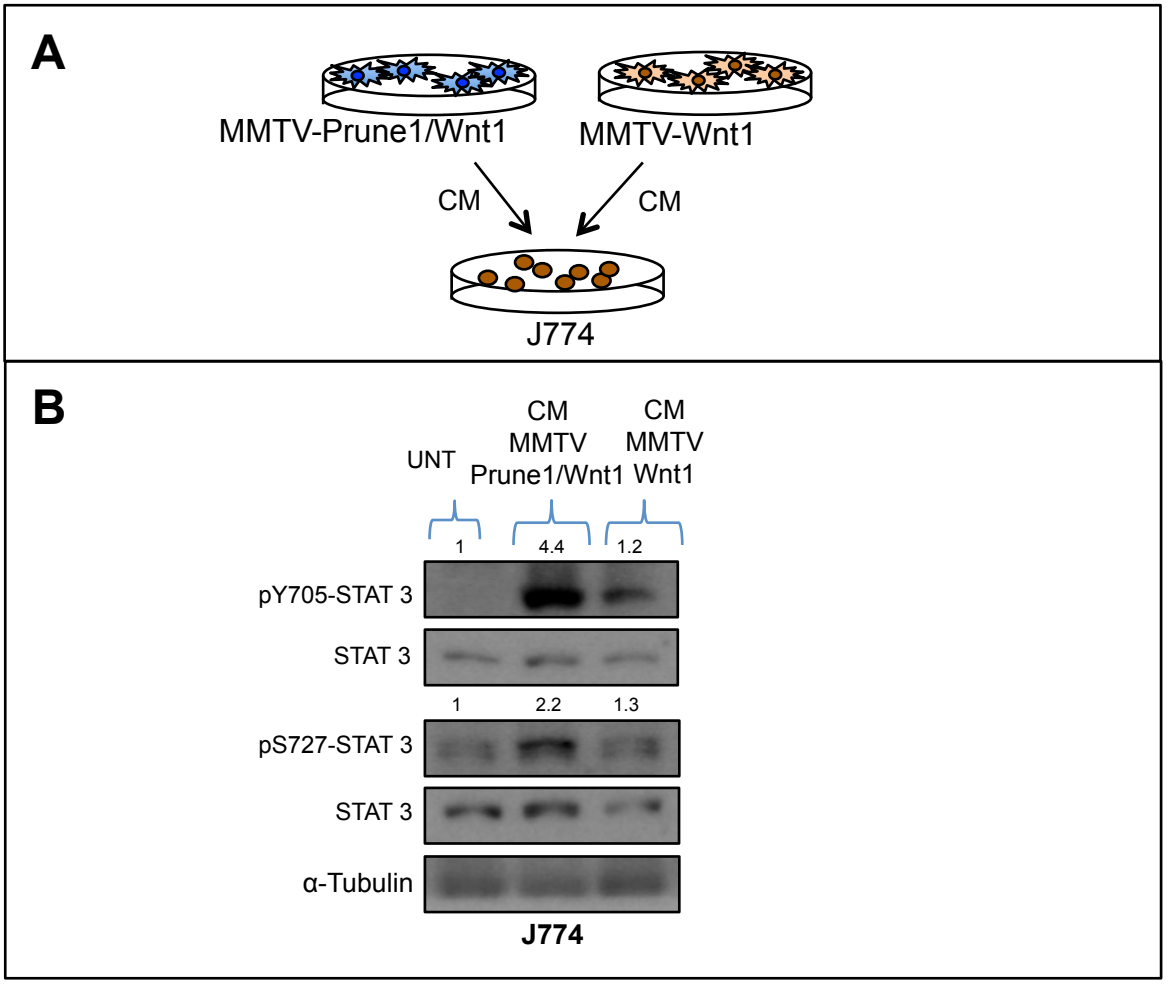

Figure 47: Prune-1 in TNBC cells activates macrophages in a paracrine manner *in vitro*. (A) Representative scheme for the experiment using MMTV-Prune1/Wnt1 and MMTV-Wnt1 primary TNBC cells. Conditioned media from these primary cells were collected after 24 hours. Macrophages (J774) were starved in for 6 hours in serum free media and then grown for 30 minutes in the conditioned media previously collected from MMTV-Prune1/Wnt1 and MMTV-Wnt1 cells. Untreated (UNT) macrophages were used as negative controls. **(B)** Immunoblotting for the indicated proteins in J774 macrophages grown for 30 minutes in conditioned media (CM) from MMTV-Prune1/Wnt1 and MMTV-Wnt1 cells. Those macrophages grown in CM collected from MMTV-Prune1/ Wnt1 cells show increased phosphorylated-STAT3 protein compared to those treated with CM from MMTV-Wnt1 cells. The densitometer analyses for the proteins were shown. α-Tubulin levels were used as loading control.

In another set of experiments, we also investigated if Prune-1 can drive the polarization of macrophages *in vitro* by evaluating the expression levels of some of the "M2-genes", such as MMP-9 and Arginase (Arg-1) 1 and IL-10 [138] [139]. We found higher Arg1, MMP9 and iL-10 levels in J774 macrophages grown for 48 hours in conditioned media from MMTV-Prune1/Wnt1 cells compared to those grown in media from MMTV-Wnt1 cells (Figure 48). Further, both primary TNBC cells were found with the ability to inhibit TNF-α, a well known marker for M1 status [138] (Figure 48).

Importantly, J774 grown in conditioned media collected from MMTV-Prune1/Wnt1 cells also show decreased levels of iNOS, another M1-marker [138].

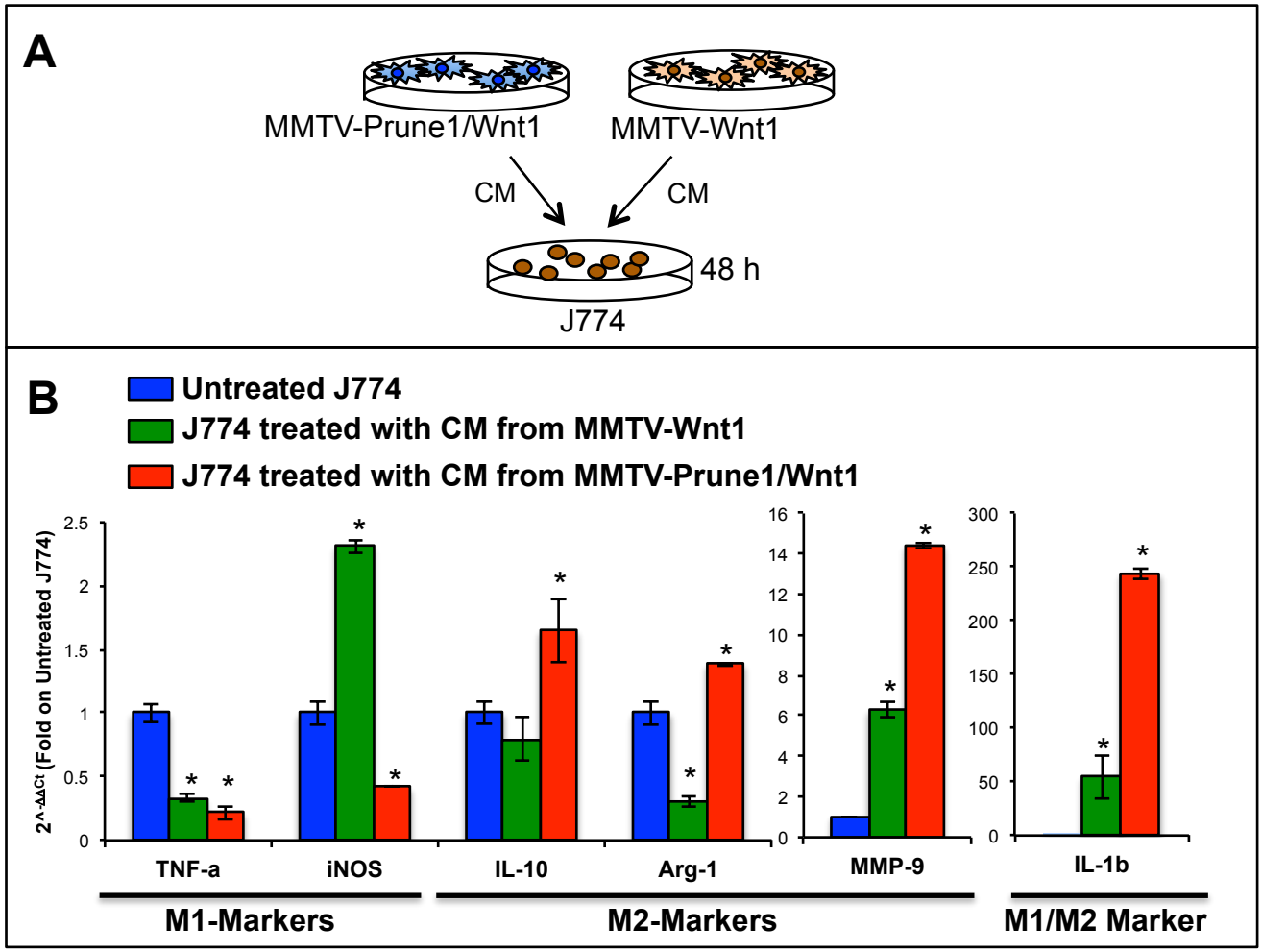

Figure 48: Prune-1 induces polarization macrophages toward an M2 status *in vitro*. (A) Representative scheme for the experiment using MMTV-Prune1/Wnt1 and MMTV-Wnt1 primary TNBC cells. Conditioned media (CM) from these primary cells were collected after 24 hours. Macrophages (J774) were starved in for 6 hours in serum free media and then grown for 48 hours in the CM previously collected from MMTV-Prune1/Wnt1 and MMTV-Wnt1 cells. Untreated macrophages were used as negative controls. **(B)** Real-Time-PCR analysis of M1-associated genes, including TNF-α and Inducible nitric oxide synthase (iNOS), and the M2-associated gene, IL-10, Arg-1, MMP-9 and IL-1β in J774 untreated (blue) or stimulated with CM collected from MMTV-Prune1/Wnt1 (red) and MMTV-Wnt1 (green) for 48 h. Increased levels of M2-associated genes (*i.e.,* IL-10, Arg-1, MMP-9 and IL-1β), with reduction in M1-markers (*i.e.,* TNF-α and iNOS) is shown in J774 treated with CM from MMTV-Prune1/Wnt1 compared to those grown in CM derived from MMTV-Wnt cells. "*" $p<0.05$.

Of interest, we found MMTV-Prune1/Wnt1 with the ability to strongly increase IL-1β levels in those J774 grown in their conditioned media (Figure 48). Nevertheless, high levels of IL-1β are present in M1-polarized but not in M2-polarized macrophages [140]. This is not in contrast with studies on dynamic macrophage polarity gradient from M1 through M2 phenotype reported high intracellular

levels of IL-1β in those macrophages polarized towards, but not at, M2 phenotype by extracellular Adenosine triphosphate (ATP; [141]). In details, this study identified pyrophosphate chains (PPi) of extracellular ATP to inhibit the release of IL-1β in "M1-toward M2-polarized" macrophages, thus leading to IL-1β intracellular accumulation. This ATP-mediated inhibition of IL-1β release, during macrophages polarization, occurred by trapping the inflammasome complex and inhibiting its activation through intracellular modulation during F-actin polymerization processes [141]. Prune-1 has an exopolyphosphatase activity (PPX/PPase) with higher affinity for short chain over long chain inorganic Polyphosphates (Poly-P) [22] Of importance, Prune-1 was also found to positively modulate microtubules polymerization processes during mitosis [29]. Future studies aimed to investigate the potential role of Prune-1 as natural source for extracellular Poly-P, including PPi, together with its potential involvement into Actin polymerization processes, may explain the intracellular accumulation of IL-1β during M1-M2 macrophages polarization.

Altogether, our results suggest that the overexpression of Prune-1 in TNBC cells has a role in the intercellular communication between tumorigenic cells and macrophages to induce their activation and M2-polarization both *in vitro* and *in vivo*.

3.10 Prune-1 induces the lung pre-metastatic niche via exosomes

The M2-polarization of TAMs in metastatic TNBC is driven by Prune-1 through the activation of intracellular signaling pathways (*e.g.,* TGF-β cascade) and paracrine extracellular secretion of soluble factors (*e.g.,* inflammatory cytokines) such as IL-17F and IL-28A.

During the last years, tumour-derived extracellular vesicle (*e.g.,* Exosomes) are emerging as new factors that promote tumour progression and metastatic dissemination with several mechanisms, including the modulation of the antitumour immune response in the tumour microenvironment [142]. In this regard, microvesicles or exosome derived from tumour cell lines were found with the ability to induce T cell apoptosis *in vitro* through Fas ligand [FASL] and Galectin 9, to induce MDSCs by impairing the differentiation of myeloid precursors into Dendritic cells, to promote Tregs function and to impair the cytotoxic actions of NK and $CD8^+$ T cells mostly due to the presence of membrane-bound TGF-β [143].

Of importance, tumour-derived exosomes are also responsible for organotropic metastasis, by preparing the pre-metastatic niche in terms of favourable microenvironment at the future metastatic site. The "organotropic distribution" occurres through a specific repertoire of exosomal integrins (ITGs) expressed on tumour-derived exosomes (distinct from tumour cells) which dictates the adhesion of the exosome to a specific target cell type in peculiar organs. This cell-type specific exosome integrins uptake also triggers signaling pathways and inflammatory responses in target cells,

resulting in the education of that organ and rendering it permissive for the growth of metastatic cells, thus directing organ-specific colonization [100]. Notably, exosomal ITG$\alpha_6\beta_4$ and ITG$\alpha_6\beta_1$ bind lung-resident fibroblasts and promote pro-migratory and pro-inflammatory by activating the Src-S100A4 axis during the pre-metastatic niche formation, thus governing lung tropism in BC, including TNBC subgroup [100].

Furthermore, exosomes were also reported with a role in the crosstalk between TNBC cells and macrophages. In this regard, exosomes-derived from TNBC cells (*i.e.,* MDA-MB-231) have the ability to induce an inflammatory response in macrophages *in vitro* and *in vivo* in terms of NF-kB signaling activation and inflammatory cytokines [106].

Since Prune-1 induces TAMs activation in a paracrine manner and promotes lung metastasis in our GEMM of metastatic TNBC, we investigated if exosomes derived from MMTV-Prune1/Wnt1 TNBC cells can modulate the lung pre-metastatic niche in these transgenic mice. In an effort to find a global picture of those Prune-1-driven exosomal proteins that are involved in the pre-metastatic niche formation, proteomic analyses were performed on the exosomes secreted by our primary TNBC cells. For this purpose, exosomes were isolated from both MMTV-Prune1/Wnt1 and MMTV-Wnt1 cell culture supernatants by adopting the methodology described [144] and exosomal markers were evaluated through western blotting analyses (Figure 49).

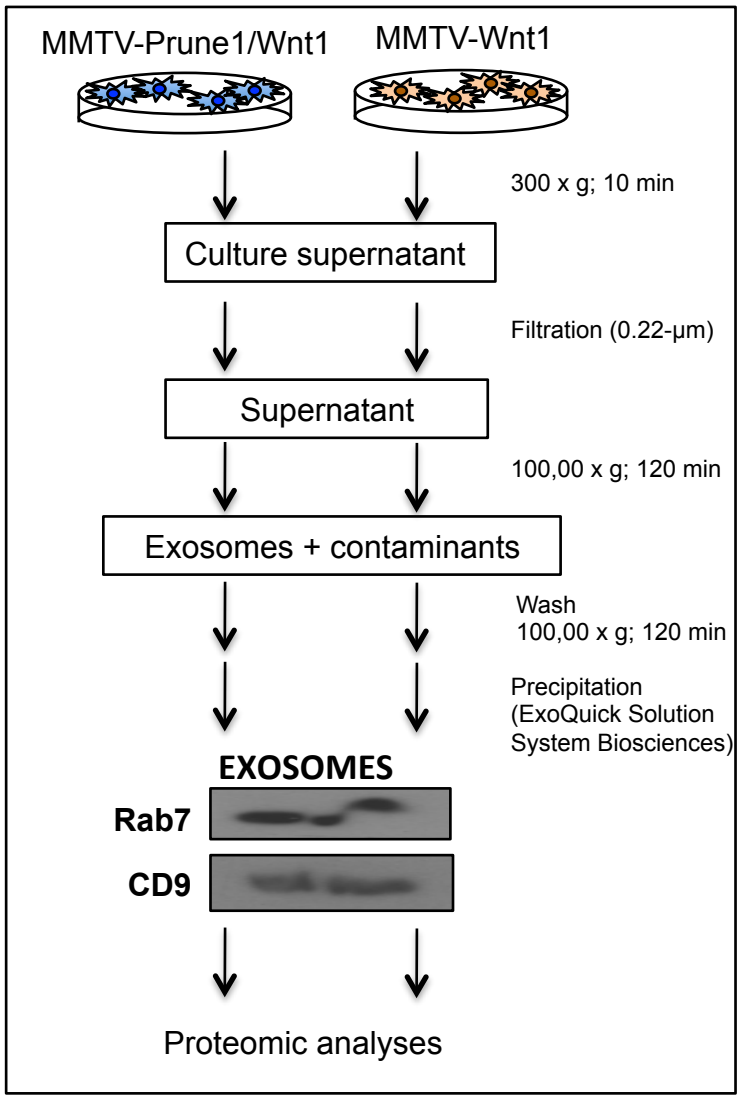

Figure 49: Representative scheme for the experiment using exosomes collected from MMTV-Prune1/Wnt1 and MMTV-Wnt1 primary TNBC cells. The isolation and purification of exosomes was performed following the methodology previously described by Clotilde Thery, et al., (Current Protocols in Cell Biology. 2006. 3.22.1-3.22.29) and using "ExoQuick Exosome Precipitation Solution"(#EXOQ5A-1, System Biosciences) to improve the yeld of purified exosomes. Representative immunoblotting with indicated antibodies (*i.e.,* Rab7 and CD9, as exosomal markers).Proteomic analyses were performed using label-free quantitative mass spectrometry technology as previously described (Cox *et al.*, Mol Cell Proteomics (2014).13(9): p. 2513-26).

Subsequently, in order to detect potential changes in the protein expression induced by Prune-1, the exosomal proteins were analyzed by taking advantage of the label-free quantitative mass spectrometry technology [145].

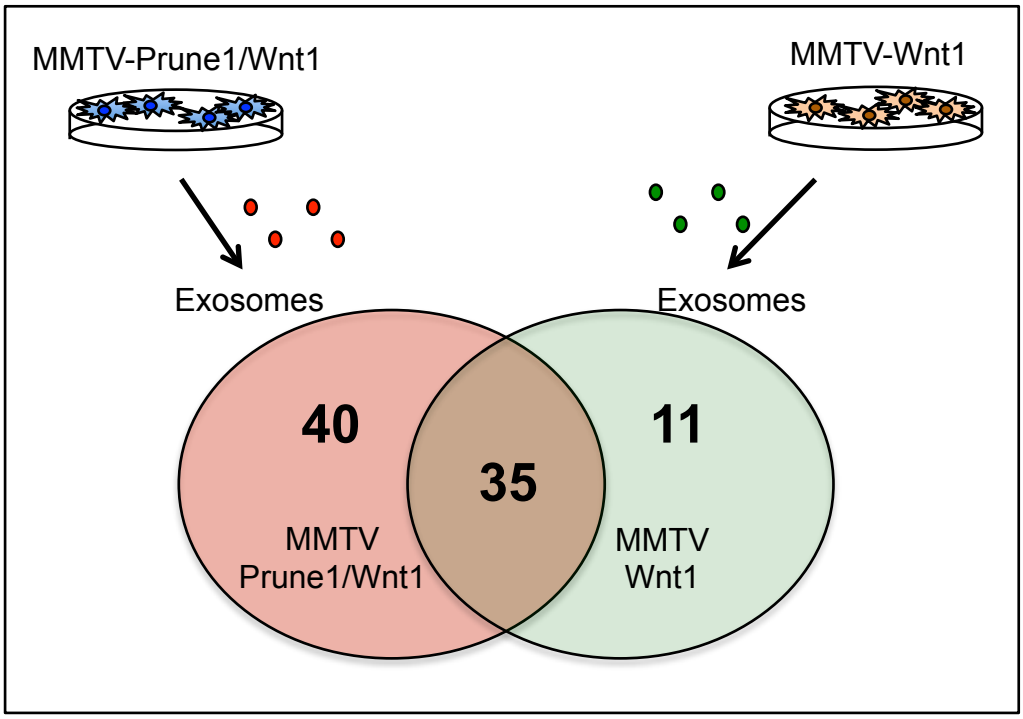

Figure 50: Representative scheme for proteomic analyses performed on exosomes. Exosomes isolated from the media supernatants of murine primary MMTV-Prune1/Wnt1 and MMTV-Wnt1 cells (as not-metastatic and metastatic TNBC cellular model, respectively) share n.35 common proteins, while exosomes derived from MMTV-Prune1/Wnt1 or from MMTV-Wnt1 have n.40 and n.11 mutually exclusive proteins, respectively. The results are representative of three independent experiments.

These analyses show that exosomes isolated from the media supernatants of murine primary TNBC cells share n.35 common proteins, while exosomes derived from MMTV-Prune1/Wnt1 or from MMTV-Wnt1 have n.40 and n.11 mutually exclusive proteins, respectively (as summarized in Figure 49).

Among the exosomal proteins secreted by MMTV-Prune1/Wnt1 cells (n.40, listed in Table 11), we identified proteins linked to EMT, such as Vimentin (Vim) and "90 kDa heat shock protein" (HSP90) [146], and with a role in BC motility and metastasis, including "Interferon induced transmembrane protein 3" (Ifitm3), Versican (Vcan), "Lysosomal-associated membrane protein 2" (Lamp2) and Syndecan binding protein (Sdcbp). Of note, Ifitm3 was found overexpressed in invasive BC with a function related to progression and motility of TNBC cells (MDA-MB-231) [147], Lamp2 overexpression in BC patients positively correlated with tumour grade [148] and Vcan was reported to enhance TNBC bone metastasis (using 4T1 cellular model) by supplying a favorable microenvironments for tumor metastasis in bone [149].

Table 11: Mutually exclusive proteins found into exosomes derived from MMTV-Prune1/ Wnt1 mice, as GEMM of metastatic TNBC.

Gene symbol	Gene name	Protein Function	Gene symbol	Gene name	Protein Function
Aqp1	aquaporin 1	Water-channel; osmotic gradient	**Ppia**	peptidylprolyl isomerase A	folding of proteins
Htra1	HtrA serine peptidase	Serine protease	**Cd81**	CD81 antigen	lymphoma cell growth
Lamp2	lysosomal-associated membrane protein 2	metastasis	**Slc16a1**	solute carrier family 16 member 1	transport across the plasma membrane
Hsp90aa1	heat shock protein 90 a1	protein folding functions	**Itih2**	inter-alpha trypsin inhibitor, heavy chain 2	carrier
Emb	embigin	outgrowth of motoneurons	**Actbl2**	actin, beta-like 2	cell motility
Anxa11	annexin A11	midbody formation	**Gnai2**	guanine nucleotide binding protein alpha inhibiting 2	transmembrane signaling systems
Emilin2	elastin microfibril interfacer 2	anchoring smooth muscle, regulate vessel assembly	**Ezr**	ezrin	Connectcytoskeletal structures to the plasma membrane
Ifitm3	interferon induced transmembrane 3	inhibits the entry of viruses	**Anxa7**	annexin A7	membrane fusion
Vim	vimentin	Motility, EMT, metastases	**Ifitm2**	interferon induced transmembrane 2	inhibits the entry of viruses
Tpi1	triosephosphate isomerase 1	Glycolysis, gluconeogenesis	**Gapdh**	glyceraldehyde-3-phosphate dehydrogenase	glycolysis
Stom	stomatin	ion channel activity	**Col6a1**	collagen type VI, alpha1	cell-binding protein
Cd82	CD82 antigen	costimulatory signals for the TCR/ CD3	**Edil3**	EGF-like repeats and discoidinI-like domains3	Adhesion, Inhibits formation of vascular structures
Mme	membrane metallo endopeptidase	destruction of opioid peptides	**Aqp5**	aquaporin 5	water channel
Sdcbp	syndecan binding protein	Multifunctional adapter protein	**Plscr1**	phospholipid scramblase 1	transbilayer migration
Vcp	valosin containing protein	Fragmentation and reassembly of golgi	**Ehd2**	EH-domain containing 2	membrane reorganization
Tinagl1	tubulointerstitial nephritis antigen-like 1	Adrenocortical zonation, repressing the CYP11B1	**Col15a1**	collagen, type XV, alpha 1	microvessels and muscle cells
Gnb1	guanine nucleotide binding protein,beta 1	transmembrane signaling systems	**Hist1h2bf**	histone cluster 1, H2bf	compact DNA
Cd9	CD9 antigen	platelet activation and aggregation	**Col18a1**	collagen, type XVIII, alpha 1	inhibits endothelial cell proliferation
Chmp4b	charged multivesicular body 4B	endosomal sorting	**Ldha**	lactate dehydrogenase A	glycolytic metabolism
Igsf8	immunoglobulin superfamily, member 8	diverse functions ascribed to CD81 and CD9	**Vcan**	versican	intercellular signaling

Notes: Annotation of exosomal protein functions by Gene Ontology (GO) terms.

Most importantly, Syndecan Binding Protein (Sdcbp; or Syntenin-1), is an adaptor molecule involved in a variety of cellular processes, including metastasis. High expression levels of Syntenin-1 in BC primary tumours was significantly related to patients OS and EFS [150], while it was found negatively correlated to ER expression [151]. Furthermore, among different BC cells, Syntenin was found overexpressed in TNBC cells with invasive/metastatic phenotype (*i.e.,* MDA-MB-231) [152] with a role in promoting cell migration and invasion both *in vitro* (by activating AKT [153], Integrin-β1 [150], MAPK [150] and TGF-β signaling and EMT [154]) and *in vivo*, thus promoting tumour growth and lung metastases. Interestingly, Syntenin-1 enhances the canonical TGF-β pathway (mediated by SMAD activation) by inhibiting the endocytosis of TGF-β type I receptor (*i.e.,* TGFBR1) mediated by Caveolin, thus preventing its internalization and degradation [155]. Therefore, the overexpression of Syntenin-1 in certain tumorigenic cells results in increased expression of TGFBR1 on cell surface, enhanced SMAD activation and induction of EMT, thus leading to metastatic spread [155]. Importantly, the expression of Syntenin-1 in melanoma metastatic microenvironment was shown to promote lung metastasis by influencing inflammatory network with induction of inflammatory cytokines (*i.e.,* IL17-A and IL-6) and both inflammatory and immunosuppressive cells (*i.e.,* Th17 cells and MDSCs, respectively) [156].

At this time, experiments of validation of this important correlation between Sdcbp and Prune-1 within TGF-β pathway are undergoing, but this will be the formal proof of another level of communication of Prune-1, thus promoting the niche formation and the lung metastases in TNBC.

In summary, our results indicate that Prune-1 is involved in extracellular mechanisms of communication between primary tumour (*i.e.,* TNBC) and distinct organs (*e.g.,* lungs) to prime a favorable local microenvironment as a pre-metastatic niche formation also by modulating the exosome protein content.

DISCUSSION AND FUTURE PERSPECTIVES

Here we have investigated the effects of Prune-1 in TNBC, the subgroup of BC with the worst prognosis compared to the other subtypes due to the aggressive clinical behaviour, the propensity to distant metastasis [19], and a lack of recognized molecular targets for therapy (*i.e.,* ER, PgR and HER2) [4]. In fact, despite optimal systemic chemotherapy, all women with metastatic TNBC ultimately die of their disease. Therefore, metastatic TNBC remains with still unmet medical needs.

It is well established that the tumour development and the malignant metastatic progression are the result of the network of communication between cancer cells and immune cells in the tumour microenvironment [62]. Tumour-infiltrating immune cells include TAMs, mast cells, dendritic cells, T and B lymphocytes, and partially differentiated myeloid progenitors (MDSCs). Once recruited into the tumor microenvironment by tumor-secreted soluble mediators, the immune cells can contribute to the malignant progression of the cancer-cell phenotype. Moreover, they establish a complex network of interplay that contributes to the promotion and maintenance of an immunosuppressive microenvironment, which itself promotes immune escape, and as a consequence, enhances tumor progression [62].

Immune cells represent a major component of TNBC microenvironment [70] mainly due to the higher propensity of TNBC cells to generate "neoantigens" for their genomic instability and mutational burden [3]. Importantly, the variegate nature of the immune microenvironment in TNBC influences the risk of relapse and response to chemotherapy [72]. In fact, new four distinct TNBC subtypes with prognostic significance were defined based on the immune and metabolic markers within the tumour microenvironment [72]. Among these newly identified subtypes, the subgroup of patients characterized by high levels of immunosuppressive markers/cells ($PDL1^{High}$, $M2\text{-}Polarized\text{-}TAMs^{High}$, $Tregs^{High}$) and in a context of high glycolitic stroma ($MCT4^{High}$) and low TILs environment, are associated with signifincantly decreased OS with poor prognosis [72]. Thus, immune and metabolic markers have further stratified TNBC into subtypes that have implications for therapies targeting immune checkpoints and tumour metabolism.

GEMM are a useful resource for studying mammary cancers *in vivo* under genetically controlled and immune competent conditions, especially for metastatic TNBC, for which targeted treatment options remain an important unmet clinical need. Nevertheless, at this time GEMMs resembling the features of metastatic TNBC have not been described yet [134].

Here, we develop a GEMM of metastatic TNBC driven by Prune-1 (MMTV-Prune1/Wnt1) as useful source for preclinical studies to determine the efficacy of novel immunotherapeutic agents (alone or in combination with standard-of-care chemotherapy regimens) for the treatment of established metastatic

disease. Importantly, our data identified Prune-1 to promote *in vivo* tumour progression and distant metastasis in TNBC by taking part to the interplay between tumorigenic and immune cells (*i.e.,* TAMs) within the tumour microenvironment. Furthermore, we found Prune-1 contributing to the generation of an immunosuppressive environment in both primary tumour and lung pre-metastatic niche through the recruitment and polarization of M2-TAMs. As summarized in Figure 51, Prune-1 acts in metastatic TNBC by promoting the activation of intracellular tumorigenic pathways (*e.g.,* TGF-β, NF-kB and PI3K/AKT cascades), the release of extracellular infammatory molecules (IL-17F and IL28), and changes in exosomes protein content, of importance Sdcbp (Syntenin-1).

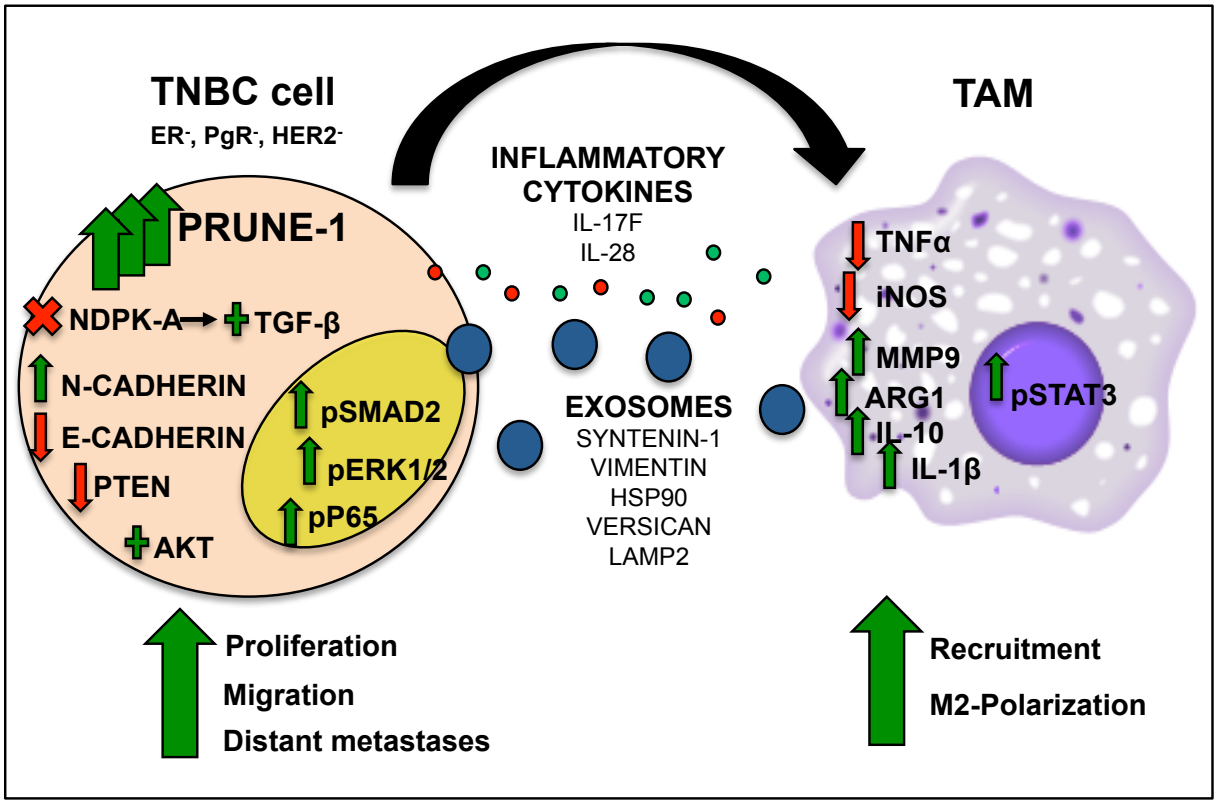

Figure 51: The proposed mechanism of action of Prune-1 in the crosstalk between tumorigenic cell and TAMs in TNBC microenvironment. Prune-1 acts in metastatic TNBC by promoting intracellular tumorigenic and inflammatory pathways activation (*i.e.,* TGF-β cascade, AKT, EMT, MAPK, NF-kB), and in a paracrine manner through the release of extracellular inflammatory molecules (*i.e.,* IL-17F and IL-28), and changes in exosomes protein content. These actions induce recruitment of TAMs in the TNBC microenvironment, promote their polarization toward anti-inflammatory/pro-tumorigenic-M2-status and prepare the soil for metastases within the premetastatic niche by modulating the exosomes protein content.

Prune-1 protein was previously identified as promoter of both tumour invasiveness and metastases, with these functions being mainly due to its interactions with specific protein partners, including NDPK-A [39, 45], and GSK-3β [36]. Through these interactions, Prune-1 modulates signaling cascades, including canonical WNT and TGF-β pathways [25], [28], which are involved in BC progression, including TNBC [59] [157], [158].

Recently, we identified a novel Prune-1-driven intracellular signaling involved in metastatic behaviour of Medulloblastoma Group 3 with poor prognosis [28]. This "metastatic axis" is guided by protein complex formation between Prune-1 and NDPK-A, whose levels were found overexpressed in those metastatic Medulloblastomas. We found Prune-1/NDPK-A protein complex to enhance the canonical TGF-β signaling (via phosphorylation of SMAD2), to up-regulate OTX2 and to inhibit the tumour suppressor PTEN, thus activating AKT pathway and promote EMT in metastatic Medulloblastoma Group 3 [28].

Here, our data in TNBC based on gene expression analyses through public available BC datasets, show higher expression levels of Prune-1 and SMAD-2/4 (as downstream effector targets of TGF-β cascade) and lower PTEN levels in TNBC samples compared to other BC datasets. We hypothesized that Prune-1 could take part to TGF-β signaling also in metastatic TNBC. In this regard, increased levels of phosphorylated/nuclear SMAD2 protein due to Prune-1 overexpression were shown both *in vitro* via Western blotting analyses performed on primary murine metastatic TNBC cells (MMTV-Prune1/Wnt1 cells) and *in vivo* through IF analyses performed on primary tumour mass derived from GEMM model of Prune-1-driven metastatic TNBC, thus confirming our hypothesis. Furthermore, increased levels of NDPK-A protein phosphorylated in Serine amino acid residues (Ser-120-122-125) that are responsible for the binding to Prune-1 were also observed in primary murine Prune-driven TNBC cells (*i.e.,* MMTV-Prune1/Wnt1 cells). This data suggest that Prune-1/NDPK-A protein complex may act as "driver" to promote metastatic dissemination also in TNBC, through enhancement of TGF-β cascade and downregulation of PTEN.

Nevertheless, NDPK-A was reported with opposite functions in BC, acting like both tumour suppressor or tumour promoter [43], [44]. Of interest, the overexpression of Prune-1 was found in those tumours that were also characterized by higher NDPK-A expression levels [42]. These data suggest that for those TNBC showing high NDPK-A expression levels, the increased Prune-1 levels might promote distant metastases through the "metastatic axis" by activating TGF-β pathway and inhibiting PTEN.

Furthermore, higher levels of extracellular NDPK-A was detected in sera from metastatic BC patients and a positive correlation between the extracellular levels of NDPK-A (secreted from TNBC cells) and the tumour growth was reported *in vivo* using xenograft mice models [43], thus suggesting a potential extracellular pro-angiogenic role for NDPK-A in TNBC. Of importance, extracellular Prune-1 was also detected in sera from patients with early stages of NSCLC [25]. Future efforts will be aimed to investigate the potential mechanism of actions of both extracellular Prune-1 and NDPK-A in metastatic TNBC for diagnostic, but also therapeutic purposes.

In this regard, a cell Competitive Permeable Peptide (CPP) containing the region of NDPK-A that is responsible for the interaction with Prune-1 protein, has been already developed in order to impair the NDPK-A/Prune-1 interaction. The therapeutic properties of CPP have been also defined *in vitro* using TNBC cell lines. In fact, the blockage of Prune-1/NDPK-A interaction using CPP reduced the proliferation rate of TNBC cells (MDA-MB-231) and inhibited AKT/mTOR and NF-kB signaling pathways [47], [48]. The CPP-mediated inhibition of NF-kB signaling in TNBC cells suggests that the anti-tumorigenic action of CPP can be investigated also *in vivo* in our GEMM of metastatic TNBC (MMTV-Prune1/Wnt1) in order to impair the recruitment and the polarization of TAMs in TNBC microenvironment.

The metastatic axis driven by Prune-1 in metastatic Medulloblastoma culminates in PTEN downregulation [28]. PTEN loss was a common feature of TNBC [3], and it was reported to anticipate the tumour onset, but not metastatic behaviour, when introduced in MMTV-Wnt1 GEMM mice [137]. However, these findings indicated that PTEN loss and activation of Wnt signaling are not sufficient to induce the metastatic spread in TNBC.

Here, we show that Prune-1 acts as metastatic driver in our MMTV-Prune1/Wnt1 mouse model and provide its mechanisms of action. We demonstrate that Prune-1 not only has the ability to promote Wnt signaling activation and PTEN inhibition, but also modulates the tumour microenvironment through the enhancement of TGF-β pathway, thus promoting metastatic spread.

Our findings further confirm that Prune-1-induced metastatic axis is mainteined also in TNBC and also suggest that Prune-1 overexpression, together with PTEN loss, can be taken into account to identified those metastatic TNBC.

TGF-β is known to regulate systemic immune surveillance of the tumour host by controlling immune responses, and it also plays a crucial role in the tumour microenvironment by modulating the proliferation, differentiation, survival and polarization status of different immune cells, including TAMs [87]. Our *in vitro* and *in vivo* results show Prune-1 to enhance TAMs recruitment and their polarization toward a pro-tumorigenic M2 status by promoting STAT3 activation, Arg1, MMP-9, IL-10 and IL-1β increase, and reducing iNOS and TNF-α expression levels in recipient macrophages. We hypothesized that Prune-1 recruits and polarize TAMs in tumour microenvironment of TNBC mainly through the activation of canonical TGF-β signaling. However, since TGF-β was reported to modulate the activation and the status of the other components of the tumour microenvironment (including MDSC, Lynphocytes, Neutrophyls, Dendritic cells and Cancer Associated Fibroblasts [CAFs]) [87], we cannot exclude the possibility that Prune-1 can also affect other immune-infiltrating cells and stromal component in TNBC microenvironment. Our data on human TNBC tissues indicate that high Prune-1 expression is also positively correlated to MDSCs ($CD11b^+$) and Tregs ($FOXP3^+$).

Furthermore, we found the anti-Prune-1 drug (AA7.1) to reduce MDSCs in the primary tumours of treated mice (Figure 29). This issue will be addressed in future studies.

Other molecular mechanisms by which Prune-1 modulates TNBC microenvironment may involve intracellular activation of other tumorigenic pathways. In this study we also provide evidences that Prune-1 in TNBC activates ERK1/2-MAPK, through the increased phosphorylation of ERK1/2 and NF-kB, through increased phosphorylation of p65 and its increased nuclear localization. An important question to be addressed is how Prune-1 promotes the ERK1/2-MAPK and NF-kB signaling pathways activation. A possible mechanism could be related to the Prune-1 ability to regulate Wnt signaling pathway, through its interaction with GSK-3β, and to the complex network of interactions existing between those signaling pathways. A crosstalk with a positive-feedback loop between the Wnt and ERK pathways has been identified in tumor cells [113]. Moreover, Wnt signaling pathway induces the expression of S100A4 [159], an important player in tumor progression and metastasis, whose expression was significantly increased in TNBC tissues with higher Prune-1 protein levels in our TNBC patient cohort. S100A4 in turn is a potent activator of the NF-kB signaling pathway [160], therefore it could act in an autocrine manner to promote the NF-kB pathway activation in Prune-1-overexpressing TNBC cells, thus providing a further link between the Prune-1-regulated signaling pathways. Further studies performed with specific inhibitors of these pathways and/or null-function mutants of the effectors of these pathways are needed to address this question, thus dissecting further the mechanism of Prune-1 action.

Furthermore, Prune-1 protein was identified as promoter of both tumour invasiveness and metastasis formation, with these functions being mainly due to its PDE activity [45]. In contrast, alterations in Prune-1 exopolyphosphatase (PPX/PPase) activity [22], due to autosomal recessive mutations, resulted in Microcephaly and PEHO-like syndrome affected patients [29], [30]. At this time we cannot exclude that Prune-1 PDE and PPX/PPase enzymatic activities play a role in modulating those signaling intracellular and/or extracellular pathways. Further, we showed increased levels of IL-1β (fold=250) in those macrophages treated with conditioned media collected from Prune-1-overexpressing TNBC cells. The intracellular accumulation of IL-1β in M2-polarizing macrophages was reported to be caused to extracellular ATP-derived pyrophosphates (PPi) [141]. For the above reasons, Prune-1 enzymatic PPX/PPase activities may be also involved in the mechanisms of macrophages polarization. Future studies will address the PPX/PPase enzymatic functions of Prune-1 also in tumorigenesis and polarization of TAMs by taking advantage of the use of specific inhibitors of Prune-1 enzymatic activities or Prune-1 mutants with null enzymatic activities.

Moreover, our *in vitro* and *in vivo* data also show that Prune-1 induces an immunosuppressive tumour microenvironment in TNBC also by releasing extracellular soluble mediators (*i.e.,* cytokines). Among

the cytokines, we found IL-17F and IL-28 as targets of the Prune-1-activated NF-kB signaling pathways [161], [162]. The molecular mechanisms that are responsible for the increased release of these tho cytokines in the conditioned media from 4T1 Prune-1 clones or in sera derived from MMTV-Prune1/Wnt1 mice in terms of increased synthesis, half-life or secretion of those proteins, will be dissected in future studies.

These Prune-1 induced-cytokines, once secreted, might also act on the tumour cells in an autocrine fashion or on immune cells (*e.g.,* macrophages) in paracrine manner within tumor microenvironment. In particular, these Prune-1 induced-cytokines could enhance the activation of Prune-1-induced signaling pathways, thus resulting in a positive feedback loop of activation. In fact, IL-17F, acting in similar manner as IL-17A, activates NF-kB and ERK1/2-MAPK signaling pathways [163], promotes the angiogenesis [164] and leads to the up-regulation of several chemokines and cytokines thus exacerbating the inflammatory tumor microenvironment [62]. These potential mechanisms of action will be dissected in future efforts.

Furthermore, we also found Prune-1 to prepare the lung pre-metastatic niche by modulating the exosomal protein content through proteomic analyses performed on exosomes collected from conditioned media derived from primary MMTV-Prune-1/Wnt1 and MMTV-Wnt1 TNBC cells. We found mutually exclusive proteins into exosomes derived from MMTV-Prune1/Wnt1 cells with a role in EMT and TGF-β signaling. These findings further validate Prune-1-induced EMT in metastatic progression [26], and describe a novel signaling mechanism of EMT independent from Prune1-induced TGF-β [28]

Finally we demonstrated *in vivo* using orthotopic xenografted immunocompetent mice model that the pharmacological inhibition of Prune-1 through AA7.1 drug [128], [28] resulted in decreased tumour growth and reduction in infiltrating M2-polarized TAMs. These results indicate that AA7.1 has immunomodulating properties. Importantly, we previously found that AA7.1 did not induce toxiciy by evaluating hematological, hepatic and renal parameters in treated mice [28]. Further, we recently reported a synergistic effect between AA7.1 and radiation in inhibiting the proliferation rate in medulloblastoma cells [28].

Future efforts will be aimed to test the pharmacological inhibition of Prune-1 via AA7.1 drug, alone or incombination with the current chemotherapy regimens and/or with immunotherapeutics (*e.g.,*immune-checkpoint inhibitors) in preclinical trials using our GEMM of metastatic TNBC.

This model of metastatic TNBC can be used in future to test non-invasive therapeutic approaches (e.g., natural compounds, [165]) alone or in combination with the chemotherapy regimens currently used in clinics. Among the emerging natural compounds with anti-tumorigenic actions and low toxicity in TNBC, Epigallocatechin Gallate (EGCG) from green Tea was found with the potential to inhibit

tumour growth *in vivo* (using orthotopic model of 4T1 cells) by inhibiting M2-polarization of TAMs through targeting exosomes-derived from TNBC cells [166].

In conclusion, our results show for the fist time that Prune-1 has a crucial role to drive metastatic spread in TNBC through two mechanisms of action. The first is related to its ability to induce migration and EMT in TNBC cells by activating different intracellular signaling pathways: TGF-β, NF-kB and PI3K/AKT (through PTEN downregulation). The second is related to its important contribution to generate an immunosuppressive microenvironment permissive to tumour growth and metastatic progression by taking part to the communication with TAMs to induce their recruitment and their polarization toward a tumour-promoting M2-phenotype. The interplay between Prune-1 and TAMs in the tumour microenvironment is mediated by the modulation of the release of inflammatory cytokines and exosomes driven by Prune-1. Among the cytokines, we found Prune-1-enhanced secretion of IL-17F and IL28 from TNBC cells. We also show for the first time that exosomes derived from Prune-1-overexpressing primary TNBC cells contain proteins with a role in EMT and metastases (*e.g.,* Syntenin-1). Targeting Prune-1 with a no-toxic drug (AA7.1) *in vivo* using orthotopic model of TNBC, results in decreased tumour growth mediated by the reduction of M2-Polarized TAMs in the tumour microenvironment. Altogether these findings were also validated in a GEMM model of metastatic TNBC, as useful source to future pre-clinical trial testing immunotherapeutics for metastatic TNBC treatment. Finally, we suggest that Prune-1 could be a new potential therapeutic target for treatment of metastatic TNBC.

ACKNOLEDGEMENT

First and foremost, I would like to thank my supervisor Prof. Massimo Zollo, my mentor, for giving me the experience to help me grow in many ways. Since my undergraduate experiences, from 2010 to date, he followed me step by step to ensure that I completed my graduated requirements and moved into this PhD program with success. I feel so very lucky to have the opportunity to work with him as a PhD student in his laboratory. Through graduated, post-graduated and PhD works with all his research team, housed in CEINGE Biotecnologie Avanzate, he has offered me valuable skills in scientific research, competitive grant writing skills, and conference presentation skills, all of which make the recipe for future success to become a higher education professional speaker and researcher. His absolute passion for what he shares with his students, with his rich and valuable knowledge in the field, is truly inspiring with an enduring enthusiasm for the subject matter being contagious! I'm very grateful for all the wonderful lessons that he has taught me over the past 4 years of my education, for his patient guidance and right advices he has provided throughout my time. He has always made time to review our experimental objectives and conclusions and give excellent guidance, despite his busy schedule. I really appreciate his help and feedback on our work and progress. Through his depth of knowledge, his expertise for the research topics, his continually questioning and positing, he has helped me strive to be a better thinker and future researcher. I have been extremely lucky to have a supervisor who gave me the strength, knowledge, ability and opportunity to undertake his research projects and to persevere and complete them satisfactorily. Without his blessings, this achievement would not have been possible. Most importantly, I just want to thank him for making himself available in a time of need with prompt responses to all my questions and queries. I definitely learned so much from him. He was very supportive and for that I really am grateful!

Then I would like to thank Prof. Piero Pucci and Prof. Kris Gevaert, my internal and external advisors, respectively, for giving me very helpful advices regarding the PhD project.

I would like to thanks to all the scientists who actively contributed to this project: Dr. Daniela Spano and Dr. Marianeve Carotenuto, who actively worked on this project laying the foundations for all the subsequent experiments; Prof. Maurizio Di Bonito, Prof. Gerardo Botti, Dr. Monica Cantile and Dr. Francesca Collina (Istituto Tumori Napoli Fondazione G. Pascale) for the anatomopathological evaluation and statistical correlations in our cohort of Triple Negative Breast Cancer patients; Prof. Kris Gevaert, my external advisor, and Dr. Jonathan Vandenbussche (VIB-UGent Center for Medical Biotechnology) for the proteomic analyses on the exosomes; Dr. Natascia Marino who generated the plasmid construct for the Transgenic Mouse Model; Prof. John Collard (Division of Cell Biology I, The Netherlands Cancer Institute, Amsterdam) who sent us MMTV-Wnt mice models; Porf. Eugene

Lukanid (Department of Molecular Cancer Biology, Institute of Cancer Biology, Danish Cancer Society, DK-2100 Copenhagen, Denmark) for S100A4 antibody; Prof. Giancarlo Troncone (Dipartimento di Sanità Pubblica, Scuola di Medicina e Chirurgia, Università Federico II di Napoli) for ER, PgR, HER2 antibodies; Dr. Adelaide Greco (CEINGE, Naples, Italy) for micro-TC imaging; Dr. Chiara Medaglia for the evaluation of the drug on Triple Negative Breast Cancer cells *in vitro*; Dr. Daniela De Martino for the *in vivo* esperiments; Dr. Cristina Maria Chiarolla, Dr. Luisa Dassi, Dr. Roberto Siciliano and Dr. Francesco Paolo Pennino for the immunohistochemical and immunofluoresce analyses.

I would like to thank my "tutors" Dr. Pasqualino de Antonellis, Dr. Marianeve Carotenuto and Dr. Daniela Spano for their time and their data criticism. I will never forget their precious lessons. They taught me how to deal scientific problems, how to solve scientific questions, how to design esperimental plans and how to decipher and interpret the obtained results. I would like to thank Dr. Daniela Spano for teaching me how to work in a team. Especially, I would like to thank Dr. Marianeve Carotenuto for her critical comments that have been very helpful during the last 2 years of my PhD program. Finally, I would like to further thank Dr. Pasqualino de Antonellis to let me understand the true sense of scientific research.

Next I would like to say thank to all the people I have met in the lab over the last 7 years because everyone taught me something, in a special manner Dr. Chiara Medaglia and Dr. Gennaro De Vita.

I would like to thank my collegues/friends Dr. Fatemeh Asadzadeh, for her very precious and helpful support during the execution of the experiments, and Dr. Iolanda Scognamiglio who followed me during the last 2 years of my PhD program working with entusiasm and optimism on the projects. I will never forget our "little team"!

I would like to thank my *ex*-collegues and friends Dr. Iolanda Boffa and Dr. Alessandra Galiero for their patience, support, charism and optimism during the revision of "miR34a paper", also known as "the miR34 time"! Thank you for everything!

I also thank my best collegue and great friend Dr. Cristina Chiarolla for our "undergraduated experiences", and for the time that we spend in "dark room" in order to chose the best expositions! I was very lucky to know her, as my "clone". I will also remember our similar passions, such as Tennent's beer and Salsa dancing, and our adventures at Bolero! Thank for spending your time to listen my "idiot problems"!

I would like also thank my collegues in the lab, Dr. Francesco Paolo Pennino, Dr. Luisa Dassi, Dr. Roberto Siciliano and graduated student Ylenia Ferrara for their important efforts during this last period of my PhD program.

Then, I would like to thank all my family. There are no words that can truly express the level of gratitude and appreciation I have for you. I would like to say thank to my mother, who strongly supported me with all her patience and for her special vegetarian food, early in the morning and late in the evening. Thank you also for looking after our pets during my working time. I would like to thank my father, even when he seems to not understand the concept of “low and constat TV volume”. I really appreciate all your sacrifices you make for me and for my brother. I would like to thank my brother Stefano, for his “night company”, during my studies.

I would like to say thank to my boyfriend Vincenzo, who has always supported me during the last 10 yeras. I really appreciate your help during the thesis writing on “christmas time”. Thank for your time and for all the times you have picked me up from the lab late in the evening!

I want to thank my bestfriend Mariarita for her kindless words and her important advices. The distance between us did not block our “madness”.

I wank to say thank to my “red wine” friends, Ugo and Lilia for all the bottles of wine on saturday night.

Finally I want to thank my little boy, Pocci, and my little sister, Thayra, that have been very precious for me. They helped me to understand my true life values and especially the respect toward every form of life and every living being.

REFERENCES

1. Siegel, R.L., K.D. Miller, and A. Jemal, *Cancer Statistics, 2017.* CA Cancer J Clin, 2017. **67**(1): p. 7-30.
2. Cancer Genome Atlas, N., *Comprehensive molecular portraits of human breast tumours.* Nature, 2012. **490**(7418): p. 61-70.
3. Bianchini, G., et al., *Triple-negative breast cancer: challenges and opportunities of a heterogeneous disease.* Nat Rev Clin Oncol, 2016. **13**(11): p. 674-690.
4. Rakha, E.A. and S. Chan, *Metastatic triple-negative breast cancer.* Clin Oncol (R Coll Radiol), 2011. **23**(9): p. 587-600.
5. Shah, S.P., et al., *The clonal and mutational evolution spectrum of primary triple-negative breast cancers.* Nature, 2012. **486**(7403): p. 395-9.
6. Lehmann, B.D., et al., *Identification of human triple-negative breast cancer subtypes and preclinical models for selection of targeted therapies.* J Clin Invest, 2011. **121**(7): p. 2750-67.
7. Masuda, H., et al., *Differential response to neoadjuvant chemotherapy among 7 triple-negative breast cancer molecular subtypes.* Clin Cancer Res, 2013. **19**(19): p. 5533-40.
8. von Minckwitz, G., et al., *Definition and impact of pathologic complete response on prognosis after neoadjuvant chemotherapy in various intrinsic breast cancer subtypes.* J Clin Oncol, 2012. **30**(15): p. 1796-804.
9. Cortazar, P., et al., *Pathological complete response and long-term clinical benefit in breast cancer: the CTNeoBC pooled analysis.* Lancet, 2014. **384**(9938): p. 164-72.
10. Byrski, T., et al., *Pathologic complete response to neoadjuvant cisplatin in BRCA1-positive breast cancer patients.* Breast Cancer Res Treat, 2014. **147**(2): p. 401-5.
11. Silver, D.P., et al., *Efficacy of neoadjuvant Cisplatin in triple-negative breast cancer.* J Clin Oncol, 2010. **28**(7): p. 1145-53.
12. Sikov, W.M., et al., *Impact of the addition of carboplatin and/or bevacizumab to neoadjuvant once-per-week paclitaxel followed by dose-dense doxorubicin and cyclophosphamide on pathologic complete response rates in stage II to III triple-negative breast cancer: CALGB 40603 (Alliance).* J Clin Oncol, 2015. **33**(1): p. 13-21.
13. Telli, M.L., et al., *Phase II Study of Gemcitabine, Carboplatin, and Iniparib As Neoadjuvant Therapy for Triple-Negative and BRCA1/2 Mutation-Associated Breast Cancer With Assessment of a Tumor-Based Measure of Genomic Instability: PrECOG 0105.* J Clin Oncol, 2015. **33**(17): p. 1895-901.
14. Isakoff, S.J., et al., *TBCRC009: A Multicenter Phase II Clinical Trial of Platinum Monotherapy With Biomarker Assessment in Metastatic Triple-Negative Breast Cancer.* J Clin Oncol, 2015. **33**(17): p. 1902-9.
15. Burkle, A., *Poly(APD-ribosyl)ation, a DNA damage-driven protein modification and regulator of genomic instability.* Cancer Lett, 2001. **163**(1): p. 1-5.
16. Tutt, A., et al., *Oral poly(ADP-ribose) polymerase inhibitor olaparib in patients with BRCA1 or BRCA2 mutations and advanced breast cancer: a proof-of-concept trial.* Lancet, 2010. **376**(9737): p. 235-44.
17. Infante, J.R., et al., *A phase 1b study of trametinib, an oral Mitogen-activated protein kinase kinase (MEK) inhibitor, in combination with gemcitabine in advanced solid tumours.* Eur J Cancer, 2013. **49**(9): p. 2077-85.

18. Dent, R., et al., *Pattern of metastatic spread in triple-negative breast cancer.* Breast Cancer Res Treat, 2009. **115**(2): p. 423-8.
19. Lin, N.U., et al., *Clinicopathologic features, patterns of recurrence, and survival among women with triple-negative breast cancer in the National Comprehensive Cancer Network.* Cancer, 2012. **118**(22): p. 5463-72.
20. Tseng, L.M., et al., *Distant metastasis in triple-negative breast cancer.* Neoplasma, 2013. **60**(3): p. 290-4.
21. Zeichner, S.B., H. Terawaki, and K. Gogineni, *A Review of Systemic Treatment in Metastatic Triple-Negative Breast Cancer.* Breast Cancer (Auckl), 2016. **10**: p. 25-36.
22. Tammenkoski, M., et al., *Human metastasis regulator protein H-prune is a short-chain exopolyphosphatase.* Biochemistry, 2008. **47**(36): p. 9707-13.
23. Zollo, M., et al., *Overexpression of h-prune in breast cancer is correlated with advanced disease status.* Clin Cancer Res, 2005. **11**(1): p. 199-205.
24. Oue, N., et al., *Increased expression of h-prune is associated with tumor progression and poor survival in gastric cancer.* Cancer Sci, 2007. **98**(8): p. 1198-205.
25. Carotenuto, M., et al., *H-Prune through GSK-3beta interaction sustains canonical WNT/beta-catenin signaling enhancing cancer progression in NSCLC.* Oncotarget, 2014. **5**(14): p. 5736-49.
26. Hashimoto, M., et al., *h-Prune is associated with poor prognosis and epithelial-mesenchymal transition in patients with colorectal liver metastases.* Int J Cancer, 2016. **139**(4): p. 812-23.
27. Carotenuto, M., et al., *Neuroblastoma tumorigenesis is regulated through the Nm23-H1/h-Prune C-terminal interaction.* Sci Rep, 2013. **3**: p. 1351.
28. Ferrucci, V., et al., *Metastatic recurrence of Group 3 medulloblastoma is driven by PRUNE-1 through targeting NME1–TGF-β–OTX2–SNAIL signalling via PTEN inhibition.* Brain, 2018, *In press*.
29. Zollo, M., et al., *PRUNE is crucial for normal brain development and mutated in microcephaly with neurodevelopmental impairment.* Brain, 2017. **140**(4): p. 940-952.
30. Salpietro, V., et al., *The phenotypic and molecular spectrum of PEHO syndrome and PEHO-like disorders.* Brain, 2017. **140**(8): p. e49.
31. Karaca, E., et al., *Genes that Affect Brain Structure and Function Identified by Rare Variant Analyses of Mendelian Neurologic Disease.* Neuron, 2015. **88**(3): p. 499-513.
32. Costain, G., et al., *Homozygous mutation in PRUNE1 in an Oji-Cree male with a complex neurological phenotype.* Am J Med Genet A, 2017. **173**(3): p. 740-743.
33. Karakaya, M., et al., *PRUNE1: a disease-causing gene for secondary microcephaly.* Brain, 2017. **140**(10): p. e61.
34. Jung, H., H.A. Seong, and H. Ha, *NM23-H1 tumor suppressor and its interacting partner STRAP activate p53 function.* J Biol Chem, 2007. **282**(48): p. 35293-307.
35. Jian, H., et al., *Smad3-dependent nuclear translocation of beta-catenin is required for TGF-beta1-induced proliferation of bone marrow-derived adult human mesenchymal stem cells.* Genes Dev, 2006. **20**(6): p. 666-74.
36. Kobayashi, T., et al., *Glycogen synthase kinase 3 and h-prune regulate cell migration by modulating focal adhesions.* Mol Cell Biol, 2006. **26**(3): p. 898-911.
37. Carotenuto, P., et al., *PRUNE and NM23-M1 expression in embryonic and adult mouse brain.* J Bioenerg Biomembr, 2006. **38**(3-4): p. 233-46.
38. Bilitou, A., et al., *Spatial and temporal expressions of prune reveal a role in Muller gliogenesis during Xenopus retinal development.* Gene, 2012. **509**(1): p. 93-103.
39. Garzia, L., et al., *Phosphorylation of nm23-H1 by CKI induces its complex formation with h-prune and promotes cell motility.* Oncogene, 2008. **27**(13): p. 1853-64.
40. Galasso, A. and M. Zollo, *The Nm23-H1-h-Prune complex in cellular physiology: a 'tip of the iceberg' protein network perspective.* Mol Cell Biochem, 2009. **329**(1-2): p. 149-59.
41. Kudoh, K., et al., *Gains of 1q21-q22 and 13q12-q14 are potential indicators for resistance to cisplatin-based chemotherapy in ovarian cancer patients.* Clin Cancer Res, 1999. **5**(9): p. 2526-31.
42. Forus, A., et al., *Amplification and overexpression of PRUNE in human sarcomas and breast carcinomas-a possible mechanism for altering the nm23-H1 activity.* Oncogene, 2001. **20**(47): p. 6881-90.
43. Yokdang, N., et al., *Blockade of extracellular NM23 or its endothelial target slows breast cancer growth and metastasis.* Integr Cancer Sci Ther, 2015. **2**(4): p. 192-200.

44. Steeg, P.S., *Metastasis suppressors alter the signal transduction of cancer cells.* Nat Rev Cancer, 2003. **3**(1): p. 55-63.
45. D'Angelo, A., et al., *Prune cAMP phosphodiesterase binds nm23-H1 and promotes cancer metastasis.* Cancer Cell, 2004. **5**(2): p. 137-49.
46. Diana, D., et al., *Mapping functional interaction sites of human prune C-terminal domain by NMR spectroscopy in human cell lysates.* Chemistry, 2013. **19**(37): p. 12217-20.
47. Ferrucci, V., et al., *A competitive cell-permeable peptide (CPP) to impair the Nme-1 (NDPK-A) and Prune-1 interaction for therapeutic applications in cancer.* Laboratory Investigation. 2018. *In press.*
48. Carotenuto, M., et al., *A therapeutic approach to treat prostate cancer by targeting Nm23-H1/h-Prune interaction.* Naunyn Schmiedebergs Arch Pharmacol, 2015. **388**(2): p. 257-69.
49. ten Dijke, P. and H.M. Arthur, *Extracellular control of TGFbeta signalling in vascular development and disease.* Nat Rev Mol Cell Biol, 2007. **8**(11): p. 857-69.
50. Massague, J., *TGFbeta in Cancer.* Cell, 2008. **134**(2): p. 215-30.
51. Ewen, M.E., et al., *p53-dependent repression of CDK4 translation in TGF-beta-induced G1 cell-cycle arrest.* Genes Dev, 1995. **9**(2): p. 204-17.
52. Pardali, K. and A. Moustakas, *Actions of TGF-beta as tumor suppressor and pro-metastatic factor in human cancer.* Biochim Biophys Acta, 2007. **1775**(1): p. 21-62.
53. Boulanger, C.A. and G.H. Smith, *Reducing mammary cancer risk through premature stem cell senescence.* Oncogene, 2001. **20**(18): p. 2264-72.
54. Siegel, P.M., et al., *Transforming growth factor beta signaling impairs Neu-induced mammary tumorigenesis while promoting pulmonary metastasis.* Proc Natl Acad Sci U S A, 2003. **100**(14): p. 8430-5.
55. Padua, D., et al., *TGFbeta primes breast tumors for lung metastasis seeding through angiopoietin-like 4.* Cell, 2008. **133**(1): p. 66-77.
56. Moses, H. and M.H. Barcellos-Hoff, *TGF-beta biology in mammary development and breast cancer.* Cold Spring Harb Perspect Biol, 2011. **3**(1): p. a003277.
57. Tan, A.R., G. Alexe, and M. Reiss, *Transforming growth factor-beta signaling: emerging stem cell target in metastatic breast cancer?* Breast Cancer Res Treat, 2009. **115**(3): p. 453-95.
58. Huber, M.A., N. Kraut, and H. Beug, *Molecular requirements for epithelial-mesenchymal transition during tumor progression.* Curr Opin Cell Biol, 2005. **17**(5): p. 548-58.
59. Ding, M.J., et al., *Association between transforming growth factor-beta1 expression and the clinical features of triple negative breast cancer.* Oncol Lett, 2016. **11**(6): p. 4040-4044.
60. Bhola, N.E., et al., *TGF-beta inhibition enhances chemotherapy action against triple-negative breast cancer.* J Clin Invest, 2013. **123**(3): p. 1348-58.
61. Spano, D. and M. Zollo, *Tumor microenvironment: a main actor in the metastasis process.* Clin Exp Metastasis, 2012. **29**(4): p. 381-95.
62. Spano D., Z.M., *Immune Cells Within the Tumor Microenvironment.* Springer-Verlag Wien 2014, 2014.
63. Quatromoni, J.G. and E. Eruslanov, *Tumor-associated macrophages: function, phenotype, and link to prognosis in human lung cancer.* Am J Transl Res, 2012. **4**(4): p. 376-89.
64. Mantovani, A., et al., *Tumour-associated macrophages as treatment targets in oncology.* Nat Rev Clin Oncol, 2017. **14**(7): p. 399-416.
65. Gabrilovich, D.I., S. Ostrand-Rosenberg, and V. Bronte, *Coordinated regulation of myeloid cells by tumours.* Nat Rev Immunol, 2012. **12**(4): p. 253-68.
66. Rochman, Y., R. Spolski, and W.J. Leonard, *New insights into the regulation of T cells by gamma(c) family cytokines.* Nat Rev Immunol, 2009. **9**(7): p. 480-90.
67. Spano, D., et al., *Dipyridamole prevents triple-negative breast-cancer progression.* Clin Exp Metastasis, 2013. **30**(1): p. 47-68.
68. Zollo, M., et al., *Targeting monocyte chemotactic protein-1 synthesis with bindarit induces tumor regression in prostate and breast cancer animal models.* Clin Exp Metastasis, 2012. **29**(6): p. 585-601.
69. Pardoll, D.M., *The blockade of immune checkpoints in cancer immunotherapy.* Nat Rev Cancer, 2012. **12**(4): p. 252-64.
70. Yu, T. and G. Di, *Role of tumor microenvironment in triple-negative breast cancer and its prognostic significance.* Chin J Cancer Res, 2017. **29**(3): p. 237-252.
71. Dieci, M.V., et al., *Prognostic value of tumor-infiltrating lymphocytes on residual disease after primary chemotherapy for triple-negative breast cancer: a retrospective multicenter study.* Ann Oncol, 2014. **25**(3): p. 611-8.

72. Adams, T.A., et al., *Composite analysis of immunological and metabolic markers defines novel subtypes of triple negative breast cancer.* Mod Pathol, 2017.
73. Hollmen, M., et al., *Characterization of macrophage--cancer cell crosstalk in estrogen receptor positive and triple-negative breast cancer.* Sci Rep, 2015. **5**: p. 9188.
74. Medrek, C., et al., *The presence of tumor associated macrophages in tumor stroma as a prognostic marker for breast cancer patients.* BMC Cancer, 2012. **12**: p. 306.
75. Sousa, S., et al., *Human breast cancer cells educate macrophages toward the M2 activation status.* Breast Cancer Res, 2015. **17**: p. 101.
76. Wang, X.X., et al., *Effect of nodal status on clinical outcomes of triple-negative breast cancer: a population-based study using the SEER 18 database.* Oncotarget, 2016. **7**(29): p. 46636-46645.
77. Yuan, Z.Y., et al., *High infiltration of tumor-associated macrophages in triple-negative breast cancer is associated with a higher risk of distant metastasis.* Onco Targets Ther, 2014. **7**: p. 1475-80.
78. Zhang, X., et al., *PD-L1 induced by IFN-gamma from tumor-associated macrophages via the JAK/STAT3 and PI3K/AKT signaling pathways promoted progression of lung cancer.* Int J Clin Oncol, 2017. **22**(6): p. 1026-1033.
79. Santarpia, M., et al., *Programmed cell death protein-1/programmed cell death ligand-1 pathway inhibition and predictive biomarkers: understanding transforming growth factor-beta role.* Transl Lung Cancer Res, 2015. **4**(6): p. 728-42.
80. Santoni, M., et al., *Triple negative breast cancer: Key role of Tumor-Associated Macrophages in regulating the activity of anti-PD-1/PD-L1 agents.* Biochim Biophys Acta, 2017.
81. Dunlap, S.M., et al., *Dietary energy balance modulates epithelial-to-mesenchymal transition and tumor progression in murine claudin-low and basal-like mammary tumor models.* Cancer Prev Res (Phila), 2012. **5**(7): p. 930-42.
82. Niu, M., et al., *Tumor-Associated Macrophage-Mediated Targeted Therapy of Triple-Negative Breast Cancer.* Mol Pharm, 2016. **13**(6): p. 1833-42.
83. Gong, D., et al., *TGFbeta signaling plays a critical role in promoting alternative macrophage activation.* BMC Immunol, 2012. **13**: p. 31.
84. Tone, Y., et al., *Smad3 and NFAT cooperate to induce Foxp3 expression through its enhancer.* Nat Immunol, 2008. **9**(2): p. 194-202.
85. von Boehmer, H. and C. Daniel, *Therapeutic opportunities for manipulating T(Reg) cells in autoimmunity and cancer.* Nat Rev Drug Discov, 2013. **12**(1): p. 51-63.
86. Ivanov, II, et al., *The orphan nuclear receptor RORgammat directs the differentiation program of proinflammatory IL-17+ T helper cells.* Cell, 2006. **126**(6): p. 1121-33.
87. Pickup, M., S. Novitskiy, and H.L. Moses, *The roles of TGFbeta in the tumour microenvironment.* Nat Rev Cancer, 2013. **13**(11): p. 788-99.
88. Flavell, R.A., et al., *The polarization of immune cells in the tumour environment by TGFbeta.* Nat Rev Immunol, 2010. **10**(8): p. 554-67.
89. Bierie, B. and H.L. Moses, *Tumour microenvironment: TGFbeta: the molecular Jekyll and Hyde of cancer.* Nat Rev Cancer, 2006. **6**(7): p. 506-20.
90. Minciacchi, V.R., M.R. Freeman, and D. Di Vizio, *Extracellular vesicles in cancer: exosomes, microvesicles and the emerging role of large oncosomes.* Semin Cell Dev Biol, 2015. **40**: p. 41-51.
91. Thery, C., L. Zitvogel, and S. Amigorena, *Exosomes: composition, biogenesis and function.* Nat Rev Immunol, 2002. **2**(8): p. 569-79.
92. Simpson, R.J., S.S. Jensen, and J.W. Lim, *Proteomic profiling of exosomes: current perspectives.* Proteomics, 2008. **8**(19): p. 4083-99.
93. Mathivanan, S., H. Ji, and R.J. Simpson, *Exosomes: extracellular organelles important in intercellular communication.* J Proteomics, 2010. **73**(10): p. 1907-20.
94. Le, M.T., et al., *miR-200-containing extracellular vesicles promote breast cancer cell metastasis.* J Clin Invest, 2014. **124**(12): p. 5109-28.
95. McCready, J., et al., *The contribution of dynamic stromal remodeling during mammary development to breast carcinogenesis.* Breast Cancer Res, 2010. **12**(3): p. 205.
96. McCready, J., et al., *Secretion of extracellular hsp90alpha via exosomes increases cancer cell motility: a role for plasminogen activation.* BMC Cancer, 2010. **10**: p. 294.
97. Higginbotham, J.N., et al., *Amphiregulin exosomes increase cancer cell invasion.* Curr Biol, 2011. **21**(9): p. 779-86.

98. Skog, J., et al., *Glioblastoma microvesicles transport RNA and proteins that promote tumour growth and provide diagnostic biomarkers.* Nat Cell Biol, 2008. **10**(12): p. 1470-6.
99. Sheldon, H., et al., *New mechanism for Notch signaling to endothelium at a distance by Delta-like 4 incorporation into exosomes.* Blood, 2010. **116**(13): p. 2385-94.
100. Hoshino, A., et al., *Tumour exosome integrins determine organotropic metastasis.* Nature, 2015. **527**(7578): p. 329-35.
101. Clayton, A., et al., *Human tumor-derived exosomes down-modulate NKG2D expression.* J Immunol, 2008. **180**(11): p. 7249-58.
102. Huber, V., et al., *Human colorectal cancer cells induce T-cell death through release of proapoptotic microvesicles: role in immune escape.* Gastroenterology, 2005. **128**(7): p. 1796-804.
103. Yu, S., et al., *Tumor exosomes inhibit differentiation of bone marrow dendritic cells.* J Immunol, 2007. **178**(11): p. 6867-75.
104. de Vrij, J., et al., *Glioblastoma-derived extracellular vesicles modify the phenotype of monocytic cells.* Int J Cancer, 2015. **137**(7): p. 1630-42.
105. Yang, M., et al., *Microvesicles secreted by macrophages shuttle invasion-potentiating microRNAs into breast cancer cells.* Mol Cancer, 2011. **10**: p. 117.
106. Chow, A., et al., *Macrophage immunomodulation by breast cancer-derived exosomes requires Toll-like receptor 2-mediated activation of NF-kappaB.* Sci Rep, 2014. **4**: p. 5750.
107. Dai, S., et al., *Phase I clinical trial of autologous ascites-derived exosomes combined with GM-CSF for colorectal cancer.* Mol Ther, 2008. **16**(4): p. 782-90.
108. Escudier, B., et al., *Vaccination of metastatic melanoma patients with autologous dendritic cell (DC) derived-exosomes: results of thefirst phase I clinical trial.* J Transl Med, 2005. **3**(1): p. 10.
109. Morse, M.A., et al., *A phase I study of dexosome immunotherapy in patients with advanced non-small cell lung cancer.* J Transl Med, 2005. **3**(1): p. 9.
110. Noguchi, T., et al., *h-Prune is an independent prognostic marker for survival in esophageal squamous cell carcinoma.* Ann Surg Oncol, 2009. **16**(5): p. 1390-6.
111. Burstein, M.D., et al., *Comprehensive genomic analysis identifies novel subtypes and targets of triple-negative breast cancer.* Clin Cancer Res, 2015. **21**(7): p. 1688-98.
112. Sorlie, T., et al., *Gene expression patterns of breast carcinomas distinguish tumor subclasses with clinical implications.* Proc Natl Acad Sci U S A, 2001. **98**(19): p. 10869-74.
113. Kim, J.Y., et al., *The relationship between nuclear factor (NF)-kappaB family gene expression and prognosis in triple-negative breast cancer (TNBC) patients receiving adjuvant doxorubicin treatment.* Sci Rep, 2016. **6**: p. 31804.
114. Bartholomeusz, C., et al., *High ERK protein expression levels correlate with shorter survival in triple-negative breast cancer patients.* Oncologist, 2012. **17**(6): p. 766-74.
115. Chen, A., et al., *Reduction in Migratory Phenotype in a Metastasized Breast Cancer Cell Line via Downregulation of S100A4 and GRM3.* Sci Rep, 2017. **7**(1): p. 3459.
116. Yoneda, T., et al., *Actions of bisphosphonate on bone metastasis in animal models of breast carcinoma.* Cancer, 2000. **88**(12 Suppl): p. 2979-88.
117. Lam, J., et al., *Baseline mechanical characterization of J774 macrophages.* Biophys J, 2009. **96**(1): p. 248-54.
118. Maurya, M.R., et al., *Analysis of inflammatory and lipid metabolic networks across RAW264.7 and thioglycolate-elicited macrophages.* J Lipid Res, 2013. **54**(9): p. 2525-42.
119. Wang, N., H. Liang, and K. Zen, *Molecular mechanisms that influence the macrophage m1-m2 polarization balance.* Front Immunol, 2014. **5**: p. 614.
120. Levy, D.E. and J.E. Darnell, Jr., *Stats: transcriptional control and biological impact.* Nat Rev Mol Cell Biol, 2002. **3**(9): p. 651-62.
121. Decker, T. and P. Kovarik, *Serine phosphorylation of STATs.* Oncogene, 2000. **19**(21): p. 2628-37.
122. Yang, X.O., et al., *Regulation of inflammatory responses by IL-17F.* J Exp Med, 2008. **205**(5): p. 1063-75.
123. Giles, D.A., et al., *Regulation of Inflammation by IL-17A and IL-17F Modulates Non-Alcoholic Fatty Liver Disease Pathogenesis.* PLoS One, 2016. **11**(2): p. e0149783.
124. Starnes, T., et al., *Cutting edge: IL-17F, a novel cytokine selectively expressed in activated T cells and monocytes, regulates angiogenesis and endothelial cell cytokine production.* J Immunol, 2001. **167**(8): p. 4137-40.

125. Dumoutier, L., et al., *Cloning of a new type II cytokine receptor activating signal transducer and activator of transcription (STAT)1, STAT2 and STAT3.* Biochem J, 2003. **370**(Pt 2): p. 391-6.
126. Zhou, Z., et al., *Type III interferon (IFN) induces a type I IFN-like response in a restricted subset of cells through signaling pathways involving both the Jak-STAT pathway and the mitogen-activated protein kinases.* J Virol, 2007. **81**(14): p. 7749-58.
127. Asadzadeh, F., et al., *In vivo bioluminescence imaging using orthotopic xenografts towards patient's derived-xenograft Medulloblastoma models.* Q J Nucl Med Mol Imaging, 2017. **61**(1): p. 95-101.
128. Virgilio, A., et al., *Novel pyrimidopyrimidine derivatives for inhibition of cellular proliferation and motility induced by h-prune in breast cancer.* Eur J Med Chem, 2012. **57**: p. 41-50.
129. Callahan, R. and G.H. Smith, *MMTV-induced mammary tumorigenesis: gene discovery, progression to malignancy and cellular pathways.* Oncogene, 2000. **19**(8): p. 992-1001.
130. Li, Y., W.P. Hively, and H.E. Varmus, *Use of MMTV-Wnt-1 transgenic mice for studying the genetic basis of breast cancer.* Oncogene, 2000. **19**(8): p. 1002-9.
131. Huang, S., et al., *Comparison of expression profiles of metastatic versus primary mammary tumors in MMTV-Wnt-1 and MMTV-Neu transgenic mice.* Neoplasia, 2008. **10**(2): p. 118-24.
132. Yu, Q.C., E.M. Verheyen, and Y.A. Zeng, *Mammary Development and Breast Cancer: A Wnt Perspective.* Cancers (Basel), 2016. **8**(7).
133. Herschkowitz, J.I., et al., *Identification of conserved gene expression features between murine mammary carcinoma models and human breast tumors.* Genome Biol, 2007. **8**(5): p. R76.
134. Pfefferle, A.D., et al., *Transcriptomic classification of genetically engineered mouse models of breast cancer identifies human subtype counterparts.* Genome Biol, 2013. **14**(11): p. R125.
135. Bocchinfuso, W.P., et al., *A mouse mammary tumor virus-Wnt-1 transgene induces mammary gland hyperplasia and tumorigenesis in mice lacking estrogen receptor-alpha.* Cancer Res, 1999. **59**(8): p. 1869-76.
136. Zhang, X., et al., *Estrogen receptor positivity in mammary tumors of Wnt-1 transgenic mice is influenced by collaborating oncogenic mutations.* Oncogene, 2005. **24**(26): p. 4220-31.
137. Li, Y., et al., *Deficiency of Pten accelerates mammary oncogenesis in MMTV-Wnt-1 transgenic mice.* BMC Mol Biol, 2001. **2**: p. 2.
138. Mantovani, A., et al., *Macrophage polarization: tumor-associated macrophages as a paradigm for polarized M2 mononuclear phagocytes.* Trends Immunol, 2002. **23**(11): p. 549-55.
139. Mantovani, A., *From phagocyte diversity and activation to probiotics: back to Metchnikoff.* Eur J Immunol, 2008. **38**(12): p. 3269-73.
140. Martinez, F.O., et al., *Transcriptional profiling of the human monocyte-to-macrophage differentiation and polarization: new molecules and patterns of gene expression.* J Immunol, 2006. **177**(10): p. 7303-11.
141. Pelegrin, P. and A. Surprenant, *Dynamics of macrophage polarization reveal new mechanism to inhibit IL-1beta release through pyrophosphates.* EMBO J, 2009. **28**(14): p. 2114-27.
142. Kahlert, C. and R. Kalluri, *Exosomes in tumor microenvironment influence cancer progression and metastasis.* J Mol Med (Berl), 2013. **91**(4): p. 431-7.
143. Thery, C., M. Ostrowski, and E. Segura, *Membrane vesicles as conveyors of immune responses.* Nat Rev Immunol, 2009. **9**(8): p. 581-93.
144. Thery, C., et al., *Isolation and characterization of exosomes from cell culture supernatants and biological fluids.* Curr Protoc Cell Biol, 2006. **Chapter 3**: p. Unit 3 22.
145. Cox, J., et al., *Accurate proteome-wide label-free quantification by delayed normalization and maximal peptide ratio extraction, termed MaxLFQ.* Mol Cell Proteomics, 2014. **13**(9): p. 2513-26.
146. Harris, D.A., et al., *Exosomes released from breast cancer carcinomas stimulate cell movement.* PLoS One, 2015. **10**(3): p. e0117495.
147. Yang, M., et al., *Knockdown of interferon-induced transmembrane protein 3 expression suppresses breast cancer cell growth and colony formation and affects the cell cycle.* Oncol Rep, 2013. **30**(1): p. 171-8.
148. Damaghi, M., et al., *Chronic acidosis in the tumour microenvironment selects for overexpression of LAMP2 in the plasma membrane.* Nat Commun, 2015. **6**: p. 8752.
149. Du, W.W., et al., *The role of versican G3 domain in regulating breast cancer cell motility including effects on osteoblast cell growth and differentiation in vitro - evaluation towards understanding breast cancer cell bone metastasis.* BMC Cancer, 2012. **12**: p. 341.

150. Yang, Y., et al., *Elevated expression of syntenin in breast cancer is correlated with lymph node metastasis and poor patient survival.* Breast Cancer Res, 2013. **15**(3): p. R50.
151. Qian, X.L., et al., *Syndecan binding protein (SDCBP) is overexpressed in estrogen receptor negative breast cancers, and is a potential promoter for tumor proliferation.* PLoS One, 2013. **8**(3): p. e60046.
152. Koo, T.H., et al., *Syntenin is overexpressed and promotes cell migration in metastatic human breast and gastric cancer cell lines.* Oncogene, 2002. **21**(26): p. 4080-8.
153. Hwangbo, C., J. Park, and J.H. Lee, *mda-9/Syntenin protein positively regulates the activation of Akt protein by facilitating integrin-linked kinase adaptor function during adhesion to type I collagen.* J Biol Chem, 2011. **286**(38): p. 33601-12.
154. Menezes, M.E., et al., *MDA-9/Syntenin (SDCBP) modulates small GTPases RhoA and Cdc42 via transforming growth factor beta1 to enhance epithelial-mesenchymal transition in breast cancer.* Oncotarget, 2016. **7**(49): p. 80175-80189.
155. Hwangbo, C., et al., *Syntenin regulates TGF-beta1-induced Smad activation and the epithelial-to-mesenchymal transition by inhibiting caveolin-mediated TGF-beta type I receptor internalization.* Oncogene, 2016. **35**(3): p. 389-401.
156. Das, S.K., et al., *Knockout of MDA-9/Syntenin (SDCBP) expression in the microenvironment dampens tumor-supporting inflammation and inhibits melanoma metastasis.* Oncotarget, 2016. **7**(30): p. 46848-46861.
157. Incassati, A., et al., *Key signaling nodes in mammary gland development and cancer: beta-catenin.* Breast Cancer Res, 2010. **12**(6): p. 213.
158. Pohl, S.G., et al., *Wnt signaling in triple-negative breast cancer.* Oncogenesis, 2017. **6**(4): p. e310.
159. Stein, T., et al., *A mouse mammary gland involution mRNA signature identifies biological pathways potentially associated with breast cancer metastasis.* J Mammary Gland Biol Neoplasia, 2009. **14**(2): p. 99-116.
160. Boye, K., et al., *Activation of NF-kappaB by extracellular S100A4: analysis of signal transduction mechanisms and identification of target genes.* Int J Cancer, 2008. **123**(6): p. 1301-10.
161. Shen, F., et al., *Identification of common transcriptional regulatory elements in interleukin-17 target genes.* J Biol Chem, 2006. **281**(34): p. 24138-48.
162. Osterlund, P.I., et al., *IFN regulatory factor family members differentially regulate the expression of type III IFN (IFN-lambda) genes.* J Immunol, 2007. **179**(6): p. 3434-42.
163. Lai, T., et al., *Interleukin 17 induces up-regulation of chemokine and cytokine expression via activation of the nuclear factor kappaB and extracellular signal-regulated kinase 1/2 pathways in gynecologic cancer cell lines.* Int J Gynecol Cancer, 2011. **21**(9): p. 1533-9.
164. Du, J.W., et al., *Interleukin-17, produced by lymphocytes, promotes tumor growth and angiogenesis in a mouse model of breast cancer.* Mol Med Rep, 2012. **6**(5): p. 1099-102.
165. Ferrucci, V., et al., *Natural compounds for pediatric cancer treatment.* Naunyn Schmiedebergs Arch Pharmacol, 2016. **389**(2): p. 131-49.
166. Jang, J.Y., et al., *Exosome derived from epigallocatechin gallate treated breast cancer cells suppresses tumor growth by inhibiting tumor-associated macrophage infiltration and M2 polarization.* BMC Cancer, 2013. **13**: p. 421.